Development and applications of a novel, thermoresponsive scaffold for three-dimensional cell culture

by

Claire Louise Rossouw

Submitted in partial fulfilment of the requirements for the degree
Philosophiae Doctor

In the Faculty of Natural and Agricultural Sciences
Department of Biochemistry
University of Pretoria
Pretoria
South Africa

SUPERVISOR:
Prof. Lyn-Marie Birkholtz
Department of Biochemistry, University of Pretoria, South Africa

CO-SUPERVISORS:
Dr. Dalu Mancama
Molecular and Biomedical Technologies, Biosciences, CSIR, South Africa

Prof. Heinrich Hoppe
Department of Biochemistry, Microbiology and Biotechnology, Rhodes University, South Africa

Dr. Sean Moolman
Licensing & Ventures, CSIR, South Africa

UNIVERSITEIT VAN PRETORIA
UNIVERSITY OF PRETORIA
YUNIBESITHI YA PRETORIA

SUBMISSION DECLARATION

I, Claire Louise Rossouw, declare that the thesis, which I hereby submit for the degree *Philosophiae Doctor* at the University of Pretoria, is my own work and has not previously been submitted by me for a degree at this or any other tertiary institution.

SIGNATURE:…….

DATE:……..

PLAGIARISM STATEMENT

I understand what plagiarism is and am aware of the University's policy in this regard.

I declare that this thesis is my own original work. Where other people's work has been used (either from printed source, internet or any other source), this has been properly acknowledged and referenced in accordance with departmental regulations.

I have not used work previously produced by another student or any other person to hand in as my own.

I have not allowed and will not allow anyone to copy my work with the intention of passing it off as his or her own work.

Student's signature Date

ACKNOWLEDGEMENTS

The completion of this dissertation was made possible by the following people whom I would like to thank:

My supervisors, Prof. Lyn-Marie Birkholtz, Dr Dalu Mancama, Prof. Heinrich Hoppe and Dr Sean Moolman for your guidance, support and encouragement. It was a privilege to work with you!

Avashnee Chetty, for stimulating discussions and for supplying the 3D scaffolds.

Kobus van Wyk, for technical assistance and help with the bioreactor experimental work.

Dr Jetsumon Sattabongkot (AFRIMS), for allowing me to train in your laboratory and for the long distance help via e-mail.

Megan Dowler (WRAIR), for your willingness to share your vast gametocyte culturing knowledge with me.

The CSIR and the 3R foundation in Switzerland for funding.

My fellow students, past and present: Dr Walter Campos and Dayaneethie Coopusamy for your help in tissue culture; Dr Tharina van Brummelen and Dr John Becker for teaching me to culture malaria parasites and Lia Rotherham for your friendship and encouragement.

My husband, Johann Rossouw, for all the weekends spent in the lab so I could feed my parasites, your unconditional love and unwavering support.

My parents, Gavin and Jane Munro and my family. I am so thankful for all the love, support and encouragement you have given me all my life.

SUMMARY

Although conventional two-dimensional (2D) cell culture is convenient for routine work, researchers are turning to three-dimensional (3D) cell culture for more accurate, physiologically representative information on the way their cells behave and respond to stimuli. Cells can now be routinely cultured in the many commercially available 3D formats.

In this study, we developed non-woven scaffolds for 3D cell culture and enhanced cell function. By making use of methods that measure the behaviour of liver cells in the 3D system we were able to demonstrate, compared to standard 2D systems, significantly higher expression of key liver enzymes involved in drug metabolism and albumin production (specifically cytochrome P450). Cell proliferation on the various scaffolds was comparable to that of a commercially available hydrogel 3D cell culture system, Algimatrix™.

When culturing cells in 3D, the means by which cells are harvested or extracted from the 3D scaffold for downstream applications is more challenging than in 2D. For this reason, many of the 3D scaffolds currently manufactured are either bio-degradable or require the use of salts to dissolve the scaffold which may negatively impact on the cells they contain. By grafting the non-woven scaffolds with the thermoresponsive polymer, poly(*N*-isopropylacrylamide) (PNIPAAm), we demonstrated that cells growing on the scaffolds are able to be released from the scaffold in a 3D conformation, non-enzymatically, through temperature changes. Selected thermoresponsive non-woven fabrics were also tested in an automated cell culture device for cell proliferation and thermally induced harvesting.

One of the applications of a 3D cell culturing system would be in exploration of the many diseases plaguing mankind, in particular malaria which is still responsible for severe disease and mortality, especially in Africa. Most available antimalarials are designed to target the pathogenic blood stages in humans and to address the constant threat of drug resistance. However, to meet the objective of malaria eradication, medicines that block parasite transmission also need to be developed. Molecules that efficiently target the parasite stages in the liver would prevent pathogenesis, symptoms and transmission. Equipped with the knowledge that the infectious sporozoites traverse several hepatocytes prior to cell infection, it may be physiologically limiting to culture the exo-erythrocytic stage *in vitro* in a 2D cell culture system where the hepatocytes are in an unnatural flat conformation, distinctly different to their *in vivo* counterparts. Moreover, monolayer cell cultures lose their tissue-related functions rapidly, greatly impairing the predictive power of such assays. Thus, the second aim of this thesis was

to establish if hepatocytes that have been cultured on 3D non-woven scaffolds improve *in vitro* sporozoite invasion compared to conventional 2D systems. Sporozoite invasion was detected in the conventional 2D monolayers using a TaqMan® assay but not in the hepatocytes growing in 3D. Future studies beyond the scope of this thesis will include modifications to the 3D scaffold to attempt achieving superior sporozoite invasion in this model system.

TABLE OF CONTENTS

LIST OF FIGURES

LIST OF TABLES

ABBREVIATIONS

AB - AlamarBlue®

APS - Ammonium Persulphate

ATR-FTIR - Attenuated Total Reflection-Fourier Transform Infrared Spectroscopy (ATR-FTIR),

DMEM - Dulbecco's Modified Eagle Medium

DPI - Days Post Inoculation

DSC - Differential Scanning Calorimetry

ECM - Extracellular Matrix

EDTA - Ethylenediaminetetraacetic acid

EEF – Exoerythrocytic Form

FCS - Foetal Calf Serum

FDA - Fluorescein Diacetate

HPI - Hours Post Inoculation

HSPG – Heparin Sulphate Proteoglycan

LCST - Lower Critical Solution Temperature

MCTS - Multicellular Tumour Spheroid

MFP - Median Flow Pore

PBS – Phosphate Buffered Saline

PCL - Poly(ε-caprolactone)

PEG - Poly(ethylene glycol)

PET - Poly(ethylene terephthalate)

PNIPAAm - Poly(*N*-isopropylacrylamide)

PP - Poly(propylene)

SEM - Scanning Electron Microscopy

SFRP - Solution Free-Radical Polymerisation

XPS - X-Ray Photoelectron Spectroscopy

APPENDIX A

CHAPTER 1

THREE DIMENSIONAL CELL CULTURE SYSTEMS AND THEIR APPLICATIONS: A REVIEW

Mammals are comprised of a large number of cell types with a variety of specialised functions including tissue scaffolding and structure; signalling and sensing; digestion and absorption; transfer of molecular oxygen; immunity; mobility and reproduction to name a few. One of the major developments in science and particularly cell biology has been the development of systems allowing the growth of these various cell types *in vitro*, literally meaning ”in glass” or outside the body. *In vitro,* biologists have been able to study amongst others cell differentiation, function, development, growth, regeneration and death.

Tissue culture was first developed in the early 1900’s as a method for studying the behaviour of tissue fragments and gradually biologists developed techniques to study the behaviour of single cells and changed the name to cell culture. In its simplest form, cell culture involves the dispersal of cells in an artificial environment composed of nutrient solutions, a suitable surface to support the growth of cells, and ideal conditions of temperature, humidity, and gaseous atmosphere. In such a system, a researcher can measure the cells’ response to culture and genetic alterations, physiological signalling molecules, prospective drugs, interaction with other kinds of cells, carcinogenic agents and pathogens. As our ability to grow, manipulate and analyse cells in this way has developed, so has our knowledge of cell function and physiology.

Increasingly the concept of three-dimension(al) (3D) is being applied in relation to *in vitro* cell culturing. *In vivo* all tissues reside in an extracellular matrix (ECM), which comprises of a complex 3D fibrous meshwork. Additionally, depending on the cell type the 3D microenvironments differ significantly (1). For example, osteoblasts are found on the surface of bone organised in sheet-like structures as cuboidal cells; hepatocytes are packed closely together in hexagonal shaped lobules and lymphocytes are suspended freely in blood or lymph vessels (1). Today, there is increasing awareness of the drawbacks of 2D *in vitro* cell culturing and the related effect on the value of the research being performed as the dynamic range of structural organisation of various cell types *in vivo* cannot be accurately emulated using 2D cell culture technology. As a result, altered metabolism and reduced functionality are observed in 2D *in vitro* cell culture (2, 3) thus, 3D cell culture matrices also known as scaffolds were introduced to overcome these limitations (1).

An analysis of the number of publications in the field of 3D cell culture indicates an increasing interest in this field. Not surprisingly, more and more scientists are shifting their focus to cells cultured in 3D as intuitively one can appreciate that with cells, form affects function (4). Figure 1.1 provides a graphical representation of the increase in the number of publications arising from studies performed by using cells cultured in 3D.

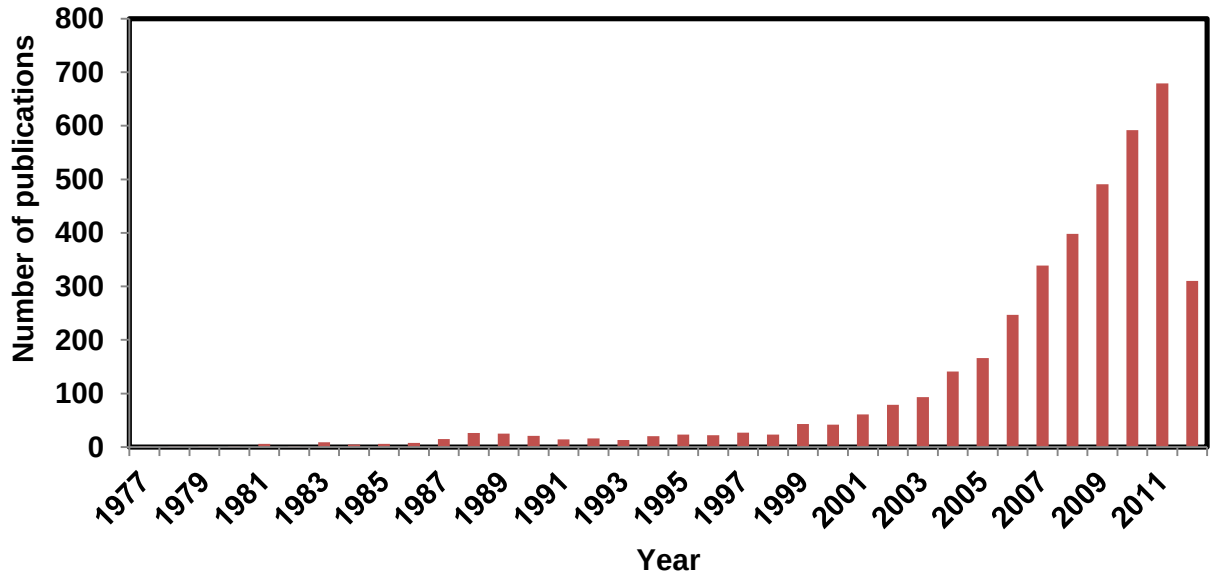

Figure 1.1. 3D cell culture publications per year (1977- June 2012). From 1977 a slow increase in the number of publications was observed in the field of 3D cell culture; a more rapid increase is observed after 2000. Source: Scopus statistics (accessed 25 June 2012).

This review looks at 3D cell culture and its growing importance in *in vitro* biology as well as the various parameters used to design and construct 3D scaffolds. Various applications of 3D cell culture in the fields of *in vitro* toxicology, anti-cancer drug screening and host-pathogen interactions are reviewed and the future of 3D cell culture is discussed.

1.1. 2D VS 3D: WHY DO WE NEED 3D?

Cells growing *in vitro* are traditionally grown on 2D surfaces of tissue culture plastic and this system has significantly improved the understanding of basic cell biology. However, 2D cell cultures bear little resemblance to the complexities of the 3D tissues from which they are derived (5). Two-dimensional monolayer cultures are convenient for routine work but impose unnatural geometric and mechanical constraints upon cells. The inherent problem with cells growing on 2D surfaces is the lack of dorsal anchorage points, which affects the balance between cells spreading or retracting. This creates an unnatural stimulatory environment for the

cells resulting in a physical imbalance, which causes the aberrant spreading of the cells (6). As such, vastly different morphology is observed for cells cultured on 2D surfaces compared to 3D as illustrated in Figure 1.2.

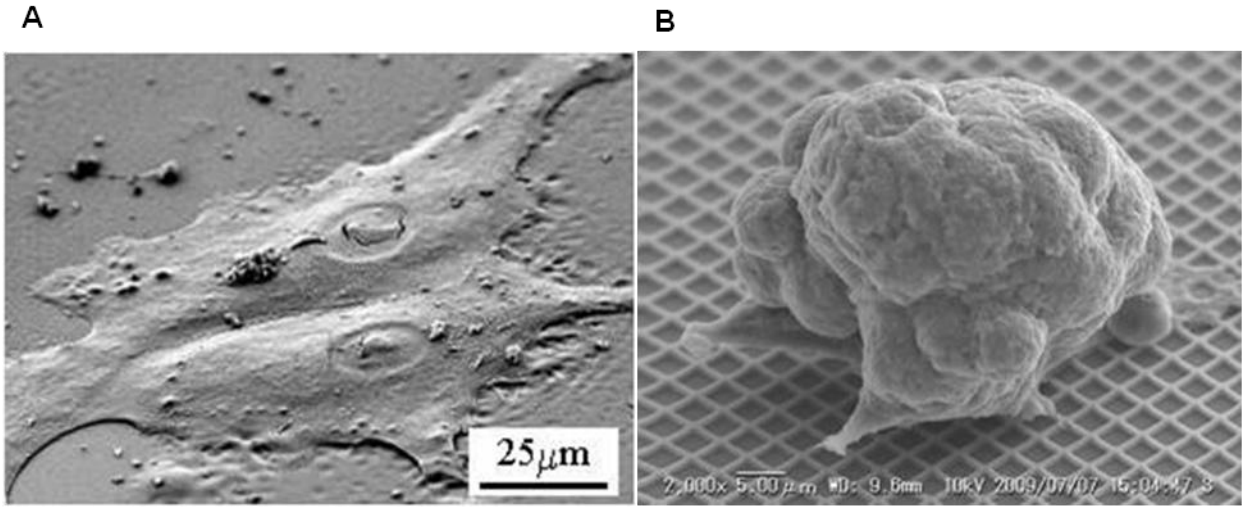

Figure 1.2. 2D and 3D cell culture morphology. **A**. Cells growing in a 2D format on the surface of tissue culture plastic show distinct flattening and spreading. **B.** Cells aggregated to form a 3D spheroid, replicating the cells' natural 3D conformation and morphology. Micrographs from (7).

Typically, cells growing in 3D are ellipsoids with dimensions of 10-30 μm whereas cells growing in 2D are flat and on average 3 μm thick (8). Cells in 3D have nearly 100% of their surface area exposed to other cells, the 3D matrix and culture medium whereas cells in 2D have approximately 50% of their surface area exposed to the cell culture media and approximately 50% exposed to the flat culture surface; only the marginal areas of the cell periphery is exposed to surrounding cells (8). Thus, 2D cultures do not mimic *in vivo* tissues as well as 3D cultures with regards to cell shape and cellular environment (9).

In addition to 3D cultures maintaining cell shape, it is also more successful in mimicking cell functionality. In native tissue, cells connect to each other as well as to the ECM to provide mechanical and biochemical signals that guide cell function. Various culture applications have shown that the growth and function of cells as multi-cellular, 3D structures are significantly different and more representative of the *in vivo* physiological state compared to 2D monolayer cultures (3, 5, 10-12). The difference lies primarily in the formation of chemical signal or molecular gradients which are important for biological differentiation, cell fate, organ development and signal transduction to name but a few. Other changes in metabolic and gene expression patterns as well as a significant reduction in the production of ECM proteins have been observed for 2D monolayer cultures (2). A change of environment for the cells, therefore, translates into a change in function and capacity for growth and differentiation. These enhanced

interactions in the 3D environment enable the cells to interpret the multitude of biochemical and physical cues from the immediate environment (6).

3D systems exhibit a much closer approximation to the *in vivo* cell microenvironment as a result of improved nutrient, oxygen and waste exchange leading to the maintenance of cell viability and function.

3D cell cultures have been used in a broad range of cell biology research, including tumour biology, cell adhesion, cell migration, metastasis, angiogenesis, epithelial morphogenesis, drug discovery applications and transport studies. Figure 1.3 illustrates several observed benefits of using 3D cell culture in place of conventional 2D cultures. Selected examples of these enhanced differences have been studied in, for example, 3D liver (6), bone (13) and neural (14) models.

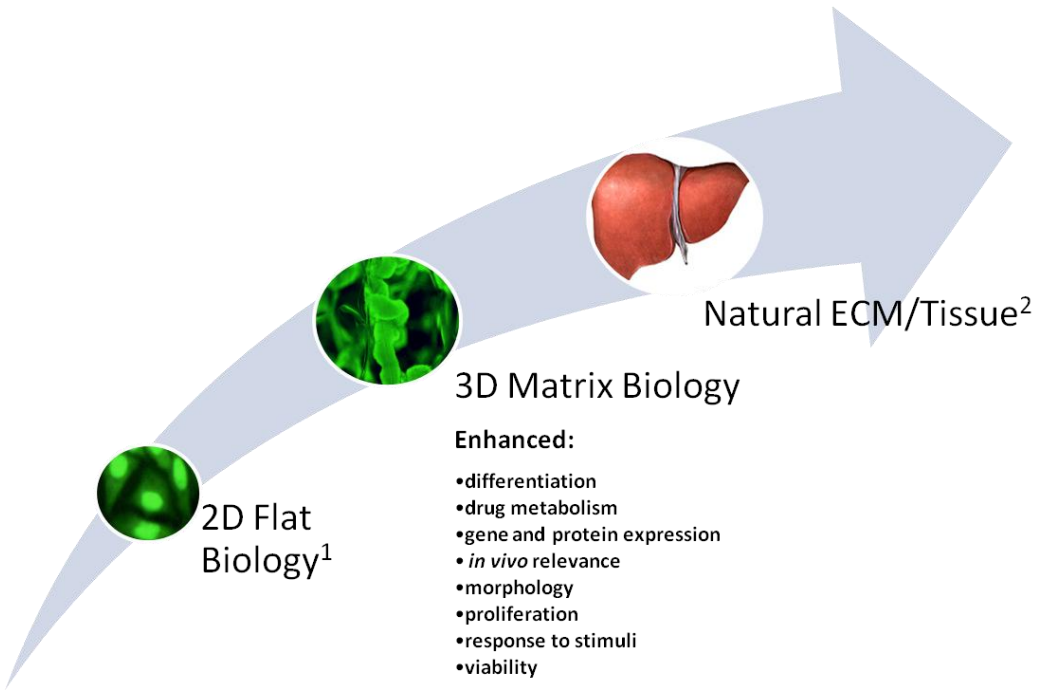

Figure 1.3. Bridging the gap between 2D cell culture and natural tissue. 3D cell cultures have demonstrated enhanced cell differentiation, drug metabolism, gene and protein expression, *in vivo* relevance, morphology, proliferation, response to stimuli and viability as compared to cells growing in 2D; [1]2D HepG2 hepatocytes (15); [2]the liver (16).

This insight into cell phenotype and function *in vitro* and the desire to have cells functioning closely to their *in vivo* counterparts has intensified the demand for the best materials able to support 3D cell growth, organisation and differentiation.

1.2. 3D SCAFFOLDS

1.2.1. Materials of choice

Material selection for 3D scaffold development is based on three fundamental criteria: the biomaterial of choice, the bulk properties of the selected material and the surface properties and/or surface modifications of the selected biomaterial as illustrated by Figure 1.4. The criteria will be different for each scaffold depending on its intended application.

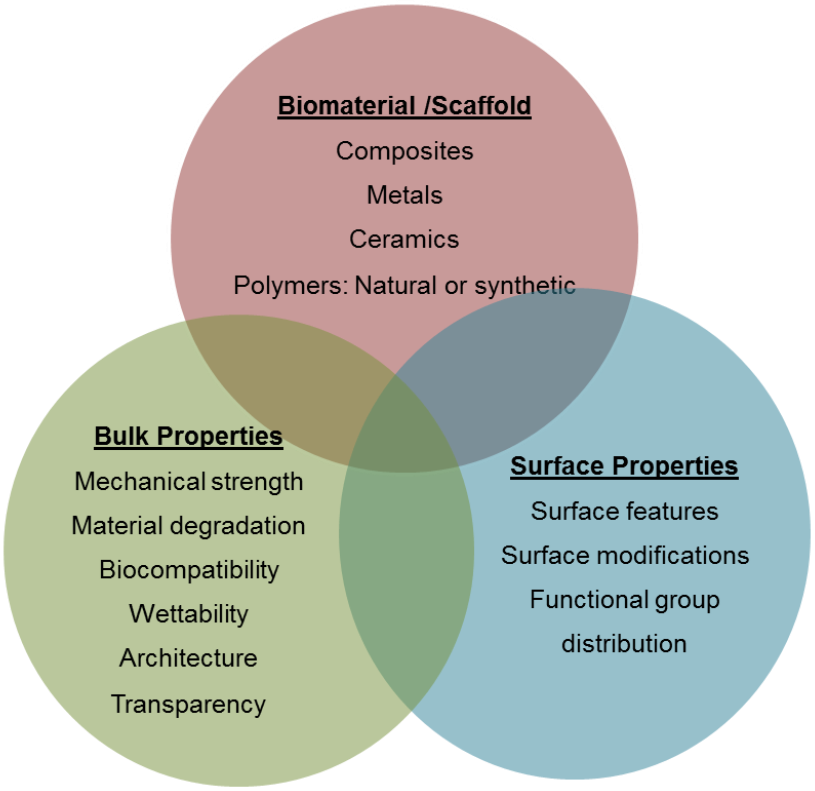

Figure 1.4. The three criteria used to design 3D scaffolds. These include the selection of the bulk material and its bulk and surface properties.

Bulk material selection is the first consideration of 3D matrix design as this will dictate various fundamental properties of the matrix, from biological effects to processability (1). For example, clinical work that requires a functioning implant may only require a temporary, biodegradable scaffold, which breaks down into metabolites without a toxic or immunogenic response. Alternatively a scaffold used as a 3D *in vitro* model needs to accurately reproduce the native tissue structure containing cells at a given stage of differentiation as well as a greater need to image these models for cell function and response (17).

Many new biomaterials have been developed to mimic the unique characteristics of natural ECM for *in vitro* cell culture applications. These biomaterials can be broadly divided into 4

categories: polymers, composites, metals and ceramics (1, 18). Among them, polymeric materials have received substantial attention because of the great flexibility in designing the composition and structure of scaffolds for specific needs (1). Polymeric 3D scaffolds can be further divided into natural and synthetic polymers as illustrated in Figure 1.5.

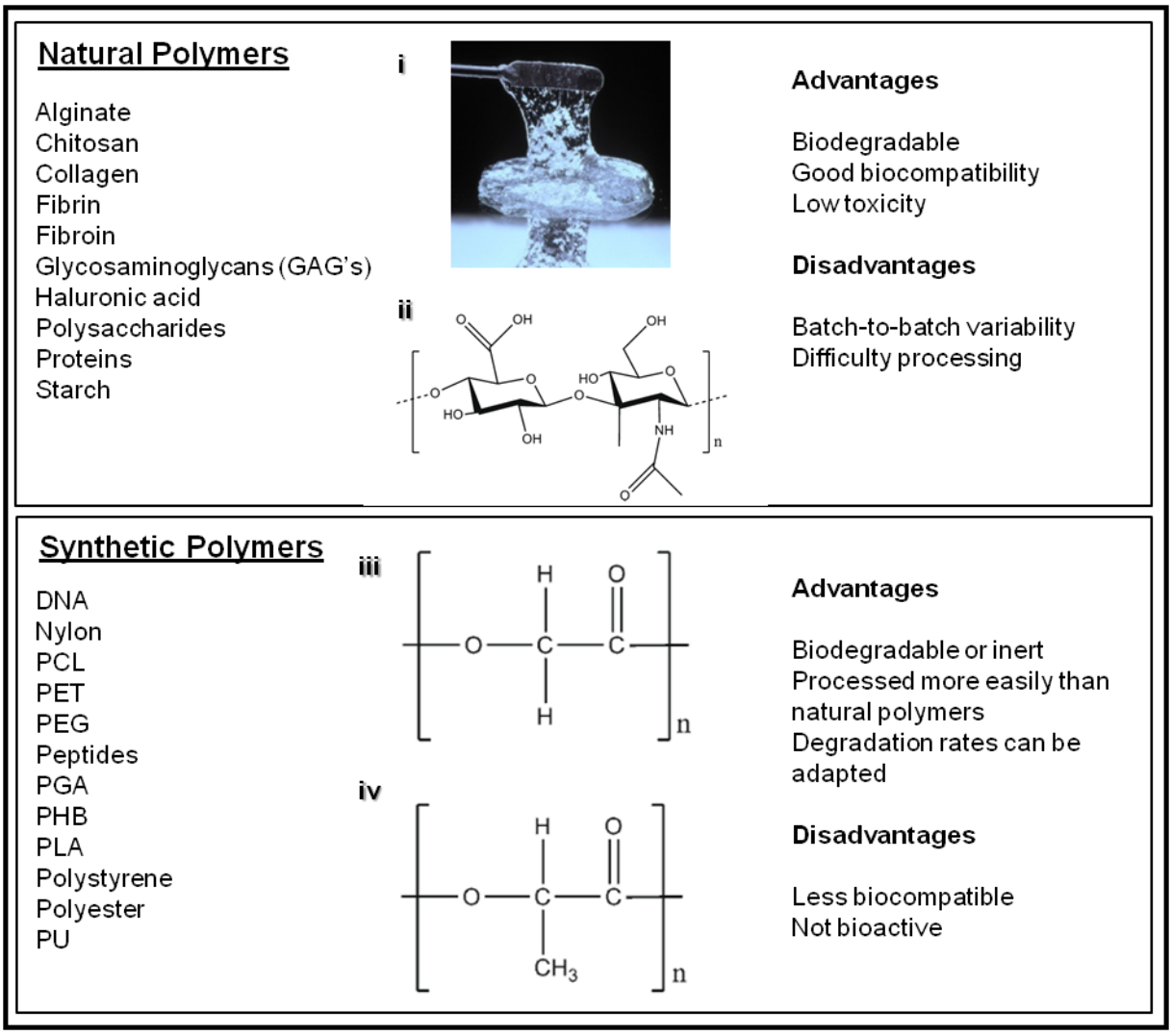

Figure 1.5. Polymer scaffolds for 3D cell culture. Polymeric scaffold are made from either natural or synthetic polymers. i-ii: An example of a natural polymer material, biodegradable haluronic acid and its chemical formula (19, 20). iii-iv: the chemical formulae of the most commonly used degradable synthetic polymers poly(glycolic acid) and poly(lactic acid) (20).

When selecting a material for scaffold fabrication various factors are important to consider. The biocompatibility of the material is an important characteristic; this is especially true if the scaffold is to be implanted into the body. The biocompatibility of the biomaterial determines the ability of the scaffold to perform its specified function without eliciting inappropriate cellular and/or host responses. Biocompatibility can be considered a graded characteristic for which the requirements change depending on the specific application of the scaffold; natural materials are typically more biocompatible than synthetic materials (1). Controlled biodegradability is an

essential requirement for implantable 3D scaffolds as the scaffolds should degrade at the rate that in-growing tissue replaces them (1). Synthetic materials generally degrade by hydrolysis (21) and natural materials generally undergo enzymatic degradation (22). Mechanical properties of the bulk materials are an important set of characteristics to consider in 3D matrix design, especially in tissue engineering for structural tissues i.e. bone. The scaffold must be able to endure sufficient loads so as not to fracture but, should not be too strong thus damaging adjacent tissue. Mechanical properties also directly shape surface mechanical properties such as surface stiffness or elasticity, which elicit clear cellular responses (1). Natural ECM is a fully hydrated gel, thus wettability is another bulk material consideration; a hydrophilic biomaterial is better at mimicking the *in vivo* aqueous environment. Transparency is another important parameter for 3D *in vitro* modelling applications where cellular behaviour within the scaffolds is to be visualised using optical, fluorescence or confocal microscopy (1).

Many types of biodegradable polymeric materials have been used for scaffold fabrication in tissue engineering applications. The gradual degradation of a biodegradable polymer is an important feature of a scaffold to aid the integration of the cells they carry with host tissues. Natural-based materials include polysaccharides (starch, alginate, chitin/chitosan, hyaluronic acid derivatives) or proteins (soy, collagen, fibrin gels, silk) and, as reinforcement, a variety of bio-fibres such as lignocellulosic natural fibres (23). Synthetic polymers include poly(lactic acid), poly(glycolic acid), poly(ε-caprolactone) (PCL) and poly(hydroxyl butyrate) (24). Many advantages and disadvantages characterise these two different classes of biodegradable polymers. The synthetic polymers have relatively good mechanical strength and their shape and degradation rate can be easily modified, but their surfaces are typically hydrophobic and lack cell-recognition signals. Naturally derived polymers have the potential advantage of biological recognition that may positively support cell adhesion and function, but they generally have poor mechanical properties (24). Synthetic polymers can be produced under controlled conditions and therefore exhibit, in general, predictable and reproducible mechanical and physical properties such as tensile strength and elastic modulus. A further advantage of synthetic polymers is the control of material impurities. Possible risks such as toxicity, immunogenicity and favouring of infections are lower for pure synthetic polymers with constituent monomeric units having a well-known and simple structure (23).

Natural and synthetic polymers exist as three main morphological formats to develop various 3D scaffolds; these are hydrogels, open- and closed cell-porous scaffolds and non-woven scaffolds.

Hydrogels have been utilised as scaffold materials for drug and growth factor delivery, engineering tissue replacements and a variety of other applications. Due to their ability to simulate the nature of most soft tissues, hydrogels are a highly attractive material for developing synthetic ECM analogs. A hydrogel is a network of polymer chains that are water-insoluble. The gels possess a high water content, facile transport of oxygen, nutrients and waste, as well as realistic transport of soluble factors (25). Furthermore, many hydrogels can be formed under mild, cyto-compatible conditions, they possess a degree of flexibility very similar to natural tissues due to their significant water content and are easily modified to possess cell adhesion ligands, desired visco-elasticity and degradability (26).

A variety of synthetic and naturally derived materials may be used to form hydrogels for tissue engineering scaffolds. Synthetic materials include poly(ethylene glycol) (PEG), macroscopically self-assembled peptides and DNA (1). DNA hydrogels are formed from branched DNA molecules with complementary sticky ends which hybridise to one another via DNA ligase to form hydrogels. Natural gels for cell culture are typically formed by proteins and ECM components (27) such as collagen (28) fibrin (29), hyaluronic acid (30), or Matrigel^{TM} (31), as well as materials derived from other biological sources such as chitosan (32), alginate (33), or silk fibrils. Since they are derived from natural sources, these gels are inherently biocompatible and bioactive (34).

Solid but highly porous scaffolds are an alternative for growing cells in 3D. The scaffolds are convenient to use, they can be manufactured in a controlled and reproducible manner, they can be moulded and shaped as needed and their structure remains stable over time. The porosity of these structures can be controlled during the production process and can, therefore, be tailored towards the types of cells to be cultured (35). Porous scaffolds fabricated from polystyrene can be used to support *in vitro* cell growth as previously described by Hayman *et al.* (35, 36) and modified by Bokhari *et al.* (5). These solid scaffolds were manufactured by polymerisation in high internal phase emulsions (HIPEs); the PolyHIPE material is characterised by its low density and open cellular construction. Bokhari *et al.* (5, 6) document the improved cell structure and function of Hep2G cells growing on this 3D culture device and an enhanced function during toxicological challenge.

Non-woven fibrous matrices are widely used scaffolds in tissue engineering (37). Many different polymers have been used to manufacture non-woven fabrics for use as scaffolds in 3D cell culture. These include polyester (38), poly(etherurethane) (39), poly(ethylene terephthalate) (PET) (37), nylon (40) and PCL (41). Non-woven fibre production is performed by the polymer of

choice being melted and extruded though capillaries which form microfibers or via electrospinning, which uses an electrical charge to draw very fine fibres (typically on the micro or nano scale) from a liquid. Non-woven materials are then formed in numerous ways including thermal bonding, needle-punching, hydro-entanglement, ultrasonic pattern bonding, chemical bonding or melt blowing (42). The advantage of using non-woven scaffolds is their large surface-area to volume ratio and the opportunity to manipulate scaffold structure and mechanical properties (43).

1.2.2. Bulk modifications

Among the scaffolds currently in use, the majority are either “simple” or “ill-defined” and many of the simple matrices are often made from only one or two components such that the physiological properties can be controlled (44). A drawback of these “simpler” polymers, however, is that cellular recognition is limited, thus restricting natural cell-matrix adhesions or abolishing them all together. These variations may impact on important cellular signalling mechanisms. On the other hand there are complex, ill-defined matrices such as Matrigel™ (44), which is a solubilised basement membrane preparation extracted from Engelbrecht-Holm-Swarm (EHS) mouse sarcoma, a tumour rich in ECM proteins. The inherent complexity of these scaffolds makes it difficult to understand cell signalling and batch-to-batch variability can negatively impact on the reproducibility of experiments (44).

“Biomimetic materials” are able to elicit specific cellular responses and direct new tissue formation mediated by biomolecular recognition (45) and modulate many aspects of synthetic matrices in an attempt to overcome the limitations of simpler polymers (46). This is achieved by altering design parameters of the selected bulk material via chemical or physical methods with bioactive molecules, such as a native long chain of ECM proteins as well as short peptides derived from intact ECM proteins that can affect specific interactions with cell receptors (45).

Bulk properties are frequently modified to replicate the multi-functional tasks of natural ECM on an artificial 3D matrix. One approach involves the incorporation of cell signalling peptides into the biomaterial such that the recognition molecules are present, not only on the surface but in the bulk of the material. One of the applications of bulk modification is the introduction of enzymatically degradable sequences, for example, photo-polymerised hydrogels containing Ala-Pro-Gly-Leu (APGL) or Val-Arg-Asn (VRN) peptides are sensitive to collagenase or plasmin degradation, respectively (45).

1.2.2. Surface modifications

Surface modification of biomaterials is a simple way to generate biomimetic materials. The surface chemical properties of a biomaterial are fundamental for dictating the adhesion and spreading of living cells (47) and one approach to endow biomaterials with bioactivity involves the incorporation of cell binding peptides into biomaterials via chemical or physiological modification to develop brand new materials (45). The incorporation of peptides into biomaterials may, for example, enhance the adhesive properties of the scaffold (48) or may render the scaffold biodegradable by specific proteases (49) such as the amino acid sequence 'A_9' for elastase mediated degradation (45).

Early work involved coating the surface of biomaterials with long chains of ECM proteins such as fibronectin, vitronectin and laminin (45). More recently, however, short peptide fragments (signalling domains of long ECM proteins) are used for surface modification. These peptides include the sequences: 'RGD' from fibronectin/vitronection for cell adhesion (48); 'IKVAV' from lamnin for neurite extension (50, 51); 'VPGIG' from elastin to enhance the elastic modulus of artificial ECM (52) or 'FHRRIKA' from the heparin binding domain to improve osteoblastic minerilization (53). These short peptide sequences have greater stability than the long chain proteins during the modification process and due to their shorter length do not form complex folded structures on the surface making them sterically available for binding (45). Additionally, the shorter peptide sequences are less expensive to produce and can be synthesised on a large scale. Surface modification peptides can be introduced through physical (54), chemical (48, 55), photochemical (56, 57), and ionic crosslinking techniques (58).

Considerations when engineering a biomimetic scaffold include the concentration and spatial distribution of the peptide or protein as well as the "spacer" for peptide modification. High peptide density may aid in cell attachment but may be antagonistic to cell migration and/or proliferation. For example, studies have shown that *in vivo,* bone scaffolds coated with the 'RGD' adhesion protein motif promotes maximal tissue growth only at intermediate values of ligand surface density (59). The spatial organisation of the RGD peptides on the surface of the biomaterials is also important as the peptides more effectively induce cell adhesion and migration when organised as clusters and not a random distribution (60, 61). The "spacer" for peptide modification is a polymer chain between the scaffold and the peptide sequence, which allows the peptide sequence to be freely extended outward of the network, increasing its availability to the target (45). Bioinert chains such as PEG with certain molecular weights (48,

57) or repetitive sequences of non-specific peptides e.g. 'GGGG' (62) have been used as spacers (45).

1.3. APPLICATIONS OF *IN VITRO* 3D CELL CULTURE

The growing body of research performed using 3D cell cultures has led to the increased use of 3D models to complement 2D cell culture and animal model studies (63). Figure 1.6 represents several applications of *in vitro* 3D models specifically in the fields of 3D cell modelling and migration, toxicology, anti-cancer drug screening and discovery, and host-pathogen interactions.

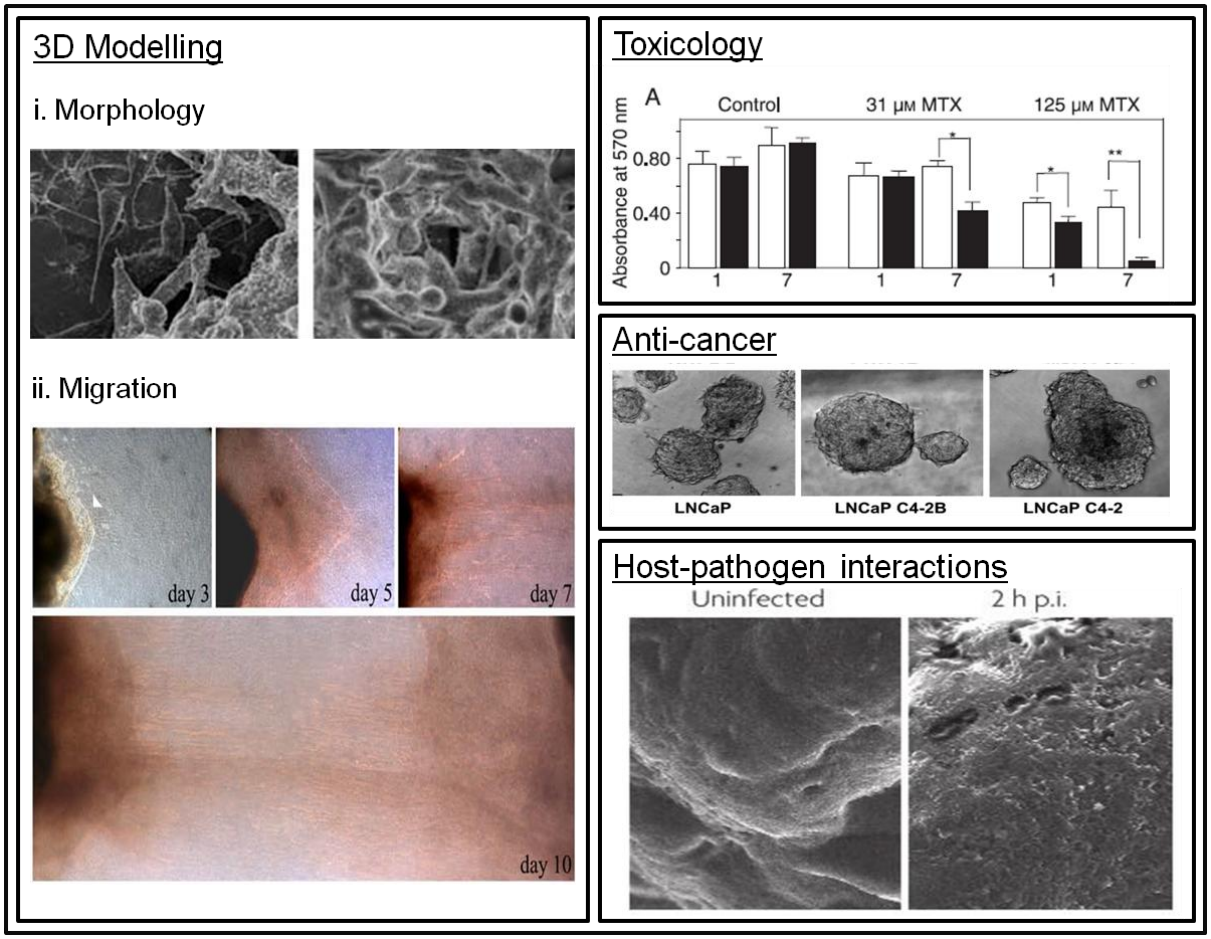

Figure 1.6. Selected *in vitro* applications of 3D cell culture. **3D Modelling: i. Morphology:** Scanning electron micrographs showing examples of HepG2 cells cultured on 2D (left panel) and 3D (right panel) polystyrene scaffolds for 7 days; SEM showed that HepG2 cells cultured on 2D surfaces were significantly more heterogeneous in structure compared to cells grown on 3D surfaces (6). **ii. Migration**: Phase contrast microscopy of the dominant axis of 3D invasion for human breast carcinoma cells explants over 10 days in a 3D collagen matrix (64). **Toxicology:** Functional activity of HepG2 cells grown on 2D (solid bars) and 3D (open bars) substrates when challenged by the cytotoxin, methotrexate (MTX) (6); **Anti-cancer:** Matrigel™ strongly supports both growth and differentiation of normal and prostate cancer spheroids which can be used to screen new chemical compounds (65) and **host-pathogen interactions:** scanning electron micrographs of Int-407 3D aggregates (control and 2 hours post infection with *Salmonella enterica* subsp. *Enterica*) (66).

The contribution made by 3D cell culture using various polymer scaffolds for *in vitro* anti-cancer drug screening, toxicology and host-pathogen interactions is further reviewed below.

1.3.1. *In vitro* anti-cancer drug screens: Tumour tissue models

State of the art *in vitro* models aim to replicate the structural, functional and mass transport properties of tumours by culturing cells in 3D (63, 67). However, the development of *in vitro* tumour tissue models has been driven by the need for better principal methods for predicting the efficacy of anti-cancer drugs (63). The development of anti-cancer drugs and therapeutics relies on screening chemical libraries of compounds using these *in vitro* tumour models to identify potential drug candidates. Current 2D cell culture models tend to suggest that anti-cancer drugs have a much higher efficacy than is subsequently observed *in vivo* and studies have indicated that the 3D architecture of tumours and the ECM all contribute to higher *in vivo* resistance to anti-cancer drugs (63).

Two 3D models exist to study/screen anti-cancer drugs. Firstly, the multicellular tumour spheroid (MCTS) model and secondly, scaffold-based cancer models. In the MCTS model, spheroids contain both surface-exposed and deeply buried cells, proliferating and non-proliferating cells and well oxygenated and hypoxic cells, much like in tumours themselves (68). In addition to oncogenic mutations, aberrant tissue organisation and signal transduction are common features in neoplasia (68) and the 3D environment in which these spheroids are grown allows a better understanding of tissue architecture and signalling in cancer. Spheroids can be studied in suspension or in hanging drops of medium, in bioreactors or in 3D matrices and are usually composed either of a homogenous cell population (valuable for high-throughput drug screening (69)) or of a multi-cellular mixture of tumour, stromal and immune cells (68). The principal limitations associated with MCTS models is the absence of vasculature, which results in lower nutrient supply to the tumour than would be observed *in vivo* and the relatively long culture period.

Scaffold-based cancer models are the second method researchers use to screen anti-cancer drugs. Various 3D scaffolds have been used to enhance our understanding of cancer biology including chitosan-alginate scaffolds which mimic the glioma microenvironment (70), and poly(lactic-co-glycolic acid) porous scaffolds that allowed the relationship between the microenvironment and tumour malignancies to be studied *in vitro* (71). Hydrogels (including Matrigel^{TM}) have been used to study breast cancer (72), Matrigel^{TM} and haluronic acid to study prostate cancer (65, 73) and alginate scaffolds were also explored as 3D models to study

cancer cell angiogenic capability (74). Cancer cells in 3D cell culture displayed high malignancies including over expression of pro-angiogenic growth factors, enhancement of tumorigenicity and insensitivity to drug treatment. For 3D cancer cell culture systems, many past studies have utilised collagen hydrogels thereby exploiting the importance of collagen as an ECM component in providing a proper platform for cell adhesion and migration (28, 75-77).

In addition to their utility in drug efficacy screens, 3D tumour models may prove useful in the development of new anticancer drugs. Both MCTS and scaffold-based models are known to better reflect *in vivo* gene and protein expression patterns and signalling pathways, making it possible to identify new cellular targets for anticancer drugs (63). It may even be possible to use 3D models for individualized therapy, that is, to predict the responsiveness of a particular patient's tumour to chemotherapy or radiotherapy (68).

1.3.2. *In vitro* toxicology models

It is estimated that for a new drug to reach the consumer market, it can cost up to $1.2 billion over a period of anywhere between 12 to 15 years. Approximately 1 in 5 drugs will fail in the human clinical trials at stage III due to hepatotoxicity (78) at an already considerable expense and cardiotoxicity is the leading cause of already approved drugs being removed from the market (63).

Friedman (79) states that "the holy grail of the [pharmaceutical] industry is to be able to predict [drug] toxicity from a cell culture." 2D cell cultures are able to predict acute hepatotoxicity (80) but cannot predict the toxicity of a drug that is metabolised *in vivo* to a toxic species - a phenomenon that cannot be adequately detected before stage III human trials (80). Due to the fact that rodents or other animals can metabolise or respond to drugs in a manner different to what humans would (81), 3D cell culture for "*in vivo*" like drug screening may help reduce the high failure rate in the development of new drugs.

The liver has many important functions in the body including albumin synthesis, fat and carbohydrate metabolism, bile secretion, elimination of harmful biochemical products such as bilirubin from the breakdown of erythrocytes and ammonia from the breakdown of proteins. Detoxification and metabolism of drugs, alcohol and environmental toxins is another important function of our liver and 3D cell culture offers opportunities for *in vivo* and *in vitro* liver toxicity models by culturing human hepatocytes (82).

Scaffold-free cellular spheroids and scaffold-based liver tissue models have been developed, and in perfused culture these systems can maintain excellent primary cell viability for two to three weeks (63). Further improvements in cell viability have been achieved by using co-culture and sandwich culture techniques, where hepatocytes are cultured with non-parenchymal cells such as epithelial cells and fibroblasts (63). 3D cell culture also enables liver specific functions, including urea and albumin production and cytochrome P450 enzyme activity, an important class of metabolic enzymes, to be maintained for up to 10 days at close to *in vivo* levels (63). Using a 3D scaffold-based model, increased cytochrome P450 enzyme CYP1A2 ethoxyresorufin to resorufin conversion activity was reported using the C3A human hepatocyte cell-line (33). An increased resistance to drug-induced apoptosis of the human hepatoma cell-line HepG2 (83) and increased albumin and urea production in hepatocytes (84) have also been observed.

In vitro cardiac tissue models have principally been developed for the study of cardiac disease and the prediction of cardiotoxicity (63). Primary cardiomyocytes would possibly offer more accurate toxicological results but, due to the logistical problems of procuring and maintaining primary tissues, 3D cardiac tissue models based on human embryonic stem cell-derived cardiomyocytes are being developed (63).

1.3.3. *In vitro* host-pathogen interactions

Despite great progress in our understanding of how pathogens successfully evade the immune system and cause disease, infectious disease still remains a huge health and economic burden particularly in the developing world, with 35% of all mortalities due to an infectious disease (85). This may potentially be reduced through the development of *in vitro* host-pathogen models that better mimic *in vivo* environments, thus, human 3D tissue models may provide superior systems for analysing the pathogenesis of disease (68).

Very little research has been published on host-pathogen interactions using 3D cell culture models, however, organotypic models cultured using the rotating wall vessel bioreactor, a cylindrical, rotating apparatus, filled with culture medium developed at the National Aeronautics and Space Administration, USA, have been used to study host pathogen interaction and are reviewed extensively by Barilla *et al.* (66). Organotypic models are formed by the natural sedimentation of cells due to gravity balanced by the bioreactor's rotation, resulting in a gentle falling of cells within the media in the chamber. The cells are attached to porous microcarrier beads or scaffolding allowing for cellular responses to chemical and molecular gradients in

three dimensions. Using this technology, host-pathogen interactions of the colon (*Salmonella enterica subsp. serovar* Typhimurium, *Cryptosporidium parvum*) (86, 87), small intestine (*S. typhimurium*, Norovirus) (88, 89), lung (*Pseudomonas aeruginosa*) (90), bladder (uropathogenic *Escherichia coli*) (91), lymphoid tissue (HIV, *Borrelia burgdorferi*) (92, 93) and lymphoblastoid (Epstein-Barr virus) (94) have been successfully studied and improved upon.

The liver pathogen hepatitis C virus (HCV) has also been studied using this technology. HCV is a liver trophic, positive-stranded RNA flavivirus causing acute and chronic hepatitis and hepatocellular carcinoma (95). HCV has infected more than 170 million people worldwide and is currently the leading cause of liver failure in the United States (96). Since its discovery in 1989, a major obstacle impeding HCV research has been the lack of robust cell culture and small animal infection models (97). Infecting cultured liver cells with the virus is extremely difficult as human hepatocytes quickly lose many of their liver-specific functions, including susceptibility to viral infection and ability to metabolise drugs, when they are cultured *in vitro*. Sainz *et al.* (97) found that when cultured in 3D, the Huh7 hepatocyte cell-line acquires a more differentiated hepatocyte-like phenotype that is highly permissive for HCV infection, thus providing an opportunity to study HCV entry and the effects of HCV infection on host cell function.

With this evidence, future engineered 3D tissues may provide a cheap *in vitro* system to replace the more expensive, and in some ways less accurate animal models, with greater control of variables for studying pathogens.

1.4. 3D CELL CULTURE: FUTURE DIRECTIONS

The motivation to mimic the 3D structure and composition of natural cellular environments has driven the rapid development of materials and fabrication techniques (1). The various 3D cell culture systems available and the major potential of these systems to improve on our knowledge of cancer biology, toxicology and how pathogens interact with their host cells have been well documented. With the demonstrated advantages of 3D cell culture, the fact remains that it is not as widely accepted as 2D cell culture due to the large deviations of structure and composition in various 3D matrices (1). Such inconsistencies prevent reproducible data and systematic analysis. Standardisation of 3D matrices should, thus, be a priority for materials scientists and biologists alike. A 3D culturing system needs to be easy to use and any technical and experimental challenges will have to be solved before 3D culture can become routine (8).

In a survey conducted by Comley in 2010 (98), participants responded with the following concerns about 3D cell culture: poor reproducibility between batches of biomimetic scaffolds, limited ability to scale up or down, difficulty in post-culturing processing and/or cell extraction from the matrix, lack of proven automated solutions, little flexibility in accommodating the many different cell-lines and types, characterising cells cultured in these geometries is difficult, poor visualisation and cost. Post-culturing processing and/or cell extraction can usually be achieved by waiting for a biodegradable scaffold to degrade or by dissolving the scaffold, usually a hydrogel, with salts. An alternative method for on-demand cell release would thus be a highly desirable feature of 3D scaffolds for *in vitro* cell analysis.

Looking to the future, optimised 3D models for toxicology screening are a priority to replace or minimise human and animal models helping to alleviate the overall cost of the drug discovery process. 3D skin models for testing pharmaceutical cosmetic compounds are also receiving wide-spread attention and currently two validated commercial skin model tissues, Episkin and EpiDerm are approved in the USA and Europe for *in vitro* corosity testing (99). Thus the investment of time towards developing and validating such *in vitro* models will likely have a significant impact on the overall success and efficiency of pharmaceutical development in the future (100).

Other niche areas set to utilise 3D cell culture lie in the areas of co-culturing, embryonic stem cell cultures (8) and 3D models for studying infectious disease (66). Co-culture of two or more cell types on scaffold systems can produce highly sophisticated models that mimic *in vivo* tissue more accurately than 2D cultures (8). Embryonic stem cells in scaffolds can promote their growth, differentiation and the formation of complex 3D structures (101); with the use of appropriate growth factors embryonic stem cells have the potential to provide an unlimited supply of pluripotent stem cells for tissue regeneration (8). As touched upon in section 1.3, 3D culture models can be a valuable tool for studying the mechanisms of infectious disease and promise to facilitate the translation of basic science from the lab to the clinic (66). Although no single *in vitro* model system will provide a complete understanding of the fundamental mechanisms governing pathogenesis, a combination of advanced cell culture models and animal models will advance our mechanistic understanding of “normal versus diseased”.

1.5. OBJECTIVES

The objective of this study was to develop a novel 3D scaffold allowing 3D cell proliferation and non-invasive cell harvesting, and to investigate the use of this technology as a tool to study host-pathogen interactions.

This study aims to address two of the issues raised above. Firstly, to address the problem of post-culturing processing and/or cell extraction from a 3D matrix by developing a scaffold capable of on-demand cell release. This system will be optimised using anchorage dependent mammalian hepatocytes; the hepatocytes will be necessary for the second aim of this thesis where the hypothesis that culturing hepatocytes in 3D would achieve superior levels of malaria sporozoite invasion *in vitro* is tested.

To address the first aim three different non-woven polymers, PP, PET and nylon were grafted with a thermoresponsive polymer poly(*N*-isopropylacrylamide) (PNIPAAm). The scaffolds were tested for their ability to permit hepatocyte proliferation and enhanced metabolic function in 3D and non-invasive cell harvesting using the various grafted scaffolds was tested (Chapter 2). Cell culture on the thermoresponsive scaffolds was scaled up using an automated cell culture device. The purpose of developing the device is for the proliferation of large numbers of cells and then, by using the thermoresponsive properties of the selected grafted non-woven scaffold, to non-invasively harvest the hepatocytes for downstream applications.

Subsequently, we aimed to test a possible application of the hepatocytes growing in 3D on the scaffolds by focussing particularly on malaria parasites as infectious agents targeting hepatocytes as a model system (Chapter 3). Mosquitoes were infected with malaria parasites (*Plasmodium falciparum*) to produce sporozoites which were harvested from their salivary glands. The ability of liver-infective sporozoites to invade hepatocytes more readily if they are growing in 3D compared to 2D was then assessed.

The knowledge gained from the study has led to the following contribution in scientific journals and conference proceedings:

Papers:

Claire L. Rossouw, Avashnee Chetty, Francis Sean Moolman, Lyn-Marie Birkholtz, Heinrich Hoppe, Dalu T. Mancama. Thermoresponsive non-woven scaffolds for “smart” 3D cell culture. Biotechnology and Bioengineering 2012; 109(8):2147–2158. (Impact Factor 3.7)

Avashnee S. Chetty, Viktoria Vargha, Arjun Maity, F. Sean Moolman, Claire Rossouw, Rajesh Anandjiwala, Lydia Boguslavsky, Dalu Mancama, and Walter W. Focke. Development of thermoresponsive PP-*g*-PNIPAAm non-woven 3D scaffold for smart cell culture using oxyfluorination-assisted graft polymerisation. Colloids and Surfaces A: Physicochemical and Engineering Aspects, 2013; 419: 37-45. (Impact Factor 2.359)

Conference proceedings:

Poster presentations:

Claire L Rossouw, Avashnee Chetty, F Sean Moolman, Lyn-Marie Birkholtz, Heinrich Hoppe, Dalu T Mancama. Optimization of an *In vitro* System to Study the Exo-erythrocytic Stage of the Human Malaria Parasite *Plasmodium falciparum*, Keystone Symposia F1 Malaria: New Approaches to Understanding Host-Parasite Interactions held at Copper Mountain Resort, Copper Mountain, Colorado, USA on Apr 11 - Apr 16, 2010.

Oral presentations:

Claire L Rossouw, Avashnee Chetty, F Sean Moolman, Lyn-Marie Birkholtz, Heinrich Hoppe, Dalu T Mancama. Thermoresponsive Non-Woven Scaffolds for “Smart” 3D Cell Culture, presented at the Emerging Researcher Symposium, CSIR, Pretoria, 13 October 2011.

Claire L Rossouw, Avashnee Chetty, F Sean Moolman, Lyn-Marie Birkholtz, Heinrich Hoppe, Dalu T Mancama. Thermoresponsive Non-Woven Scaffolds for “Smart” 3D Cell Culture, presented at the South African Society of Biochemistry and Molecular Biology Congress, Champagne Sports Resort, Kwa-Zulu Natal, 29 January – 1 February 2012.

CHAPTER 2

HEPATOCYTE PROLIFERATION AND THERMALLY INDUCED CELL DETACHMENT ON NON-WOVEN PP, PET AND NYLON THREE-DIMENSIONAL SCAFFOLDS

2.1. INTRODUCTION

Historically, anchorage-dependent cells have been cultured on flat surfaces of glass and, more recently, on modern tissue culture plastics. Once the cultured cells have reached the desired level of confluency, they are sub-cultured or passaged. The process of dissociating the cells from the surface of the tissue culture plastic typically requires the use of enzymes such trypsin, collagenase or pronase. Trypsin, an endopeptidase produced in the gastro-intestines of mammals, is most commonly used. All three enzymes act by digesting proteins, thus during the process of cell dissociation, they modify surface exposed cellular proteins and cell membrane composition. This process has a detrimental effect on the cells if one wishes to use them downstream in immunological or physiological assays. Additionally, ECM components and cell-cell junctions are also digested by trypsination.

Non-enzymatic methods for cell dissociation include solutions containing ethylenediaminetetraacetic acid (EDTA), cell scraping and cell freezing. Cell scraping is typically conducted using a rubber cell scraper in the culture flask in a pre-warmed, balanced salt solution and then dissociating the cells by gentle vortexing or trituration (repeated, gentle pipetting); this results in viable and intact cells. Freezing is another alternative for cell harvesting and although cells are not usually viable after freezing, many membrane characteristics and immunological properties remain intact. This technique is often used for harvesting protease sensitive biological materials rather than whole cells (102).

Over the past three decades, extensive research has been conducted on the use of thermoresponsive, “smart” polymers used in 2D cell culturing to allow non-invasive harvesting of cells and cell sheets. The temperature-sensitive polymer, poly(*N*-isopropylacrylamide) (PNIPAAm) has been covalently grafted onto 2D polystyrene cell culture tray surfaces to facilitate cell attachment and trypsin-independent cell release induced by a temperature change (103).

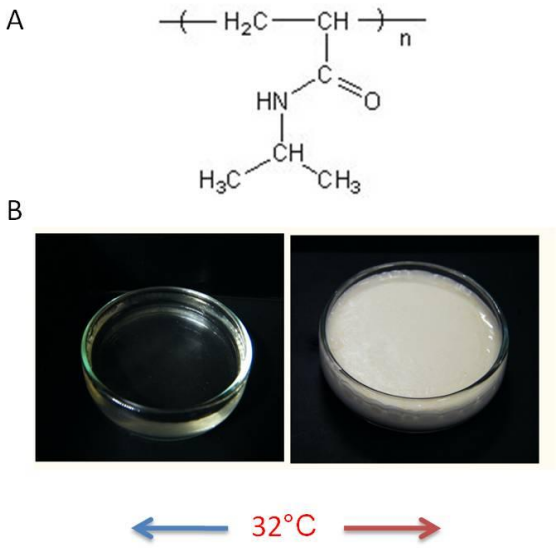

Figure 2.1. Poly(*N*-isopropyl acrylamide). **A.** The structure of the *N*-isopropyl acrylamide monomer. **B.** Poly(*N*-isopropyl acrylamide) below its lower critical solution temperature (LCST, hydrated, hydrophilic) of 32°C and above its LCST (dehydrated, hydrophobic).

PNIPAAm switches reversibly between hydrophobic and hydrophilic states when the temperature crosses its lower critical solution temperature (LCST) of approximately 32°C (Figure 2.1). This is due to the presence of the hydrophilic amide groups and the hydrophobic isopropyl group on its side chain. When the temperature is below the LCST the hydrophilic chains are hydrated and the polymer swells; as the temperature increases past the LCST, the hydrophobic interaction becomes stronger, the balance between hydrophilic/hydrophobic interactions break down, and the polymer collapses (104). This allows cells to attach onto the PNIPAAm surface at 37°C when the surface is hydrophobic while spontaneously releasing cells from the hydrophilic surface at 25°C (103). The major advantage of using PNIPAAm in 2D cell culture is that cells are non-invasively harvested as intact cell sheets with critical cell surface proteins, growth factor receptors, and cell-to-cell junction proteins remaining intact (Figure 2.2) (105-107).

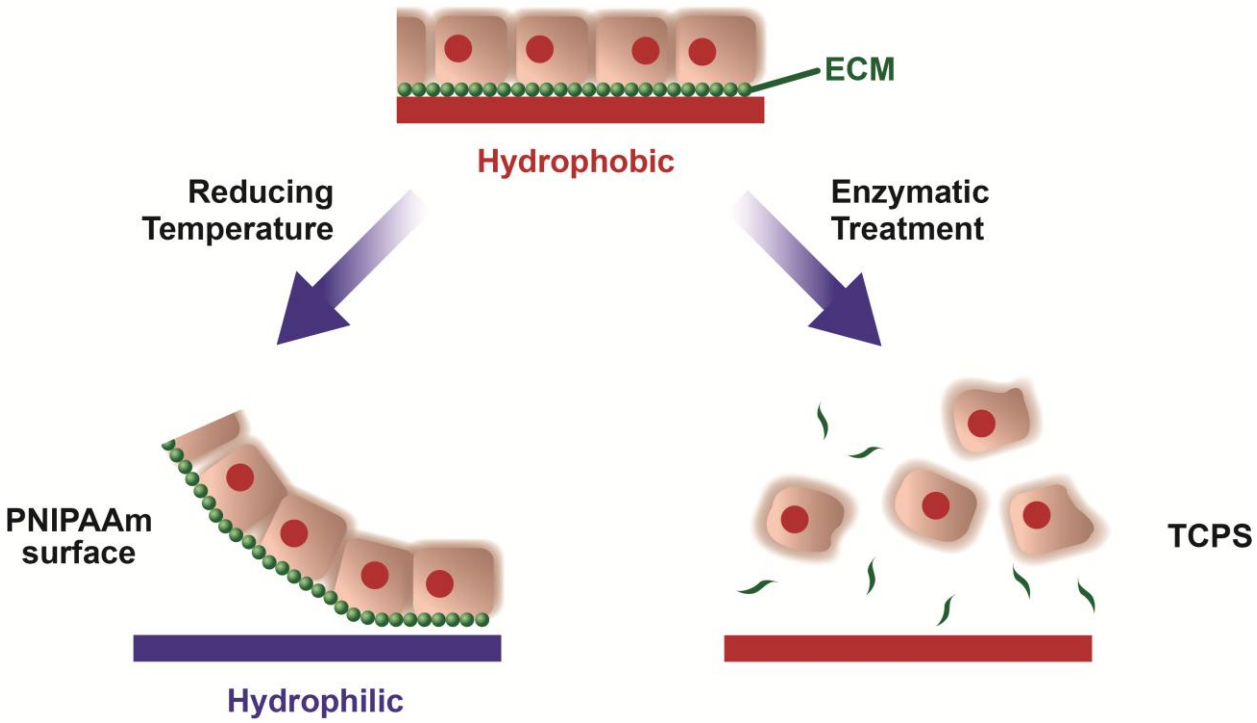

Figure 2.2. Temperature-responsive culture dishes. During cell culture, cells deposit extracellular matrix (ECM) molecules and form cell-to-cell junctions (top). Cells harvested from temperature-responsive dishes (left) are recovered as intact sheets along with their deposited ECM (green), by simply reducing the temperature. With typical proteolytic harvesting of cells growing on tissue culture poly(styrene) (TCPS) by trypsination, both ECM (green) and cell-to-cell junction proteins are degraded for cell recovery. Figure modified from (108).

As iterated in Chapter 1, although 2D cell culture is convenient for routine work, researchers are turning to 3D cell culture for more accurate, physiologically representative information on the way their cells behave and respond to stimuli. Cells can now be routinely cultured in 3D. However, the means of harvesting the cells from the scaffolds is more challenging than in 2D. To this extent, many of the 3D scaffolds currently manufactured are either bio-degradable or require the use of salts to dissolve the scaffold, which may negatively impact the cells they contain. This study, therefore, proposes combining 3D cell culture technology with the temperature responsive polymer PNIPAAm, shown to allow non-invasive cell release in 2D, to create a novel 3D scaffold for simple 3D cell culture and easy, non-invasive cell harvesting.

2.1.1. Scaffold selection

Selection of the type of 3D scaffold for grafting with PNIPAAm was thoroughly considered. In order to create a 3D matrix within which cells would be seeded and proliferate eliminated the idea of making the whole scaffold out of PNIPAAm hydrogel. Firstly, it would have been too expensive and secondly, above the polymer's LCST, it is in a dehydrated conformation that would result in the whole gel collapsing at 37°C under standard cell culture conditions (109).

Grafting PNIPAAm onto another hydrogel polymer was considered but cell retention would be problematic. A hydrogel grafted with PNIPAAm would possibly not release the cells when one lowered the temperature as the cells may become trapped in the hydrogel due to pore size distribution and tortuosity issues. Using a 'soluble' hydrogel was also considered; once the cells have populated the hydrogel it is dissolved to recover the cells. However, that would have made the 3D system not easily re-usable, and not suited for semi-continuous cell production in a bioreactor should the need arise.

Non-hydrogel scaffolds such as foams were also considered, but foams are typically very dense, with lower percentage open pores or free volume and have higher tortuosity than for example, non-woven scaffolds. This study required a scaffold where pore size distribution could be varied over a substantial range, and non-woven scaffolds allow this, whilst having a high percentage free volume. It was also thought that a non-woven scaffold would possess the best chance of releasing cells easily from the scaffold due to their interconnected open pore structure. In addition, non-woven scaffolds can be cut or rolled into any shape required.

2.1.2. Cell culture automation

In parallel to the increasing demand for cells that more closely mimic *in vivo* characteristics, bench scientists to large-scale bio-manufacturers are turning to solutions that allow hands-free growth, maintenance, and monitoring of cells for just-in-time delivery of cells into downstream applications. Furthermore, studies have shown that cells grow significantly better under dynamic culture conditions as a result of continuous cycling of nutrients as well as the removal of metabolic wastes (110). In some instances, the sheer force produced by the flowing medium can act as a mechanical stimuli signal that further promotes stem cell differentiation towards certain cell-lineages (110). The use of a non-destructive, three-dimensional automated cell culturing system could potentially revolutionize the cell culture fraternity and many large corporations such as Hamilton are investing in this technology (111).

2.1.3. Objectives

This chapter describes the biological contributions to a transdisciplinary approach to create thermoresponsive, non-woven scaffolds amenable to automated cell culturing. In this collaborative effort, scaffold selection and fabrication was performed by Rajesh Anandjiwala (Materials Science and Manufacturing (MSM), CSIR). Subsequently, in this study, these

scaffolds were grafted with PNIPAAm and tested for their ability to functionally support cell growth in 3D and allow non-invasive release of the cells from the matrix.

Based on the identified system functional requirements as well as normal bioreactor perfusion circuit design criteria, a preliminary design of an automated cell culture system was developed by Mr Kobus van Wyk of Blue Line Designs (Pretoria, South Africa). Here, the selected thermoresponsive, non-woven fabrics tested for cell growth and release were further analysed in the automated cell culture device for cell proliferation and thermally induced harvesting.

2.2. MATERIALS AND METHODS

2.2.1. Scaffold fabrication

Three different non-woven polymer scaffolds were investigated in this study as substrates for cell proliferation. Fabrics made from poly(propylene) (PP) and poly(ethylene terephthalate) (PET) non-woven polymers with a median flow pore (MFP) size of 150-300 µm were developed based on needle-punching technology. Needle-punched non-woven fabrics are created by mechanically orienting and interlocking the fibres of a spun-bonded or carded web. This mechanical interlocking is achieved with thousands of barbed felting needles repeatedly passing into and out of the web. The non-woven mats used as scaffolds were thermo-fused at 145°C (PP) and 180°C (PET), in order to prevent the dissociation of the fibres during cell culture. Nylon non-woven scaffolds with pores sizes in the range of 40-80 µm were developed due to the lower fibre density of the nylon compared to PP and PET fibres, and thermofused at 200°C. The non-woven scaffolds were manufactured and characterised by Rajesh Anandjiwala (MSM, CSIR) for porosity, water permeability, compressibility, fabric density, tensile strength, area weight and thickness (data not shown).

2.2.2. Grafting methods

PP, PET and nylon non-woven scaffolds were grafted with PNIPAAm using a solution free-radical polymerisation (SFRP) technique by Avashnee Chetty (MSM, CSIR). Briefly, the grafting methods investigated involved swelling of pure (or functionalised) non-woven scaffolds in an initiator solution followed by SFRP in an aqueous NIPAAm monomer solution with heat activation (70ºC or 50ºC). Two functionalisation methods were investigated prior to grafting, i.e. oxyfluorination (performed using a proprietary method at Pelchem (Pty) Ltd, South Africa) or a chemical oxidation method using ammonium persulphate (APS). Grafting of PNIPAAm onto the surface of the fibres was confirmed by attenuated total reflection-fourier transform infrared spectroscopy (ATR-FTIR), differential scanning calorimetry (DSC), X-ray photoelectron spectroscopy (XPS) and scanning electron microscopy (SEM). Table 2.1 summarises the various scaffolds received from MSM (CSIR) for testing.

Table 2.1. Non-woven scaffolds used for this study. The various non-woven scaffolds both control (Cont) and grafted (*g*-NIPAAm) received from Avashnee Chetty (MSM, CSIR) for cell culture testing.

Scaffold material	Scaffold name	Mean pore size (µm)
Control scaffolds (not grafted)		
Poly(propylene)	PP-Cont	127
Poly(ethylene terephthalate)	PET-Cont	127
Nylon	Nylon-Cont	40-80
Grafted scaffolds		
Poly(propylene)	PP-*g*-NIPAAm-1	127
	PP-*g*-NIPAAm-1a	127
	PP-*g*-NIPAAm-2	127
	PP-*g*-NIPAAm-A	127
	PP-*g*-NIPAAm-B	127
	PP-*g*-NIPAAm-B1	100
	PP-*g*-NIPAAm-B2	150
	PP-*g*-NIPAAm-B3	200
Poly(ethylene terephthalate)	PET-*g*-NIPAAm-2	127
	PET-*g*-NIPAAm-A	127
	PET-*g*-NIPAAm-B	127
Nylon	Nylon-*g*-NIPAAm-A	40-80
	Nylon-*g*-NIPAAm-B	40-80

A commercially available 3D culturing system, AlgiMatrix™ (Gibco®, Invitrogen Corporation, Carlsbad, California, USA), was included in the study to serve as a control in order to benchmark our scaffolds' performance for cell proliferation. The AlgiMatrix™ 3D system is based on hydrogel technology and has been used to proliferate hepatocytes (112).

2.2.3. Cell-scaffold interaction

HC04 (MRA-156, MR4, ATCC® Manassas, Virginia) and HepG2 (ATCC HB-8065™, ATCC®) hepatocyte cell-lines were used in the study. HC04 cells are human hepatocytes immortalised by Sattabongkot *et al.* from healthy, human primary liver cells to support the *in vitro* development of human malaria species (113). HepG2 cells are human hepatocellular liver carcinoma cells routinely used worldwide for *in vitro* liver studies. Scaffolds of size 5 x 5 x 3 mm were sterilised in 70% ethanol for 1 h, rinsed three times in 1x PBS and allowed to dry in a laminar hood. The scaffolds were soaked overnight at 37°C in the cell culture media specific for

the cell-line used (see below), to reduce any surface tension effects (114) as well as to ascertain whether the scaffolds had been effectively sterilised prior to seeding the non-woven scaffolds with the hepatocytes.

HepG2 cells were cultured in Dulbecco's Modified Eagle Medium (DMEM, Lonza Walkersville, Inc. Maryland, USA) with 2 mM L-glutamine and supplemented with 10% (v/v) foetal calf serum (FCS), 1% (v/v) antibiotics (10000 unit/10 mg/mL Pen/Strep, Sigma-Aldrich Chemie, GmbH, Steinheim, Germany). HC04 cells were cultured in 1:1 DMEM:Hams F12 media (Lonza) with 2 mM L-glutamine and supplemented with 10% (v/v) FCS, 100 g/mL penicillin and 10 µg/mL streptomycin (Sigma-Aldrich Chemie). The cells were cultured in T75 culture flasks (Nunc, Roskilde, Denmark) in a humidified incubator at 37°C and 5% CO_2 (standard conditions) and were subcultured once or twice a week depending on the confluence. When the cells were approximately 70% confluent they were trypsinised and resuspended at the correct concentration for seeding onto the scaffold. Briefly, the cell culture media was aspirated from the HC04 and HepG2 hepatocytes growing in culture flasks and the cell layer was gently rinsed with phosphate buffered saline (PBS, pH 7.4, Lonza Walkersville) to remove any residual cell culture media containing FCS, which inhibits the action of trypsin. The cells were covered with a thin layer (approximately 10 mL) of trypsin-versene (EDTA) (Lonza Walkersville) and incubated for 5 min at 37°C whereafter 20 mL of culture media was added to the detached cells to inactivate the trypsin. The cells were added to a 50 mL centrifuge tube (BD Biosciences, San Jose, California), pelleted by centrifugation at (50*g*) and the supernatant was aspirated off the cell pellet. Viable cells were counted using trypan blue dye exclusion on a haemocytometer and the hepatocytes were resuspended to a concentration of 1 x 10^6 cells/mL. A 200 µL aliquot of this was gently dripped onto each of the non-woven scaffolds (Table 2.1) and Algimatrix™ scaffolds in a 96-well plate, resulting in a final concentration of 2 x 10^5 cells seeded onto each scaffold.

The scaffolds were incubated at 37°C for 2 h to allow cell attachment. Thereafter, the scaffolds were removed from the 96-well tissue culture plate using sterile tweezers and individually placed into the well of a 12-well tissue culture plate with 2 mL cell-specific media and cultured in a humidified incubator under standard conditions. Scaffolds containing the HepG2 and HC04 hepatocytes were maintained in culture for a period of 21 days with media changes performed every 48 hours post inoculation (hpi).

2.2.4. Cell viability and proliferation

2.2.4.1. AlamarBlue® assay

The AlamarBlue® (AB, Invitrogen Molecular Probes®, Eugene, Oregon, USA) cell viability reagent functions as a cell health indicator. It was used to estimate the number of viable cells growing in the 3D scaffold (*in situ*) without the need to release the cells from the scaffolds (115, 116). The active ingredient is resazurin, a non-toxic cell-permeable compound; resazurin is a blue, non-fluorescent compound which, upon entering a healthy cell, is reduced to resorufin that is a red, highly fluorescent compound.

A standard curve for the AB assay was generated in order to determine cell proliferation by correlating a known cell number with the fluorescent intensity of the solution after an optimised incubation time. Standard curves were generated for both the HepG2 and HC04 cell-lines in a 24-well tissue culture plate. Cell suspensions were prepared as described in section 2.2.3 to an initial concentration of 2 x 10^6 hepatocytes/mL, from which the cells were serially diluted (1:2) in cell culture media thus generating a cell concentration range from 2 x 10^6 hepatocytes/mL to 3.125 x 10^4 hepatocytes/mL (117). The cell dilutions (500 µL each) were seeded into triplicate wells of the 24-well tissue culture plate and incubated at 37°C. After an initial 2 - 3 h attachment period, the culture media was removed and the cells were re-fed with 450 µL fresh, pre-warmed media containing 50 µL (10% v/v final concentration) AB. After an optimised incubation period of 30 min at 37°C in the dark, 100 µL of the reduced media from each well was transferred in duplicate to individual wells of a black-walled 96-well plate and the fluorescence was read using a microplate reader (Tecan GENios, Tecan Group Ltd. Männedorf, Switzerland) at excitation and emission wavelengths of 520 nm and 590 nm, respectively. The series of cultures with known cell numbers were correlated to their respective fluorescence values to generate the standard curve.

All of the scaffolds listed in Table 2.1 and the AlgiMatrix™ alginate scaffolds were subsequently seeded with either 200 µL of a 1 x 10^6 cells/mL HC04 cell suspension or with HepG2 cells. Duplicate samples of 6 independent biological replicates (n=6) were used for each scaffold. The scaffolds were placed in into the wells of low cell-binding 6-well tissue culture plates with 3 mL of specific cell culture media for each cell type. The cells on the scaffolds were maintained under standard conditions and the media changed every 48 hpi. The AB assay was performed using the scaffolds 0, 3, 7, 11, 15 and 21 days post inoculation (dpi). These time points were selected based on previous work by Mandal and Kundu (116), Shor *et al.* (115) and Wagner *et*

al. (114). The day 0 time point served as a leak test and was used to ascertain how many cells were retained in the different scaffolds after 2 hpi. Five scaffolds per treatment were then transferred individually to the wells of a 24-well tissue culture plate containing 450 µL of fresh, pre-warmed cell culture media with 50 µL (10% v/v) AB. As a negative control (blank), 10% AB was added to media without cells. The cells were re-incubated at 37°C for 30 min in the dark, after which the plates were gently swirled to ensure equal mixing of the dye solution. Subsequently, 100 µL of the media was aliquoted in duplicate into the wells of a black-walled 96-well plate and the fluorescence was read as described above. The blank values were subtracted from the fluorescent values and the data were converted to viable cell number per scaffold using the standard curve generated above. The media was removed from the wells in which the scaffolds were placed and these were frozen at -70°C for subsequent DNA quantification.

2.2.4.2. DNA quantification using Hoechst 33258

Hoechst 33258 (Invitrogen Molecular Probes®) is a bisbenzimide DNA intercalator which binds to the AT rich regions of double stranded DNA. Hoechst 33258 excites in the near UV (350 nm) and emits in the blue (450 nm) regions.

In order to generate standard curves from crude cell lysates, as outlined by Rago *et al.* (118), the HC04 and HepG2 cell-lines were seeded into 24-well tissue culture plates as described above. After cell adhesion to the tissue culture plates, the medium was removed, cells were washed once with distilled water to remove residual cell culture media as well as any dead cells and 500 µL distilled water was subsequently added. The cells were incubated at 37°C for 1 h followed by three freeze-thaw cycles at -70°C to lyse the cells. Equal volumes of the cell lysate and Hoechst 33258 (20 µg/mL) were added to a total volume of 200 µL in a black 96-well plate and mixed well. A negative control (blank) was generated by adding the working dye solution to a sample of distilled water without cells. Fluorescence was measured and the blank subtracted from the values obtained to generate a standard curve as described above.

After establishment of standard curves, DNA quantification was performed on scaffolds, frozen away from section 2.2.4.1. by the addition of 500 µL distilled water to wells containing the scaffolds and incubation at 37°C for 1 h. This was then followed by three freeze-thaw cycles to lyse the cells on the scaffolds including continuous mixing (by swirling the plates to mix the liquid content) throughout. Equal volumes of the cell lysates and Hoechst 33258 (20 µg/mL) were added in duplicate to the wells of a black-walled 96-well plate and fluorescence measured

as described above. A blank was included to serve as a negative control and was subtracted from the fluorescent values obtained. The number of viable cells per scaffold was calculated by extrapolation from the standard curve.

2.2.5. Imaging cell-scaffold-interaction

The HC04 and HepG2 cells growing on the scaffolds were visualised with fluorescent microscopy using fluorescein diacetate (FDA, Sigma-Aldrich Chemie) to monitor cell attachment and morphology on 3, 7, 11, 15 and 21 dpi (112). The non-specific esterase activity in the cytoplasm of viable cells converts non-fluorescent FDA to fluorescein, a green fluorescent dye. FDA was diluted to 5 mg/mL in acetone. Of this, a 1:250 dilution in 1x PBS was incubated with cells on the scaffolds (enough to cover the scaffold) for 5 min, after which the cells were gently rinsed in PBS to remove any residual dye. Both the top and bottom of the scaffolds were viewed for cell attachment at the days mentioned above at 40x magnification using a standard fluorescence microscope (Olympus BX41, Olympus Microscopy, Essex, UK) equipped with a 490 nm bandpass filter with a 510 nm cut-off filter for fluorescence emission.

2.2.6. Hepatocyte metabolic activity measurement

The production of albumin is often used as an indicator of hepatocyte metabolic activity. Levels of albumin were determined using the Albumine Fluorescence Assay Kit (Sigma-Aldrich Chemie) based on an established method which uses Albumin Blue (119). Albumin Blue is an anionic fluorescent probe that binds to albumin in a specific way to undergo strong fluorescent enhancement with an excitation and emission wavelength of 600 and 630 nm, respectively. Specific levels of albumin secretion were normalised to total protein levels as determined by a standard Bradford assay (5).

2.2.6.1. Bradford standard curve

The Bradford assay is a protein determination method that involves the binding of Coomassie Brilliant Blue G-250 dye to proteins (120). Upon binding to protein, the doubly protonated red cationic form detected at 470 nm is converted to a stable unprotonated blue form that is detected at 595 nm. A standard curve was created using a 250 µL microplate assay with a bovine gamma-globulin standard set with seven concentrations of gamma globulin (2, 1.5, 1, 0.75, 0.5, 0.25 and 0.125 mg/mL). Briefly, 5 µL of the gamma globulin standard dilutions and 250 µL of the 1x dye reagent were combined, in triplicate, in individual wells of a 96-well

microplate; a blank consisting of only the 1x dye reagent was also included. The samples were incubated at room temperature for 5 min and the absorbance measured at 595 nm on a Bio-Tex EL808 plate reader (A.D.P, Weltevreden Park, South Africa). The values from the blank samples were subtracted from the absorbance values and the data from the replicates were averaged. A standard curve was created by plotting the 595 nm values against their corresponding concentration in µg/mL.

2.2.6.2. Albumin assay

A standard curve was generated using the calibrator solution in the Albumine (human) Fluorescence Assay Kit (Sigma-Aldrich Chemie). The calibrator solution (human albumin stock solution) of 2000 mg/L was diluted to final concentrations of 2, 10, 30, 100 and 200 mg/mL in distilled water. Calibrator solution (35 µL of each dilution) was mixed with 175 µL assay reagent and the fluorescence was read on a microplate reader (Tecan GENios) at excitation and emission wavelengths of 600 and 630 nm, respectively.

PP-Cont (un-grafted scaffolds, mean pore size of 200 µm, Table 2.1) were punched into disks (15 mm in diameter and 3 mm thick, n=3), seeded with 1.5 x 10^6 HC04 or HepG2 hepatocytes and cultured for 21 dpi; media changes were performed every 24 h. Culture supernatant samples were collected every 24 hpi for albumin quantification on days 3, 7, 10, 14 and 21 dpi. The 24 h culture supernatant from a 70% confluent 75 cm^2 flask of HC04 or HepG2 hepatocytes was used as the 2D comparison. Sample solution (35 µL each in triplicate) was mixed with 175 µL assay reagent and the fluorescence was read on a microplate reader. The fluorescent values were blanked to a well containing only the assay reagent. Total albumin was calculated by extrapolation from the standard curve and normalised to total protein in the media as determined by the Bradford assay. Statistical analysis was performed using a paired t-test of unequal variance where $P<0.01$ and $P<0.05$.

2.2.7. Cytochrome P450 mRNA expression

PP-Cont non-woven scaffolds with a mean pore size of 200 µm, seeded with HC04 hepatocytes (as in section 2.3.3) were frozen away on 10, 14 and 21 dpi. Scaffolds seeded with HepG2 hepatocytes were frozen away at 21 dpi. To investigate the effect of scaffold pore size and/or grafting on gene expression, PP-*g*-PNIPAAm scaffolds with mean pore sizes of 100, 150, 200 µm (PP-*g*-PNIPAAM-B1, PP-*g*-PNIPAAM-B2, PP-*g*-PNIPAAM-B3; Table 2.1) were seeded with HC04 hepatocytes and frozen away on 21 dpi. Hepatocytes growing in a control 75 cm^2 cell

culture flask were harvested via trypsination at 70% confluence and frozen at -80°C until further use.

2.2.7.1. RNA extractions

RNA was isolated under RNAse-free conditions according to the method described by Clark *et al.* (121), a method that utilises both Tri-Reagent and the RNeasy kit (Qiagen GmbH, Hilden, Germany). The monophasic, phenol/guanidine thiocyanate solution in TRI-Reagent inhibits RNase activity and lyses the sample material. The homogenate is then separated into aqueous and organic phases by the addition of chloroform followed by centrifugation. RNA partitions in the aqueous phase, DNA in the interphase and proteins in the organic phase. The RNA was then precipitated from the aqueous phase with ethanol (EtOH).

Total RNA was extracted from the frozen hepatocytes on 3D scaffold and cell pellets from 2D cell culture using the RNeasy kit (Qiagen). The hepatocytes on the 3D scaffolds and the cell pellets were fully defrosted to room temperature and a volume of 600 µL RLT buffer (lysis buffer, proprietary) was added to each sample and mixed; this mixture was centrifuged at 7000*g* through a Qia-Shredder column (Qiagen) for physical cell rupture. The flow-through was collected and mixed with 600 µL TRI-reagent in a 2 mL microfuge tube. After a 5 min incubation at room temperature, 400 µL chloroform was added, vortexed and incubated at room temperature for 10 min. The samples were collected by centrifugation at 7000*g* for 15 min and the upper aqueous phase of each was transferred to a clean tube without disturbing the interphase. The RNA was precipitated with 700 µL 70% (v/v) EtOH, loaded onto RNeasy columns and centrifuged for 15 s at 8000*g*. The RNA was washed with 350 µL buffer RW1 (proprietary) followed by an on-column DNAse treatment using 27 units DNAse 1 (Qiagen) to degrade any residual contaminating DNA. The RNA was then washed again with buffers RW1 and RPE following which the column was placed in a clean microfuge tube and RNA eluted in 30 µL of RNAse-free water by incubation at room temperature for 3 min and centrifugation at 8000*g* for 1 min and stored at -70°C. The concentration of RNA was determined by measuring the absorbance at 260 nm by UV spectrophotometry with a NanoDrop-1000 (Thermo Fisher Scientific, Waltham, MA, USA). An absorbance of 1 unit at 260 nm corresponds to 40 µg/mL RNA. The ratio between the absorbance values at 260 and 280 nm gives an estimate of RNA purity; pure RNA has an A260/A280 ratio of 1.9-2.1.

2.2.7.2. cDNA synthesis and qRT-PCR

First strand cDNA was synthesised using the high-capacity RNA-to-cDNA Kit (Life Technologies Corporation, Carlsbad, CA, USA) according to kit instructions. The High Capacity RNA-to-cDNA Kit is a streamlined reverse transcription kit designed for optimum performance with the TaqMan® Gene Expression Master Mix, Power SYBR® Green PCR Master Mix and other PCR enzymes. SYBR® Green is an asymmetrical cyanine dye used to detect polymerase chain reaction (PCR) products by binding to double-stranded DNA formed during the PCR reaction. As the PCR progresses, more PCR product is created; since the SYBR® Green dye binds to all double-stranded DNA, the result is an increase in fluorescence intensity proportionate to the amount of PCR product produced.

The RNA-to-cDNA Kit includes 20x Enzyme Mix (Multiscript MuLV reverse transcriptase and RNase inhibitor protein) and 2X RT Buffer Mix (includes dNTPs). RNA (2 µg) was added to 2X RT buffer and 20x enzyme mix. The mixture was incubated at 37°C for 60 min followed by 5 min at 95°C to stop the enzymatic reaction; the cDNA was stored at -20°C.

Cytochrome P450 (CYP) 2C19, 2C9, 1A2, 2D6, 3A4 and 3A5 mRNA expression levels were determined using quantitative real time-PCR (qRT-PCR). The qRT-PCR was conducted according to manufacturer's instructions: each 20 µL reaction contained the following reagents: 1X Power SYBR® Green PCR Master Mix II (Life Technologies), 200 nM of both the forward and reverse primers, 10 µg cDNA template and the balance up to 20 µL, nuclease-free water. The thermal cycles were as follows: 95 °C for 10 min followed by 40 cycles of denaturing at 95°C for 15 s and extension at 60°C for 1 min. The samples were run and analysed on a 7500 Fast Real-Time PCR System (Applied Biosystems, Forster City, CA, USA). A melting curve analysis was performed to ensure that there was not more than one PCR product being produced in the reaction. Relative quantification of gene expression levels was determined using the comparative Ct method ($2^{-\Delta\Delta Ct}$) (122) and normalised to the β-actin gene (97). Statistical analysis was performed as described in 2.2.6.2.

2.2.8. Thermal release of cells from the various scaffolds.

Hepatocytes were cultured on all grafted scaffolds (5x5x3 mm, Table 2.1) for 10 days. The scaffold had been ethanol sterilised as outlined in section 2.2.3 and a duplicate set of scaffolds were autoclaved (121°C for 20 min); this was done to assess if the method of sterilisation had an effect on the functionality of the grafted PNIPAAm layer. On day 10 post inoculation the

scaffolds were gently rinsed in sterile PBS pre-warmed to 37°C to remove loose or dead cells and were placed (3 per well) into a 6-well plate containing 2 mL of cooled (20°C) culture media. Nine scaffolds were used per grafting and sterilisation method: three scaffolds which remained in the incubator at 37°C, three at 20°C for 1 h and three at 20°C for 2 h to establish the length of time necessary for temperature-mediated cell detachment; a maximum of 2 h was used as previously described by Canavan *et al.* (123). The cell culture plates containing the scaffolds were periodically agitated by gentle swirling during the incubations, where-after the scaffolds were removed and the released cells on the bottom of the wells photographed under bright field illumination using a 4x objective and an Olympus BX41 microscope fitted with a CC-12 digital camera (Soft Imaging Systems GbmH, Münster, Germany).

2.2.9. Automated cell culture and thermal cell release

An automated cell culture system was proposed as a means to scale up 3D cell culture on the non-woven scaffolds. High-density cell proliferation and non-invasive cell harvesting via thermal release was tested. The automated cell culture system was designed by Kobus van Wyk (Blue Line Designs, Pretoria, South Africa) in consultation with the project team at the CSIR. A prototype automated system was constructed to test the design and specific culture parameters for successful cell proliferation prior to designing a final system for testing (Figure 2.3).

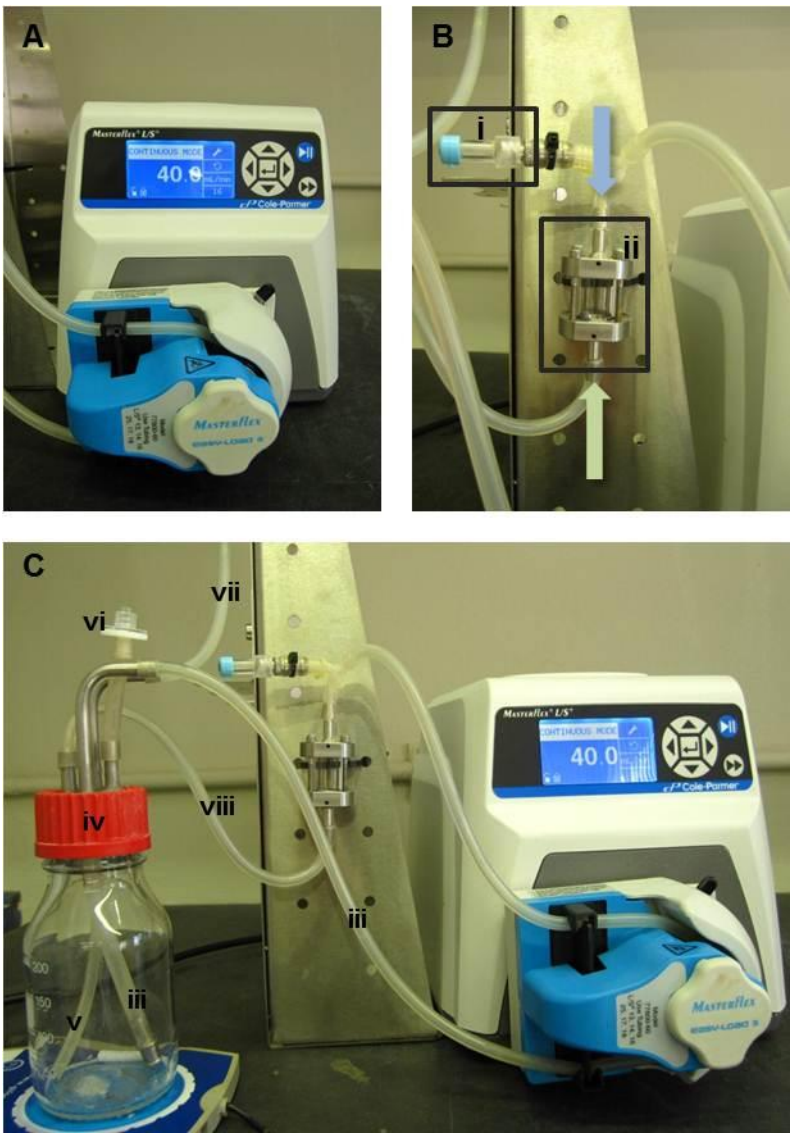

Figure 2.3. The prototype automated cell culture device. **A.** The peristaltic pump. **B. i:** sampling port; **ii:** the bioreactor (without scaffolds, 4 mL volume); blue and green arrows: media in/out. **C.** The full system, **iii:** media to bioreactor; **iv**: media reservoir; **v:** gas inlet (into the cell culture media); **vi**: gas vent; **vii**: gas line from tank; **viii:** media return line (from the bioreactor).

The prototype automated cell culture device was subsequently tested. Initial experiments were conducted in a small, prototype bioreactor as illustrated in Figure 2.3 to test the suitability of the PP non-woven scaffolds as a scaffold in the continuous perfusion system by optimising several parameters. Pure PP non-woven scaffolds with 200 µm pores were used in the initial experiments. In the final system PP-*g*-PNIPAAm-B2 (Table 2.1) was selected for use in the bioreactor; the pore size of this scaffold is on average 200 µm. This scaffold with bigger pores was selected such that when the scaffold disks are stacked onto one another there will be more space for released cells to migrate out of the bioreactor for harvesting. Scaffolds with smaller pores may become clogged with cell clusters or the cells clusters may become trapped in the fibre network.

Chapter 2: Hepatocyte proliferation and thermally induced cell detachment on 3D scaffolds

HC04 hepatocytes were seeded (1.5 million cells per non-woven disk of 15 mm diameter) into either the medium reservoir and allowed to circulate through the system where they would become entrapped within the non-woven scaffold or, in a separate experiment, cells were seeded directly into the bioreactor containing the non-woven scaffolds via the sampling port. The media in the reservoir was either static or gently stirred with a small magnetic stirrer. Typically, 3 non-woven scaffolds were used per bioreactor. Hepatocytes were seeded into the bioreactor for 3 h followed by a media change to remove and quantify any cells that had not seeded into the non-woven scaffolds. Media was perfused at 2 mL/min while seeding or allowed, in the case of direct seeding into the bioreactor, to settle without perfusion into the scaffolds.

Media perfusion (axial flow) was tested from either the bottom-up or top-down through the bioreactor containing the non-woven scaffolds to assess which method formed fewer bubbles/air locks and allowed better retention of the hepatocytes within the non-woven scaffolds. Media was perfused at 0.5 mL/min for general cell maintenance.

Media changes were performed when the glucose levels were measured using an Accu-Check Active® glucometer (Roche Pharmaceuticals, Basel, Switzerland) to be below 10 mmol/L approximately half the starting concentration. Once cell seeding and media perfusion parameters were established, cells were seeded into the bioreactor and their proliferation and viability were monitored over a set period of time. Based on the results of the prototype testing, a final system was designed, constructed and tested for its ability to cultivate large numbers of cells. Thermal release of hepatocytes on grafted scaffolds was then assessed in a basic proof-of-concept experiment.

2.3. RESULTS

2.3.1. Grafting methods

Grafting methods that yielded a layer of PNIPAAm on the surface of non-woven scaffolds as verified by Avashnee Chetty (MSM, CSIR) by ATR-FTIR, DSC, XPS and SEM are listed in Table 2.2.

Table 2.2. A summary of successful methods used to achieve a grafted layer of PNIPAAm onto the surfaces of poly(propylene) (PP), poly(ethylene terephthalate) (PET) and nylon non-woven polymers (blue shaded area). The green shaded panel represents scaffolds of different pore sizes grafted as per PP-*g*-PNIPAAm-B and the grey panel summarises the variations of grafting method PP-*g*-PNIPPAm-B to serve as additional controls for thermal release assessment.

Sample Name	Polymer properties			Grafting method				
	Polymer	MFP (µm)	Mass g/m^2	Pre-treatment	Initiator	NIPAAm added	Temp (°C)	Time (h)
PP-Cont	PP	127	-	-	-	-	-	-
PET-Cont	PET	127	-	-	-	-	-	-
Nylon-Cont	Nylon	40-80	-	-	-	-	-	-
PP-*g*-PNIPAAm-1	PP	127	-	APS[1]	Ceric ion/nitric acid	✓	70	24
PP-*g*-PNIPAAm-1a	PP	127	-	APS	Ceric ion/nitric acid	✓	50	24
PP-*g*-PNIPAAm-2	PP	127	-	-	APS	✓	70	24
PET-*g*-PNIPAAm-2	PET	127	-	-	APS	✓	70	8
PP-*g*-PNIPAAm-A	PP	127	-	Oxyfluorination[2]	APS	✓	*70*	7
PP-*g*-PNIPAAm-B (Test 1)	PP	127	-	Oxyfluorination[3]	APS	✓	*70*	7
PET-*g*-PNIPAAm-A	PET	127	-	Oxyfluorination[2]	APS	✓	70	7
PET-*g*-PNIPAAm-B	PET	127	-	Oxyfluorination[3]	APS	✓	70	7
Nylon-*g*-PNIPAAm-A	Nylon	40-80	-	Oxyfluorination[2]	APS	✓	70	7
Nylon-*g*-PNIPAAm-B	Nylon	40-80	-	Oxyfluorination[3]	APS	✓	70	7
PP-*g*-PNIPAAm-B1	PP	100	200	Oxyfluorination[3]	APS	✓	70	7
PP-*g*-PNIPAAm-B2	PP	150	100	Oxyfluorination[3]	APS	✓	70	7
PP-*g*-PNIPAAm-B3	PP	200	95	Oxyfluorination[3]	APS	✓	70	7
Test 2	PP	127		Oxyfluorination[3]	APS	x	70	7
Test 3	PP	127		-	APS	✓	70	7
Test 4	PP	127		-	APS	x	70	7

[1]Ammonium Persulphate
[2]Dynamic oxyfluorination 5:95 F:N_2, 3 min exposure
[3]Static oxyfluorination 20:80 F:N2 and other gas mixtures, 30 min exposure

2.3.2. Cell viability and proliferation

Since quantifying the number of viable cells in a 3D scaffold is not possible by conventional cell counting methods, the AB assay was used to estimate the number of the cells growing on the scaffold without prior detachment from the scaffold.

The AB assay was performed to determine the number of viable HC04 and HepG2 hepatocytes within the various grafted and control scaffolds. Cell numbers were extrapolated from standard curves generated from serial dilutions of cells in a 24-well plate (Figure 2.4).

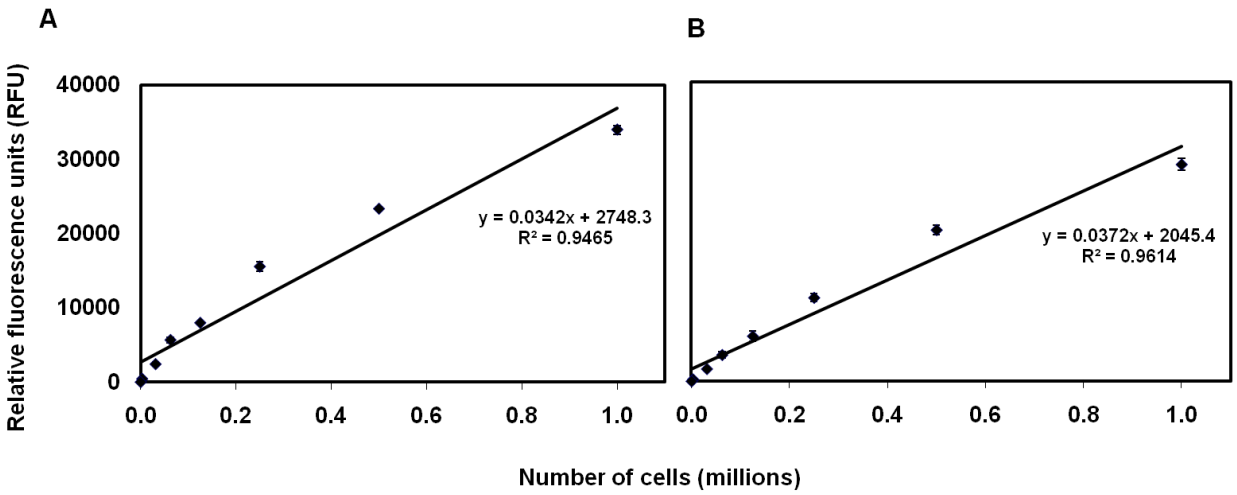

Figure 2.4. AlamarBlue® assay standard curves for HC04 (A) and HepG2 (B) hepatocytes. The standard curves were generated from a pre-determined number of hepatocytes growing in a 24-well tissue culture plate by a 30 min incubation with 10% (v/v) AlamarBlue®. The data are presented as the average of three replicates per cell number plotted against fluorescence ± standard deviation.

Cells proliferated efficiently as evident from cell number increases over time on all the 3D control and grafted scaffolds (Figure 2.5). The HC04 hepatocytes grown on the PP scaffolds had a first maximum on day 7 with a general decline in numbers on day 11, but cell numbers were observed to recover thereafter. This phenomenon was noted on all scaffolds regardless of the cell-line except in a few instances e.g. HC04 cells growing in the Algimatrix™ alginate scaffolds and grafted nylon scaffolds. On the PP scaffolds, the PP-*g*-PNIPAAm-1a and PP-*g*-PNIPAAm-B supported the highest number of HC04 hepatocytes; these results were comparable to the proliferation seen within the Algimatrix™ scaffold. HepG2 hepatocytes growing on PP scaffolds were best supported by PP-*g*-PNIPAAm-1, PP-*g*-PNIPAAm-1a and PP-*g*-PNIPAAm-B; these scaffolds supported more cells than the Algimatrix™ scaffold. HC04 and HepG2 hepatocytes growing on the PET scaffolds were, by comparison, better supported by the Algimatrix™ scaffold as well as the control scaffold. HepG2 hepatocytes did not proliferate well on the grafted PET scaffolds. Both cell-lines grew well on the nylon scaffolds.

HC04 hepatocytes grown on Nylon-*g*-PNIPAAm-B matched the proliferation trend seen for the Algimatrix™ scaffold and, together with Nylon-cont, surpassed the Algimatrix™ proliferation when supporting HepG2 hepatocytes.

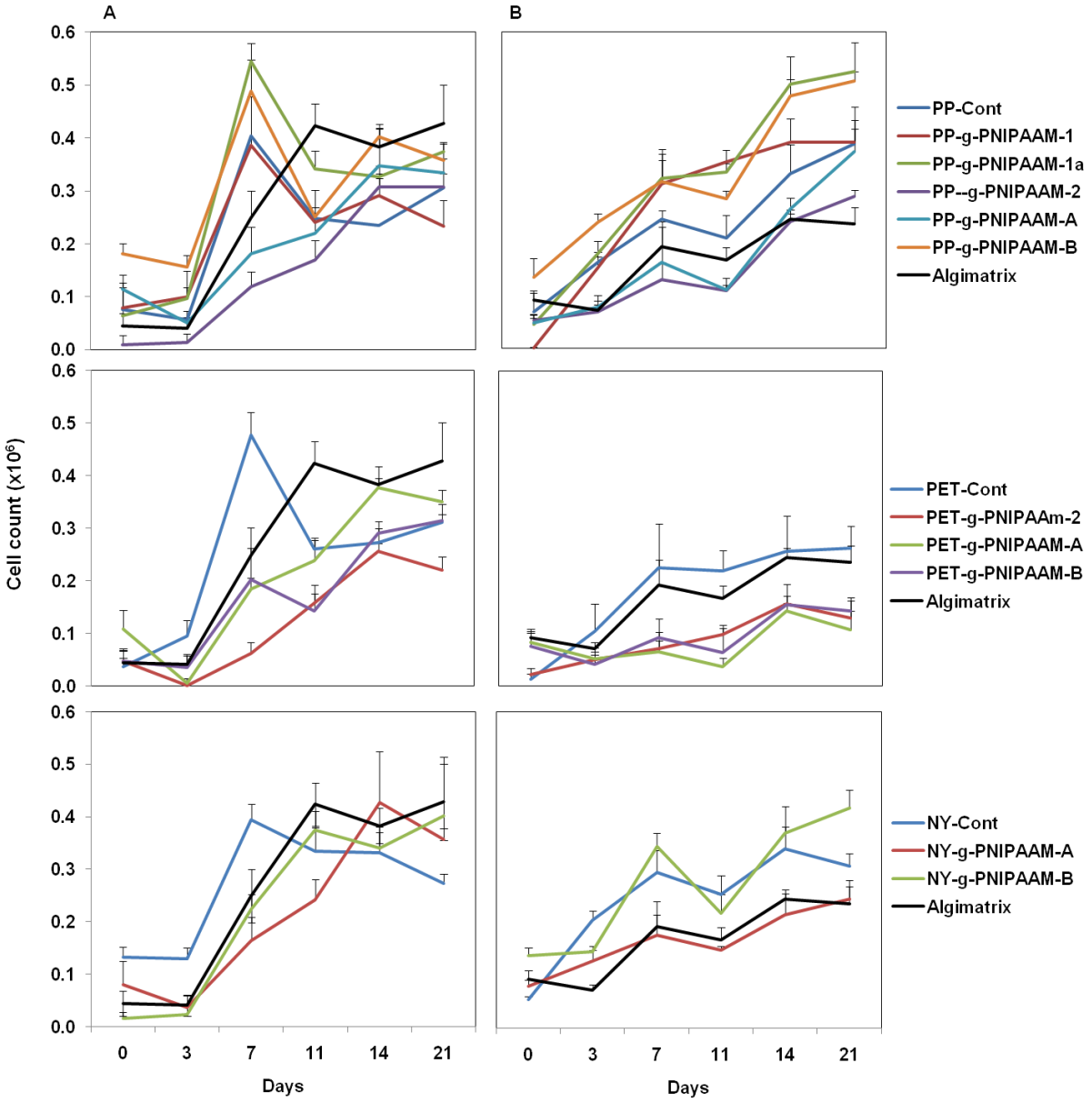

Figure 2.5. Cell proliferation on poly(propylene) (PP), poly(ethylene terephthalate) (PET) and nylon non-woven scaffolds, determined by the AB assay. HC04 (A) and HepG2 (B) hepatocyte cell-lines growing on different scaffolds as summarised in Table 2.2. were assayed for viability and proliferation using AB on 0 (hepatocyte retention in the scaffolds), 3, 7, 11, 14 and 21 dpi and are represented as number of cells. The data are presented as the average of five individual scaffolds ± standard deviation.

Total DNA content of the cells was measured on 3, 7, 11, 14 and 21 dpi as an alternative means to measure cell proliferation on the 3D scaffolds; cell numbers were extrapolated from a standard curve generated for Hoechst 33258 (Figure 2.6).

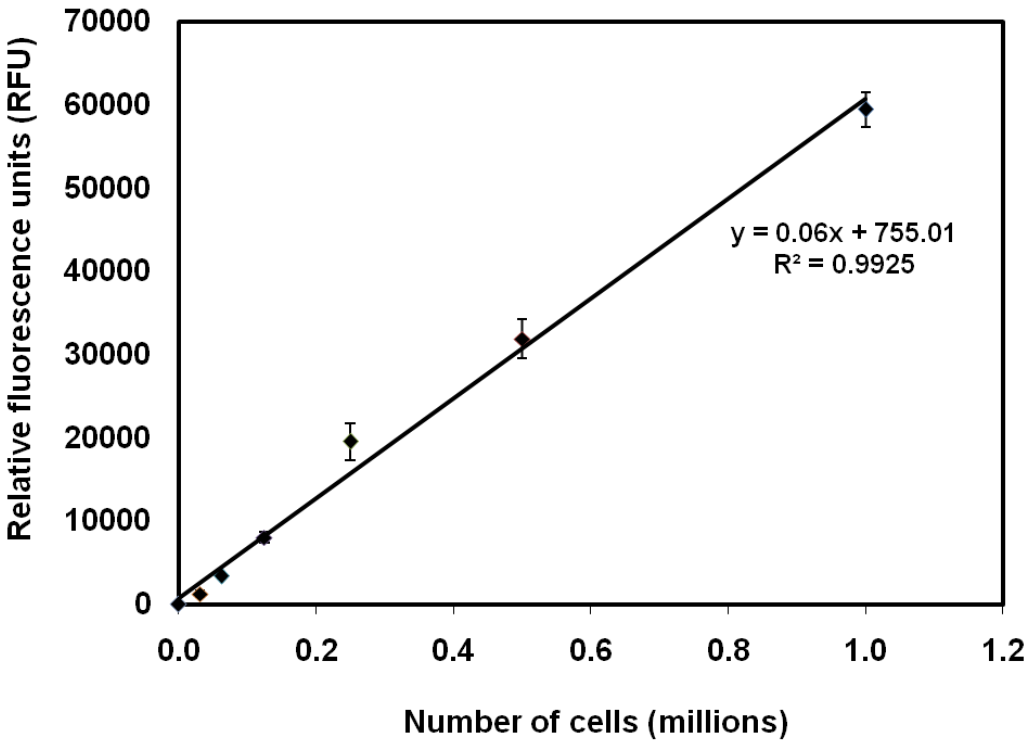

Figure 2.6. Hoechst 33258 standard curve using crude cell lysates as described by Rago *et al.* (118). A standard curve from crude cell lysates was generated from a predetermined number of hepatocytes (HC04 or HepG2) growing in a 24-well tissue culture plate with Hoechst 33258 at a final concentration of 10 µg/mL. The standard curve from HC04 hepatocytes is illustrated. The data are presented as the average of three replicates per cell number plotted against fluorescence ± standard deviation.

Cell numbers derived from the DNA quantification results indicated that up to 5-fold more HC04 hepatocytes were growing on the scaffolds than suggested by the AB assay (Figure 2.6). The HC04 hepatocytes growing on the PP, PET and nylon scaffolds showed an approximate linear increase in numbers over time; however, there was not one scaffold that stood out as being far superior (or inferior) to the control scaffolds and Algimatrix™. Overall, DNA quantification-derived cell numbers of the HepG2 hepatocytes on the scaffolds more closely resembled the trend observed in the AB assay. As with the HC04 cells, no difference in growth on the grafted scaffolds as compared to the control scaffolds and Algimatrix™ was observed (Figure 2.7). A general decrease in HepG2 DNA levels was seen on day 11 on the PET and nylon scaffolds and on day 14 on the PP scaffolds after which DNA levels recovered or remained relatively constant.

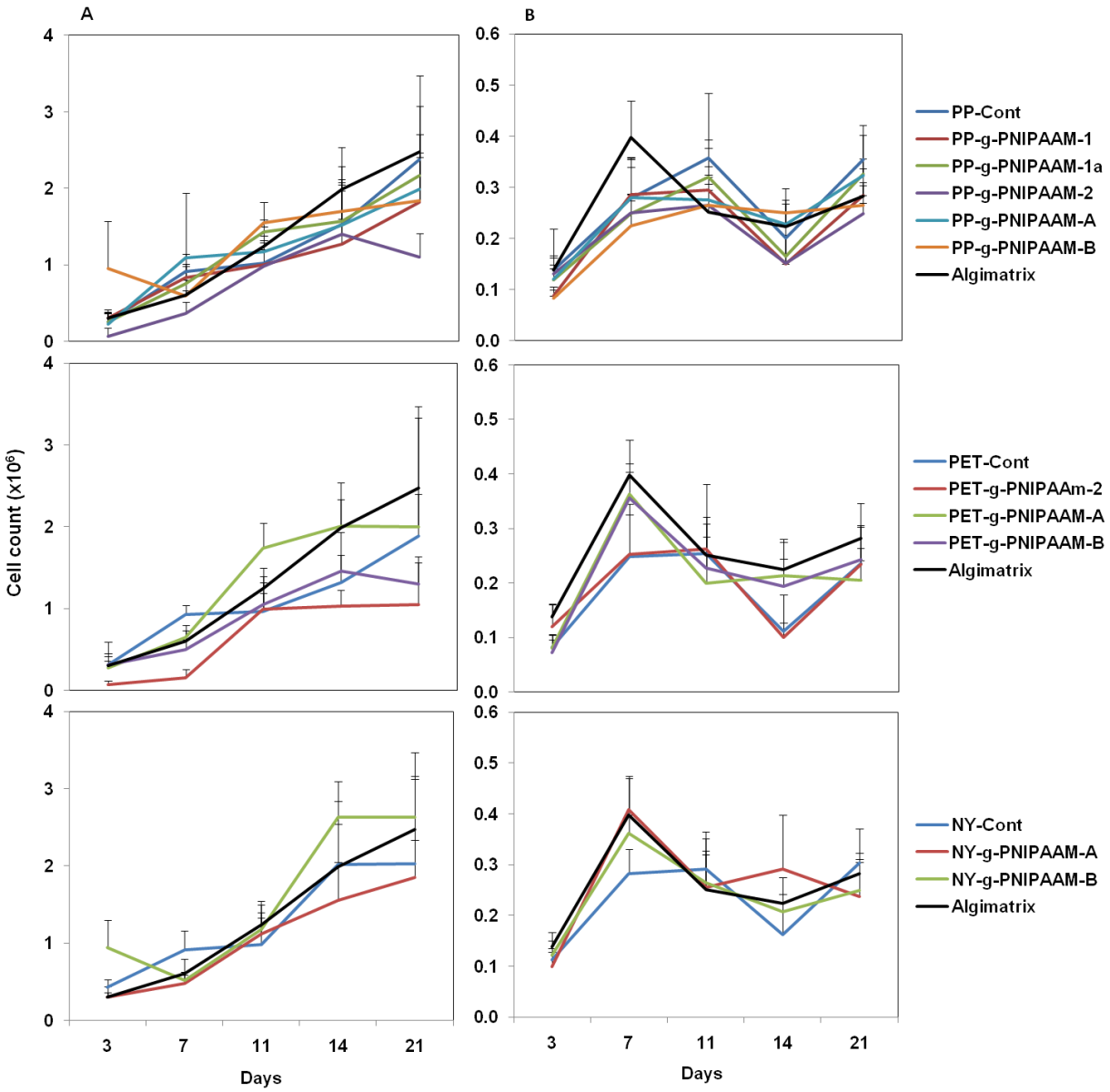

Figure 2.7. Cell proliferation of hepatocytes growing on poly(propylene) (PP), poly(ethylene terephthalate) (PET) and nylon non-woven scaffolds, determined by DNA staining. The proliferation of HC04 (A) and HepG2 (B) hepatocyte cell-lines growing on different scaffolds (as summarised in Table 2.2) was calculated using Hoechst 33258 fluorescence on 3, 7, 11, 14 and 21 dpi. The data are presented as the average of five individual scaffolds ± standard deviation.

2.3.3. Fluorescence microscopy and albumin quantification

As an indicator of cell viability and functionality, fluorescence microscopy and albumin production was used to determine cell morphology and metabolic activity. Representative cell morphology and proliferation of the HC04 and HepG2 hepatocytes on the PP-*g*-PNIPAAm-B scaffold over 21 days is shown in Figure 2.8. HC04 hepatocytes grow along the non-woven fibres and at later time points form large cell clusters whereas the HepG2 hepatocytes have a greater tendency to form spheroids soon after seeding. The large cell clusters and spheroids

are a desirable morphology for certain 3D cell culture applications as spheroids are highly metabolically active and physiologically representative cell formations.

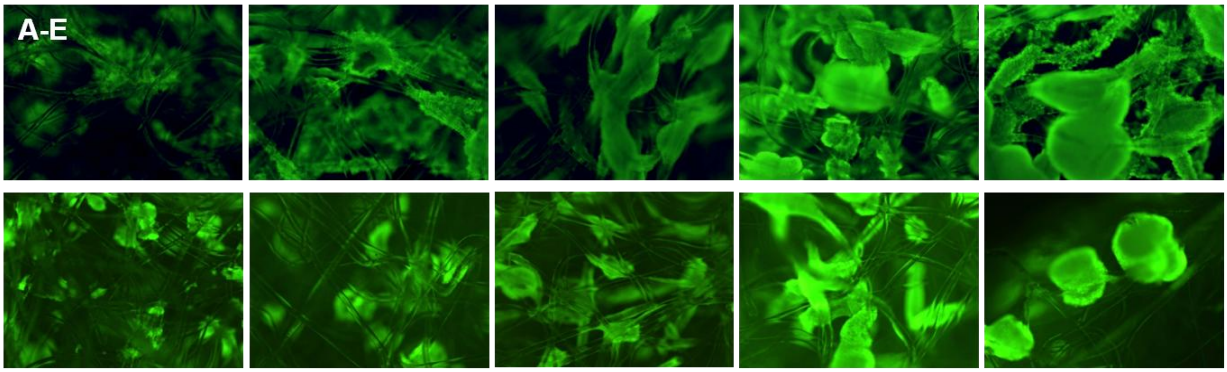

Figure 2.8. Representative fluorescence micrographs of HC04 (top panel) and HepG2 (bottom panel) hepatocytes growing on the PP-*g*-PNIPAAm-B scaffold after 3, 7, 11, 14 and 21 dpi (A-E). Cells were stained with Fluorescein Diacetate (FDA) and visualisation was performed at 40x magnification using a standard fluorescence microscope (Olympus BX41) equipped with a 490 nm bandpass filter with a 510 nm cut-off filter for fluorescence emission.

Hepatocyte metabolic activity was measured by quantifying albumin production (indicating active protein biosynthesis) of hepatocytes grown on pure PP scaffolds (mean pore size of 200 µm). Albumin production in 2D and 3D cultures was quantified on 3, 5, 7, 10, 14 and 21 dpi and normalised to total protein. Fluorescent values obtained in each assay were plotted against their respective standard curves (Figure 2.9) and the data were expressed as expression fold change as compared to the 2D values.

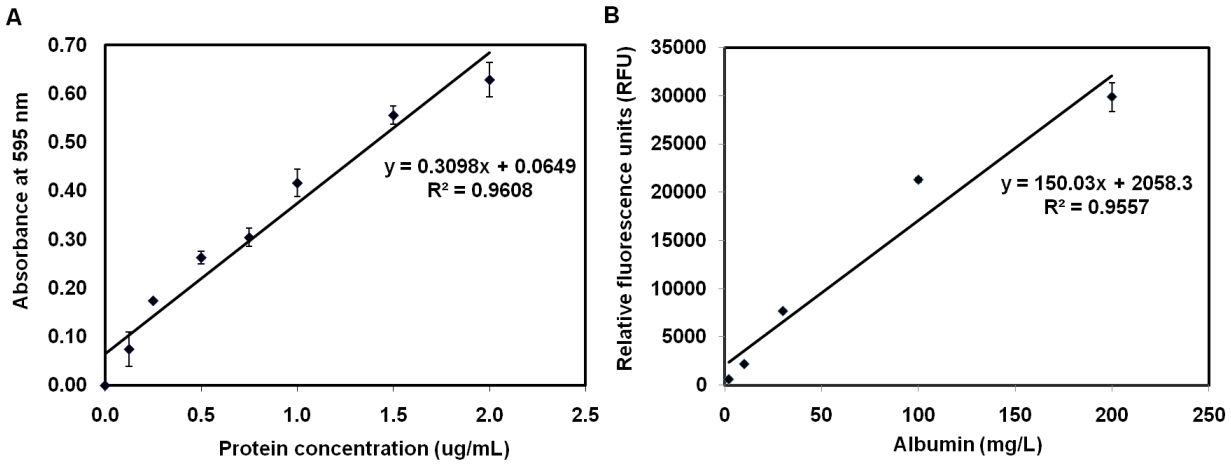

Figure 2.9. Bradford assay and albumin standard curves. **A.** The Bradford standard curve was performed as a 250 µL microplate assay using the bovine gamma-globulin standard set with seven concentrations of gamma globulin: 2, 1.5, 1, 1.75, 0.5, 0.25 and 0.125 µg/mL. The data are presented as the average of three replicates per concentration plotted against absorbance at 595 nm ± standard deviation. **B.** The albumin standard curve was generated using the calibrator solution in the Albumine Fluorescence Assay Kit (Sigma-Aldrich). The albumin stock solution was diluted to final concentrations of 2, 10, 30, 100 and 200 mg/mL and the fluorescence was read at excitation and emission wavelengths of 600 and 630 nm respectively. The data are presented as the average of three replicates per concentration plotted against fluorescence ± standard deviation.

Albumin production of hepatocytes cultured in 3D was compared to albumin production in hepatocytes cultured in 2D.

HC04 hepatocytes secreted, on average, twice the amount of albumin when cultured on the 3D PP non-grafted scaffolds as compared to the 2D monolayer, indicating that cells growing in the 3D context were more metabolically active than their 2D counterparts (Figure 2.10). In contrast, the HepG2 cells took longer to exceed the levels of albumin secreted by the 2D monolayer, achieving a maximum 1.5-fold increase at 21 dpi.

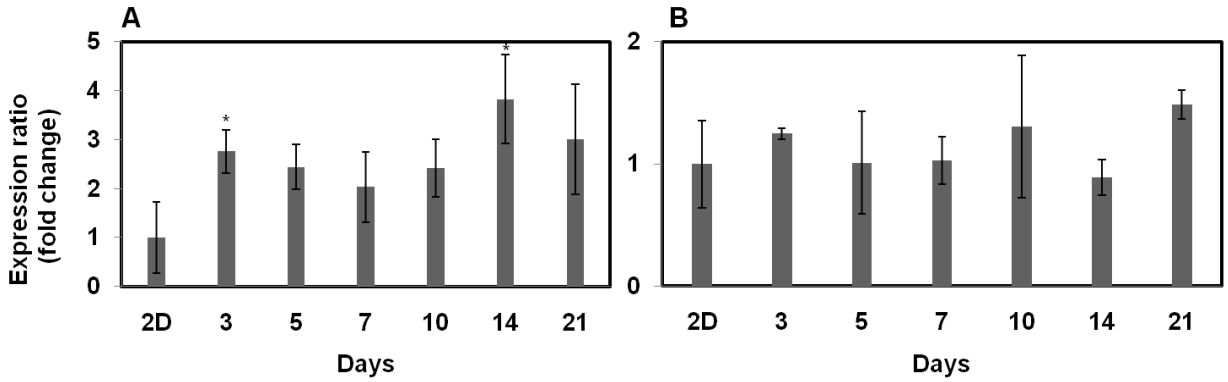

Figure 2.10. Relative albumin secretion in HC04 (A) and HepG2 (B) hepatocytes growing on a 3D non-woven control scaffold (pore size 200 µm). Known quantities of human albumin were used to establish a calibration curve and the quantities of albumin secreted into culture media were normalised to total protein levels in the media as determined by the Bradford assay to correct for differences in cell numbers. The data are indicated as fold change of cells growing in 3D compared to cells grown as a 2D monolayer. Data are the average of three individual scaffolds ± standard deviations; * indicates significance at $P<0.05$ (student T-test).

2.3.4. Cytochrome P450 mRNA expression

CYP gene expression was monitored using qRT-PCR in HC04 cells grown on PP-Cont non-woven scaffolds modified to have a mean pore size of 200 µm (Figure 2.11 A) and compared to the CYP gene expression in hepatocytes growing in 2D in order to compare cell metabolic function. CYP genes code for enzymes that are involved in the oxidation of organic compounds to enhance excretion and play a major role in the metabolism of drugs and xenobiotics. It has been hypothesised that hepatocytes growing in 3D may display enhanced drug metabolism due to higher levels of endogenous CYP gene expression.

Primers designed for CYP gene expression analysis are listed in Table 2.3. The expression of these genes was normalised against that of β-actin as housekeeping gene. Primers were designed using Primer3 (124).

Table 2.3. Primer sequences for cytochrome qRT-PCR.

Gene	Accession number	Forward primer (5'→3')	Reverse Primer (5'→3')	Product length (bp)
CYP2C19	NM_000769.1	TGCACGAGGTCCAGAGATACAT	TTTAACGTCACAGGTCACTGCAT	71
CYP2C9	NM_000771.3	CCTGACTTCTGTGCTACATGACAA	ATTGCCACCTTCATCCAGAAA	85
CYP1A2	NM_000761.3	CTCCTCCTTCTTGCCCTTCA	GTTTACGAAGACACAGCATTTCTTG	97
CYP2D6	NM_001025161.1	TGTGCCCATCACCCAGATC	TCACGTTGCTCACGGCTTT	95
CYP3A4	NM_017460.3	GCAAGAAGAACAAGGACAACATAGAT	GCAAACCTCATGCCAATGC	85
CYP3A5	NM_000777.2	TGGGACCCGTACACATGGA	GACAAAACATTTCCCAACAAAGG	81
β-actin	NNM_001101	CCTGGCACCCAGCACAAT	GCCGATCCACACGGAGTACT	70

Expression levels of *CYP2C9, 2C19, 3A4* and *3A5* increased over time as the 3D scaffold became more densely populated, with *CYP1A2, 2C19* and *3A5*, up-regulated compared to the 2D control. *CYP2C19* for example, was expressed 79-times higher (significance $P<0.05$) in the cells growing on the scaffold compared to the 2D control, using β-actin as the internal qRT-PCR reference control for cell numbers. For two genes, namely *CYP2C9* and *3A4*, levels of gene expression remained equal to, or below, that seen for HC04 cells grown in 2D. This experiment revealed the highest level of CYP expression to be at 21 dpi (Figure 2.11 A). On this basis, similar quantification of the selected CYP genes was performed at 21 dpi using HepG2 hepatocytes grown on the scaffolds.

qRT-PCR revealed that CYP genes *1A2, 2C9* and *2C19* were up-regulated at day 21 while the expression levels of CYP genes *3A4* and *3A5* were less than that of the 2D control. *CYP2D6* was expressed at a similar level to that of the 2D control (Figure 2.11 B). When the CYP gene expression levels were assessed on scaffolds of different mean pore size that had been grafted (using grafting method of scaffold PP-*g*-PNIPAAm-B) it was noted that gene expression was increased for all the selected genes as depicted in Figure 2.11 C. No specific conclusion can be drawn as to which pore size performed the best; however, the scaffolds PP-*g*-PNIPAAm-B1 (100 µm mean pore size) and PP-*g*-PNIPAAm-B2 (150 µm mean pore size) appeared to support higher levels of gene expression than PP-*g*-PNIPAAm-B3 (200 µm mean pore size).

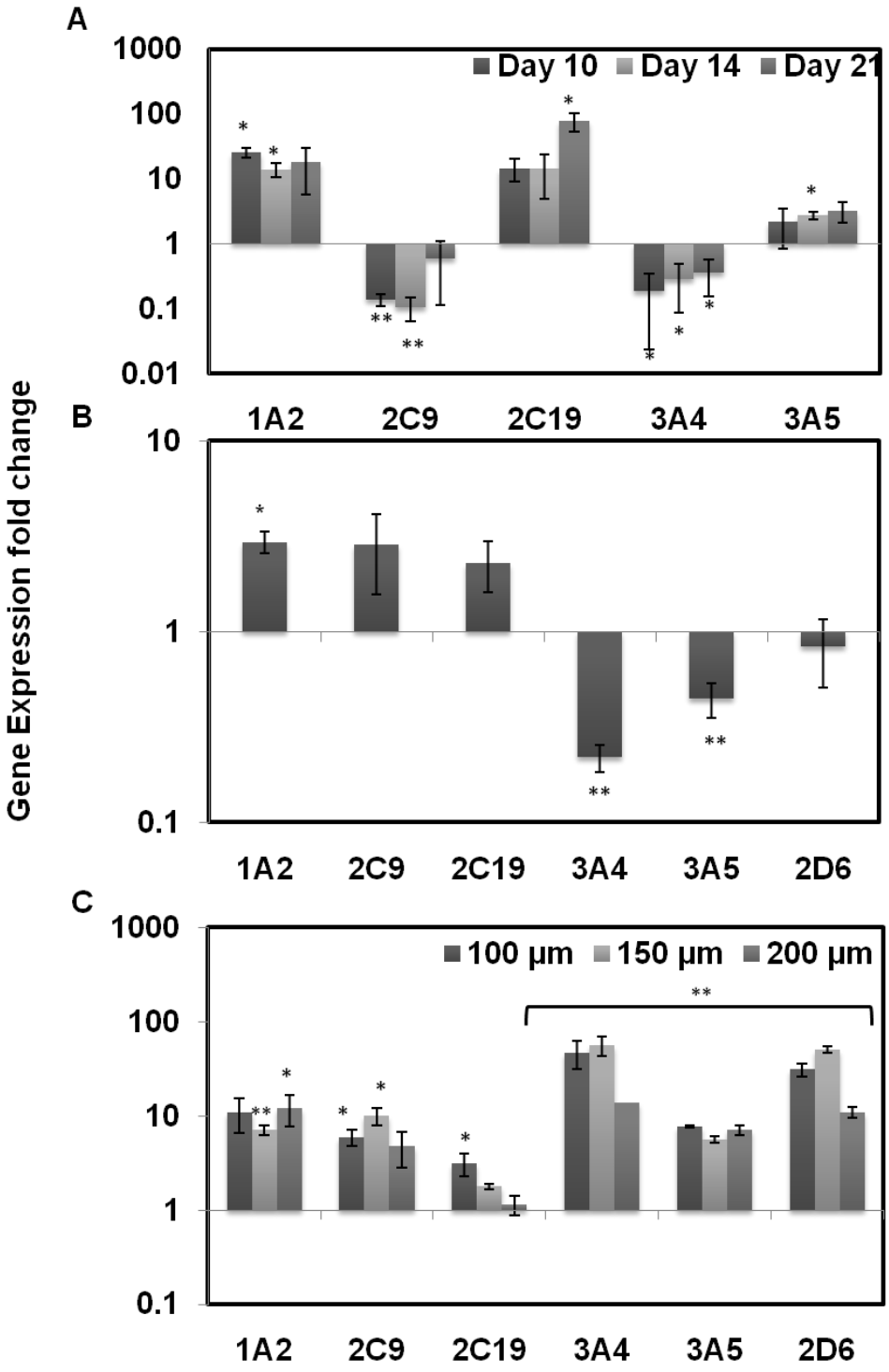

Figure 2.11: CYP gene expression of 3D hepatocytes relative to 2D hepatocytes. **A.** HC04 hepatocyte CYP gene expression after 10, 14 and 21 days of growth on the non-grafted, 200 um pore size, poly(propylene) (PP) scaffolds. **B.** HepG2 cytochrome gene expression after 21 days of growth on the same PP non-woven scaffolds as described for graph A. **C.** HC04 cytochrome gene expression after 21 days of growth on scaffolds PP-*g*-PNIPAAm-B1 (100 µm), PP-*g*-PNIPAAm-B2 (150 µm) and PP-*g*-PNIPAAm-B3 (200 µm). Expression of each transcript, relative to a 2D HC04 monolayer culture, was determined using the $2^{-\Delta\Delta Ct}$ method by normalising to β-actin expression and is graphed as fold induction compared to 2D. Data are represented as the average of three independent experiments performed in triplicate ± standard deviations. * indicates significance at $P<0.05$ and ** indicates significance at $P<0.01$ (student T-test).

2.3.5. Thermal release

An initial thermal release trial was conducted to ascertain which non-woven polymer, grafting and sterilisation method (autoclaving or ethanol) permits optimal cell release at 20°C using HC04 hepatocytes that had grown on the scaffolds for 10 dpi. Thermal release of HC04 hepatocytes at 20°C was observed most significantly after 2 h on the PP-*g*-PNIPAAm-A and PP-*g*-PNIPAAm-B scaffolds that had been ethanol sterilised (Figure 2.12). No other scaffold displayed significant thermal cell release. Although some scaffolds did appear to release cells, including PET-*g*-PNIPAAm-A (autoclaved, 1 h release), PET-*g*-PNIPAAm-B (ethanol, 2 h release) and Nylon-*g*-PNIPAAm-A (autoclaved, 2 h release), these scaffolds were also observed to drop non-woven fibres, ruling out the possibility that thermal release alone was responsible for the released cells. This result was subsequently confirmed using HC04 and HepG2 cells (Figure 2.13).

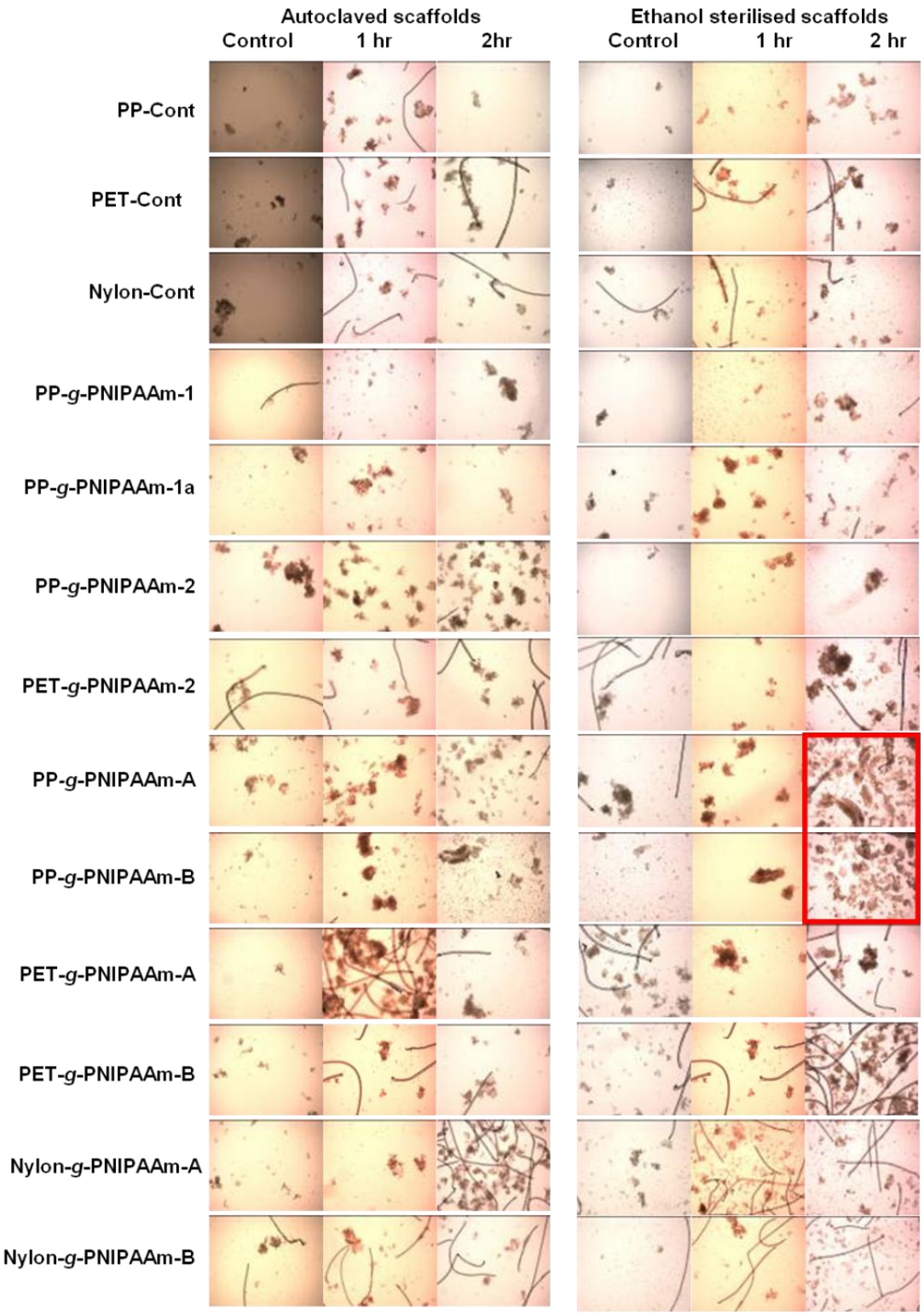

Figure 2.12. Thermal release of HC04 hepatocytes from grafted and control scaffolds 10 dpi. Autoclaved and ethanol sterilised scaffolds were allowed to incubate at 37°C (control) and 20°C for 1 h and 2 h to assess the potential of each scaffold to undergo temperature induced cell release. The red box around PP-*g*-PNIPAAm-A and PP-*g*-PNIAPPM-B (both ethanol sterilised) after 2 h at 20°C indicates successful thermal release of the cells from the scaffolds based on a visual comparison as compared to their respective controls which were maintained at 37°C. Images of the dropped cells were taken using bright-field illumination and a 4x objective on a standard microscope (Olympus BX41).

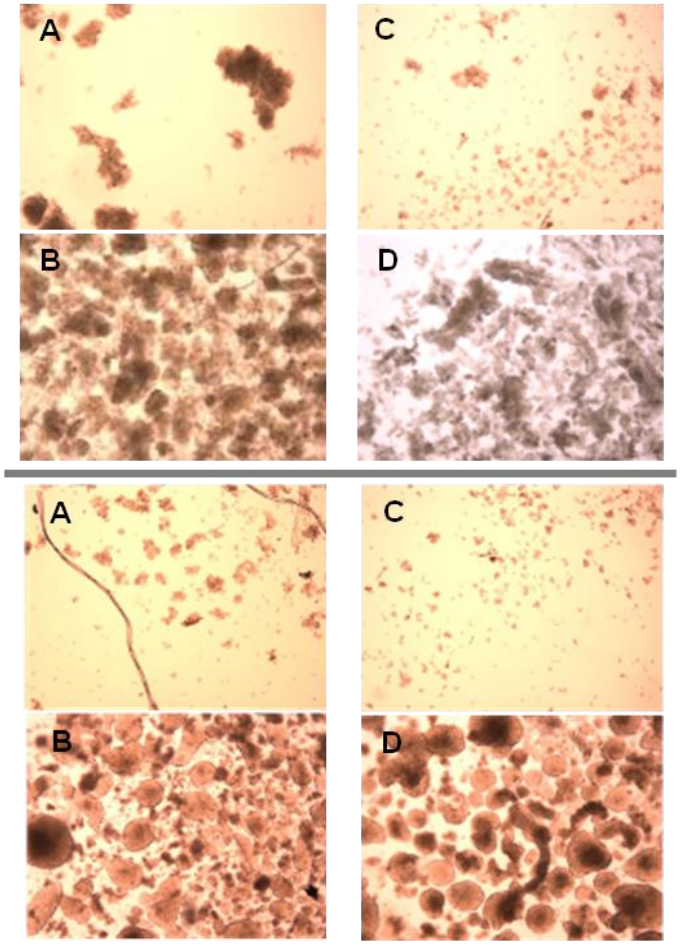

Figure 2.13. Thermal release of HC04 and HepG2 hepatocytes. Cells were grown on either PP-*g*-PNIPAAm-A (left hand panels) or PP-*g*-PNIPAAm-B scaffolds (right hand panels) for 10 days**.** Cell release was compared between scaffolds kept at 37 °C (A, C) or at 20°C (B, D) for 2 h for both HC04 (top panels, A-D) and HepG2 cells (bottom panels, A-D). Images of cells dropped from the scaffolds were taken using a standard microscope (Olympus BX41) at 40x magnification.

Additional controls were included to verify that none of the other components of the grafting process other than the presence of PNIPAAm was responsible for the observed cell release. Scaffold PP-*g*-PNIPAAm-B which had been oxyfluorinated and grafted displayed greater capacity for thermal release than the “test 2” and “test 4” scaffolds (Table 2.1), which had not been grafted with PNIPAAm. In addition scaffold PP-*g*-PNIPAAm-B released more cells than scaffold “test 3” which had been grafted but had no prior surface functionalisation i.e. oxyfluorination (Figure 2.14).

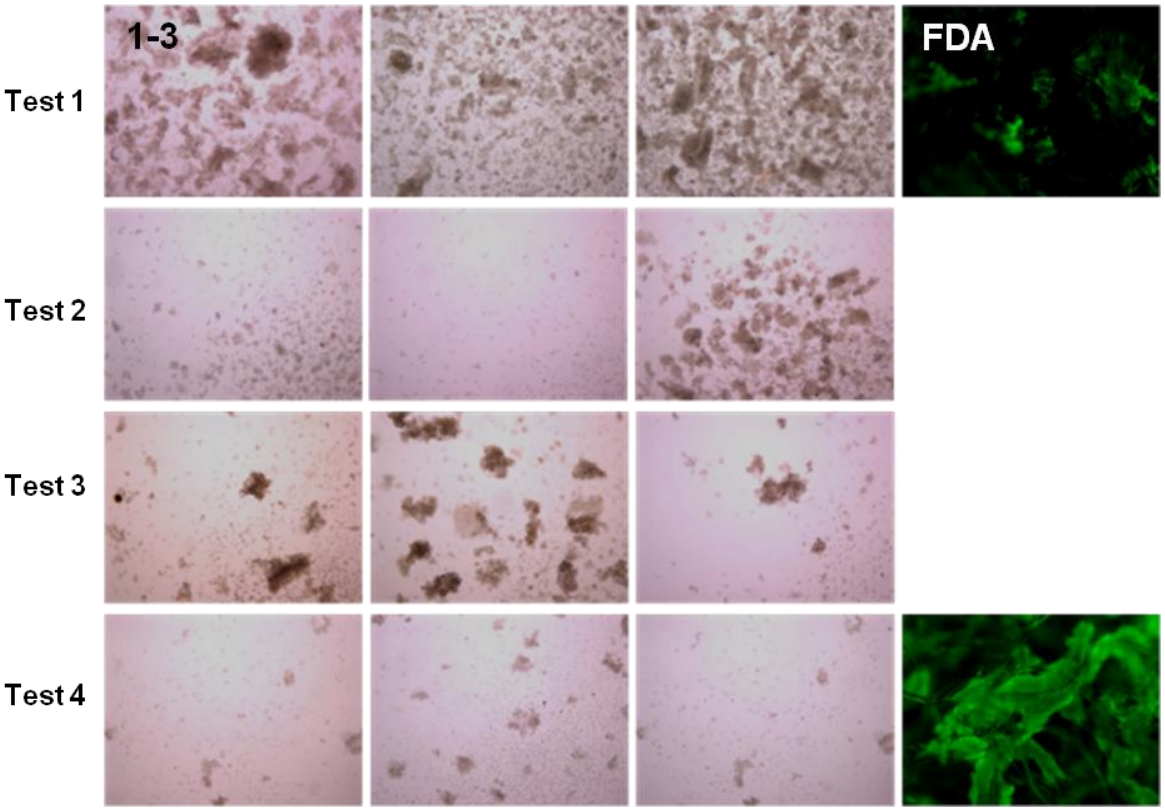

Figure 2.14. Additional controls used to assess if omitting any stages of the grafting process have any effect on thermal release. Panels 1-3 are HC04 hepatocytes dropped from biological replications of each of the grafting variations, Test 1 – Test 4 as summarised by Table 2.2. Thermal release of cells that had been growing on ethanol sterilised scaffolds (Test 1-4) for 10 days took place at 20°C for 2 h. Thermal release images of the dropped cells were taken using a standard microscope (Olympus BX41) with a 4x objective. HC04 hepatocytes remaining on the scaffolds Test 1 (grafted) and Test 4 (not grafted) after thermal release were visualised using fluorescein diacetate (FDA, Sigma) at 40x magnification using an Olympus BX41 microscope equipped with a 490 nm bandpass filter with a 510 nm cut-off filter for fluorescence emission.

It can thus be concluded that only the addition of PNIPAAm during the grafting procedure will result in release of cells from the scaffolds when the temperature is lowered below the LCST and that no other exogenous factors contribute to the observed cell release. In addition to this, grafted scaffolds with different pore sizes were tested to see if this had any effect on thermal release of the cells; after 10 days in culture it was observed that pore size does not significantly affect cell release from the scaffolds with mean pore sizes of 100, 150 or 200 µm, based on visual estimation (Figure 2.15).

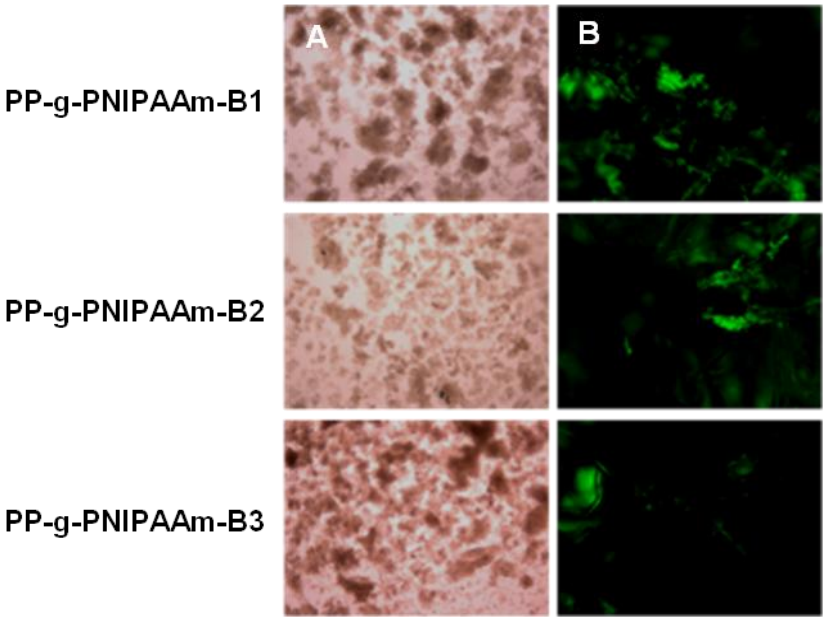

Figure 2.15. Effect of non-woven scaffolds' pore size on thermal release. HC04 hepatocytes were released after 10 days of growth from ethanol sterilised scaffolds: PP-*g*-PNIPAAm-B1 (mean pore size 100 µm) PP-*g*-PNIPAAm-B2 (mean pore size 150 µm) and PP-*g*-PNIPAAm-B3 (mean pore size 200 µm) as summarised in Table 2.2 at 20°C for 2 h. Images of the dropped cells were taken using a standard microscope (Olympus BX41) at 40x magnification. Fluorescent images of the cells remaining on the scaffolds after thermal release were taken using fluorescein diacetate (FDA, Sigma) using an Olympus BX41 microscope equipped with a 490 nm bandpass filter with a 510 nm cut-off filter for fluorescence emission.

A quantitative estimation of cell recovery rates from the scaffolds was also conducted. Scaffolds PP-*g*-PNIPAAm-B1, PP-*g*-PNIPAAm-B2 and PP-*g*-PNIPAAm-B3 were seeded with HC04 hepatocytes. At 14 dpi, the number of total cells on the scaffolds was estimated using the AB assay. Trypsin treatment of the scaffolds or thermal release was used to remove cells from the scaffolds (n=3). Viable cells released from the scaffolds were counted using trypan blue dye exclusion. Trypsin treatment of scaffolds PP-*g*-PNIPAAm-B1 and PP-*g*-PNIPAAm-B2 yielded approximately as many cells as the thermal release, however, more viable cells were released from PP-*g*-PNIPAAm-B3 after trypsin treatment than thermal release. In all instances with the exception of scaffold PP-*g*-PNIPAAm-B3 treated with trypsin (Table 2.4), fewer cells were released than the total estimated to be growing on the scaffold using AB thus indicating that neither trypsin nor thermal release is fully effective in releasing all the cells.

Table 2.4. Hepatocyte cell release from scaffolds PP-*g*-PNIPAAm-B1, PP-*g*-PNIPAAm-B2 and PP-*g*-PNIPAAm-B3 via trypsin treatment or thermal release. Total hepatocyte numbers on the scaffolds prior to cell release were estimated using AB. Viable cells released from the scaffolds were counted using trypan blue dye exclusion on a haemocytometer. The data are presented as the average of three individual scaffolds.

	PP-*g*-PNIPAAm-B1	PP-*g*-PNIPAAm-B2	PP-*g*-PNIPAAm-B3
Total Cells	556 206	608 985	468 552
Trypsin	270 000	190 000	530 000
Thermal Release	230 000	230 000	250 000

Viable cells released from the scaffolds were seeded into a 6 well plate and re-attachment and growth was observed as an additional indication of viability post release (data not shown).

2.3.6. Automated cell culture device

The automated system was designed such that a final (potentially commercial) system would contain a permanent base unit containing the re-usable hardware fitted with a single-use set of consumable components, which would be pre-packed and sterilised. The system hardware would be a once-off acquisition that would be re-used for consecutive cell culturing experiments and would include the perfusion pump, heating/cooling equipment, valves and the permanent base unit (the platform upon which the tubing and bioreactor will be mounted). The consumable set would contain the “wetted” perfusion components including all the perfusion tubing, pinch valve segments, sampling ports, T-sections, etc; the media reservoirs; the bioreactor unit; the oxygenator unit; instrumentation probes that are in direct contact with the perfusion media (oxygen probes, etc.); and the gas supply sterility filters.

Functioning of the automated system will involve circulation of cell culture medium from the medium reservoir to the bioreactor which will contain the non-woven scaffolds; cells are then seeded into the bioreactor; sufficient time is allowed for the bioreactor to be populated with cells and then cell release is affected by lowering the temperature of the cell culture medium to detach cells from the scaffolds grafted with PNIPAAm. The medium containing cells would then be recovered and centrifuged separately for cell separation from the media; this process is illustrated in Figure 2.16. For the purposes of our study the entire automated cell culture device was placed into an incubator set at 37°C to regulate the temperature.

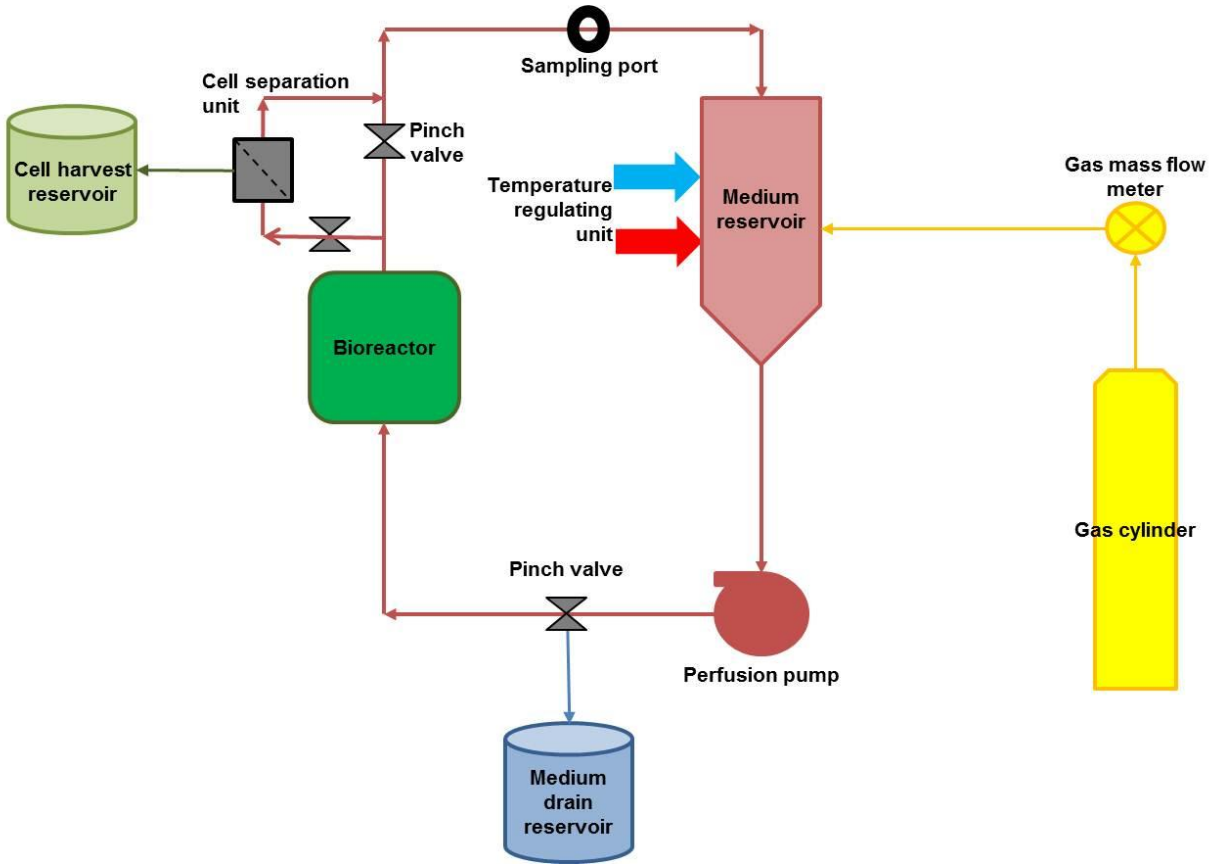

Figure 2.16. The perfusion circuit layout and system components of the proposed automated cell culture system (Figure courtesy of AJ van Wyk, Blueline Designs, re-drawn by C. Rossouw).

2.3.6.1. Prototype

PP un-grafted scaffolds (mean pore size of 200 µm) were punched into disks (15 mm in diameter and 3 mm thick). Three scaffolds were used in the bioreactor per experiment, which was pre-cultured overnight (pump speed 5 mL/min) to remove any debris and to ascertain whether the bioreactor and scaffolds had been adequately sterilised. The overnight media was replaced with fresh, warm media (37°C). The data for the different seeding methods using HC04 hepatocytes are presented in Table 2.5. By seeding the hepatocytes directly into the bioreactor and allowing them to attach over a period of 2-3 h most of the hepatocytes were retained in the bioreactor. In addition, an experiment was conducted when the bioreactor was run over a period of 7-10 dpi to ascertain that if the cells were not growing well on the scaffolds, where within the automated system they were becoming trapped. Once the automated system was stopped the media was drained and the scaffolds with cells attached gently removed from the bioreactor. The scaffolds, medium reservoir, bioreactor and tubing were trypsinised and the cells were harvested and counted by trypan blue dye exclusion on a haemocytometer.

Table 2.5. Experimental parameters assessed using the prototype automated cell culture device

Bioreactor Seeding Method			
Delivery Into media reservoir	**Pump Speed**	**Media flow direction**	**Viable cells in media after 3 h**
Media static			
$2x10^6$	2 mL min^{-1}	Up into bioreactor	24 000
$2x10^6$	2 mL min^{-1}	Up into bioreactor	16 000
Media stirred			
$4.5x10^6$	2 mL min^{-1}	Up into bioreactor	64 000
$4.x10^6$	2 mL min^{-1}	Up into bioreactor	69 000
Into bioreactor			
4.5 x 10^6	Static	Up into bioreactor	27 000
4.5 x 10^6	Static	Up into bioreactor	12 000

Cell proliferation				
Trial 1				
Number of cells seeded	**Pump Speed**	**Media flow direction**	**Days in culture**	**Number of viable cells**
4.5 x 10^6 (into bioreactor)	0.5 mL min^{-1}	Up into bioreactor	7	Media reservoir 0 Bioreactor glass $60x10^4$ Within tubing $5x10^6$ Non-woven scaffolds $8x10^6$ **Total:** 13.6x 10^6
Trial 2				
Number of cells seeded	**Pump Speed**	**Media flow direction**	**Days in culture**	**Number of viable cells**
4.5 x 10^6 (into bioreactor)	0.5 mL min^{-1}	Up into bioreactor	7	Media reservoir 0 Bioreactor glass $1x10^6$ Within tubing $1.5x10^6$ Non-woven scaffolds $2.3x10^6$ **Total:** 4.8 x 10^6
Trial 3				
Number of cells seeded	**Pump Speed**	**Media flow direction**	**Days in culture**	**Number of viable cells**
4.5 x 10^6 (into bioreactor)	2 mL min^{-1}	Down into bioreactor	10	Media reservoir 0 Bioreactor glass 0 Tubing 0 Non-woven scaffolds 49.9 x 10^6 **Total:** 49.9 x 10^6
Trial 4				
Number of cells seeded	**Pump Speed**	**Media flow direction**	**Days in culture**	**Number of viable cells**
4.5 x 10^6 (into bioreactor)	2 mL min^{-1}	Down into bioreactor	10	Media reservoir 0 Bioreactor glass 0 Tubing 0 Non-woven scaffolds 39.7 x 10^6 **Total:** 39.7 x 10^6

By adjusting the direction of the media flow and its speed we observed up to a 10 fold increase in cell numbers over a 10 day period in trials 3 and 4.

An additional trial was conducted (trial 3 conditions, Table 2.5) in order to visually assess hepatocyte distribution between the scaffolds within the bioreactor. The scaffolds were removed from the bioreactor and stained with fluorescein diacetate as described in section 2.2.5. (Figure 2.17). Viable hepatocytes were observed to be attached to the scaffolds throughout the bioreactor.

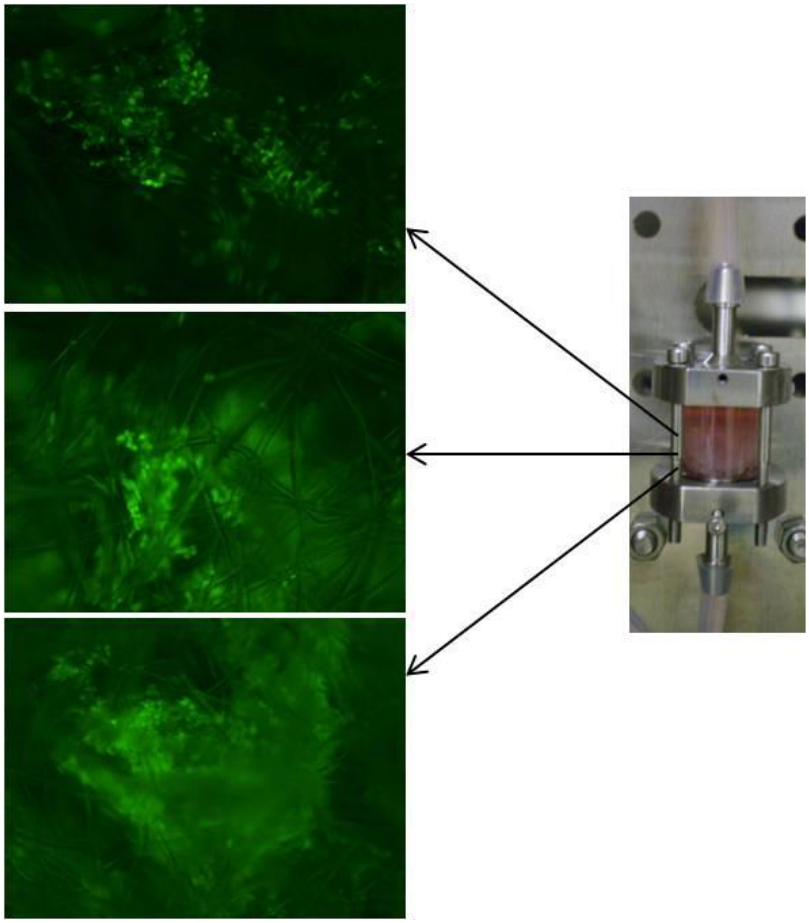

Figure 2.17. HC04 hepatocytes growing on the three non-woven scaffolds housed in the bioreactor. Fluorescent images of hepatocytes growing on the scaffold from the top, middle, and lower layers of the bioreactor 7 dpi. This illustrates that the seeding method enable cells to be distributed throughout the scaffolds in the bioreactor. The hepatocytes were stained with fluorescein diacetate (FDA, Sigma) and visualised at 40x magnification using an Olympus BX41 microscope equipped with a 490 nm bandpass filter with a 510 nm cut-off filter for fluorescence

2.3.6.2. Final system design and testing

During the initial cell culturing experiments on the final system, cells were seeded dynamically i.e. they were introduced in suspension in the medium reservoir and pumped through the bioreactor and scaffold. This seeding method resulted in cells adhering to all surfaces of the

system and less on the non-woven scaffolds. During subsequent cell culturing experiments, the seeding procedure was optimized such that the cells were seeded statically above the bioreactor via a sampling port and allowed to settle via gravity onto the non-woven scaffolds in the bioreactor. The static conditions were maintained for 3 h before the bioreactor was perfused. The results obtained from this seeding methodology indicated much higher cell numbers attached to the scaffold, resulting in overall better performance of the cell culturing system. It was thus decided to adopt a gravity assisted, static seeding methodology in the final automated cell culture. Cells would be seeded from the sampling port located at the top of the bioreactor with perfusion of the system only commencing 3 h after seeding.

The initial cell culturing experiments revealed that the cells were adhering to the bottom of the medium reservoir as well as the inside lumen of the tubing. This was due to the gravitational settling of cells within the reservoir. Experimental manipulation by means of agitation of the medium reservoir using a magnetic stirrer resulted in fewer cells adhering to the bottom of the reservoir. In the final perfusion system design this aspect was addressed by designing the medium reservoir with an angled bottom medium intake that will allow any cells in suspension to settle towards the bottom of the reservoir from where they would be pumped back to the bioreactor i.e. media would flow out the bottom of the reservoir (Figure 2.18A). Once back in the bioreactor the cells would have the opportunity to adhere to the non-woven scaffold. Any anchorage dependant cell will tend to adhere to any available surface, this means that cells will adhere to the inside surface of the tubing and one of the best ways to limit the effect of cells adhering to the tubing is to reduce the length (i.e. surface area) of the tubing. In the final perfusion system design emphasis was placed on reducing the overall length of tubing of the system.

Air trapped in the prototype bioreactor resulted in uneven perfusion of the non-woven scaffolds. The entrapped air would accumulate below the scaffold on the outlet side of the bioreactor. Thus, the new design has incorporated a way in which to remove air bubbles forming below the scaffold as illustrated in Figure 2.18B and C. In addition this problem was somewhat overcome by perfusing the media down though the bioreactor as opposed to up though the bioreactor. The final automated system is photographed in Figure 2.18.

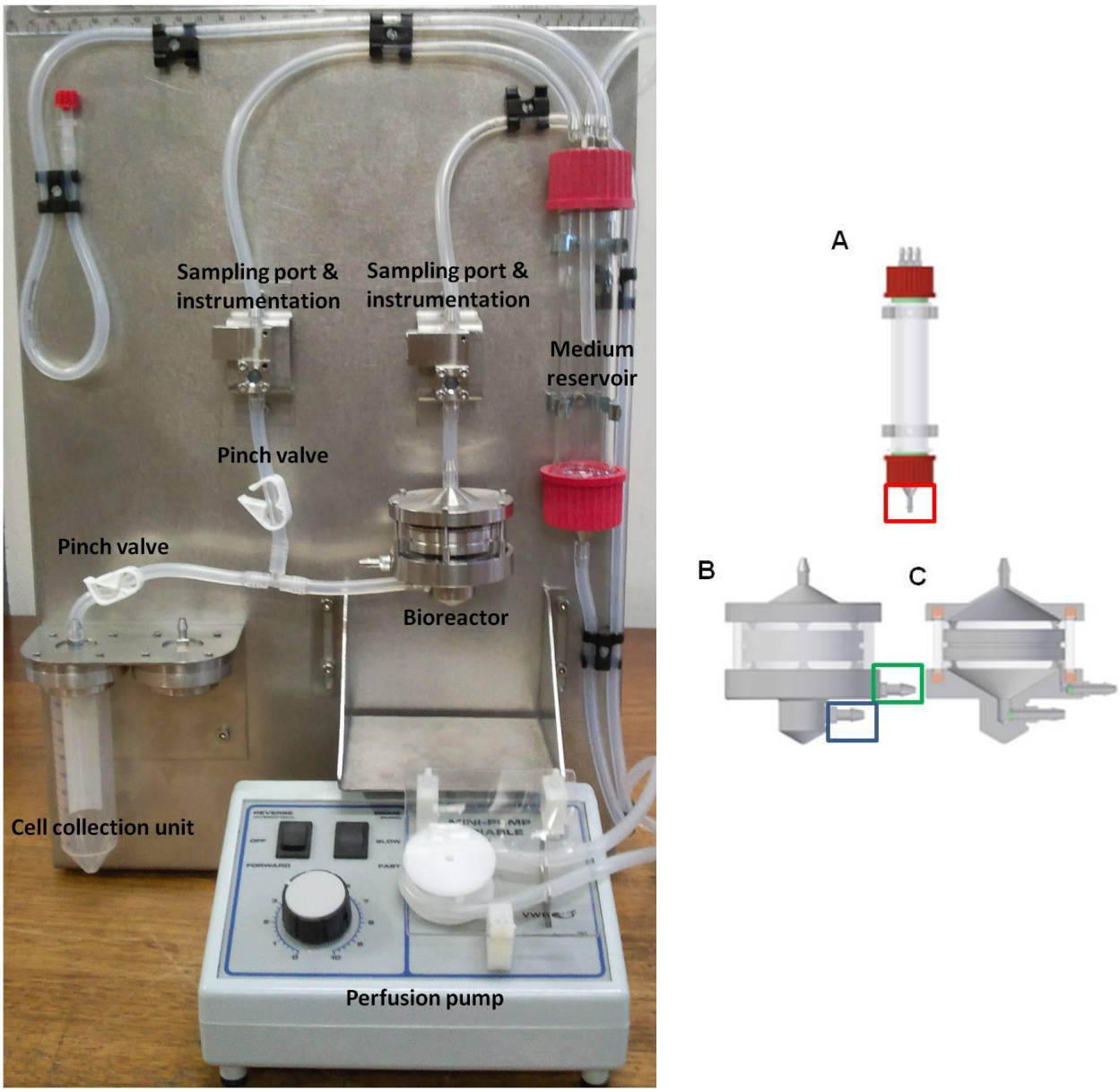

Figure 2.18. The final automated cell culture system. The new automated system is photographed on the left. **A.** The new medium reservoir. Media is pumped out of the bottom of the reservoir (red box) thus preventing cells settling on the bottom of the reservoir and eliminating the need to stir the media. **B.** The new bioreactor with medium outlet (blue box) and air bubble outlet (green box). **C.** A schematic cross section of the bioreactor.

The final automated system was tested using the parameters from trial 3 and 4 (Table 2.5), however, the pump speed was modified. In order to keep the bioreactor filled with media at all times the pump speed was set to 10 mL/min. Two million HC04 hepatocytes per non-woven scaffold (total 6 million) were seeded into the bioreactor via the sampling port and grown for 10 days. A control experiment using PP-Cont non-woven scaffolds (200 µm pores) was first performed. Thermal release was attempted by draining the warm (37°C) cell culture media and replacing it with media at room temperature (20°C). The media was perfused for 2 hours and the cell culture media containing any released hepatocytes was collected. Viable cells were counted using trypan blue dye exclusion and a haemocytometer. The non-woven scaffolds were

then removed from the bioreactor and the cells remaining on the non-woven scaffolds trypsinised as in section 2.2.3 and collected. Viable hepatocytes were counted using trypan blue dye exclusion and a haemocytometer. This experiment was repeated using PP-*g*-PNIAPPA-B1 non-woven scaffolds. The data are presented in Figure 2.19.

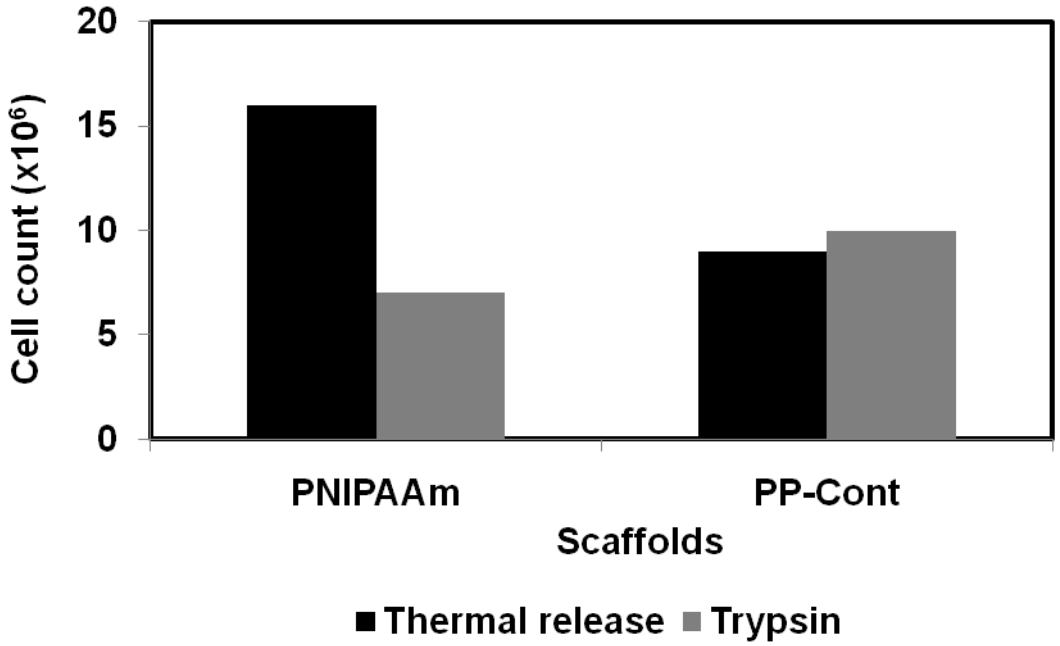

Figure 2.19. HC04 hepatocytes released from grafted (PP-*g*-PNIPAAm-B1) and control (PP-Cont) non-woven scaffolds 10 dpi in the final automated system. Approximately 16 million cells were released by the grafted non-woven scaffold after temperature reduction and a further 7 million were released from the non-woven scaffolds after trypsination. Nine million hepatocytes were released from the control non-woven scaffolds after the temperature reduction and a further 10 million after trypsination.

The data indicate that, of the cells released, just under 50% (9 million) of the hepatocytes growing on the control scaffolds are released when the temperature of the circulating cell culture media is dropped and the rest of the cells (10 million) are subsequently release via trypsin on the control scaffolds. Approximately 16 million hepatocytes were released from the grafted scaffolds (PP-*g*-PNIPAAm-B1) and less than half that number (7 million) remained on the scaffolds when the balance of the cells was released via trypsin were counted. This experiment was not repeated due to the limited number of grafted scaffolds available so reproducibility of this experiment was not assessed. These preliminary data do however, support the hypothesis that cells can proliferate in the bioreactor and be released by reduction of temperature.

2.4. DISCUSSION

A growing body of evidence has emerged where cells grown *in vitro* in 3D structures have been shown to be significantly different and more representative of the physiological state of the native source tissue than those grown in conventional 2D monolayer cultures. The development of new culturing systems that enhance this capability is therefore expected to lead to significant advances in the predictive accuracy of multiple *in vitro* cell culture applications, including the fundamental study of cell growth and signalling, host-pathogen interactions, and the drug discovery process. In this study, the need was identified to develop a scaffold which could not only support cell attachment and enhanced proliferation, but could furthermore be capable of releasing 3D cell structures non-invasively for downstream applications. This is the first report for the development of 3D, thermoresponsive, non-woven scaffolds able to release cells from a 3D matrix without the use of enzymatic detachment or degradation of the scaffold. The feasibility of using three different polymers for enhanced 3D cell culture, grafted by various means with PNIPAAm, was investigated.

AB (non-destructive assay) and Hoechst 33258 (destructive assay) were used independently for determining the number of viable cells growing on the non-woven scaffolds as, to date, there is not one wholly accepted method for cell enumeration in 3D (125). For the majority of scaffolds tested using the AB assay, cell numbers, for both HC04 and HepG2 hepatocytes, were observed to initially increase after seeding but subsequently declined between days 7 and 11; thereafter cell numbers recovered and increased. Similar results have previously been observed by Shor *et al.* (115) in the interaction of osteoblasts with PCL / hydroxyapatite scaffolds. It has been suggested that this observed trend is due to the inability of the dye to penetrate the scaffolds and react with the cells in the interior of the scaffolds. The recovery in cell numbers can be attributed to cells subsequently populating areas of the scaffold where the dye can more easily penetrate. The cell numbers estimated using the AB assay will not be accurately representative of the inner construct environment if a metabolite concentration gradient existed between the interior and the exterior of the construct and is therefore dependent on the efficiency of metabolite diffusion into and out of the construct. This can be overcome to a degree by swirling the wells containing the scaffolds during the incubation period to assist dye diffusion, however, this diffusivity of reagents into the 3D environment can ultimately become a confounding factor in this type of assay and it is thus important to use AB in combination with another cell quantification assay. The AB assay did, however, reveal that the cells were able to proliferate on the grafted scaffolds at a level comparable to, and in some instances better than

that of the commercially available alginate scaffold, Algimatrix™ and the control scaffolds, suggesting an absence of scaffold-induced cytotoxicity.

The Hoechst 33258 assay indicated that the HC04 cells proliferated rapidly on the scaffolds whereas the growth of the HepG2 hepatocytes was relatively static over time. This can be largely attributed to the different way in which these cells grow. Fluorescence microscopy revealed that the HC04's displayed guided growth according to the non-woven fibre orientation forming 3D structures as depicted in Figure 2.9 and populating the majority of the scaffold surface area. HepG2 cells formed spheroids with a small area of attachment to the non-woven fibres soon after seeding into the scaffolds thus they did not populate the scaffolds as rapidly or as extensively as the HC04 cells. This discrepancy in morphology is also evident when looking at the images of cells liberated during thermal release (Figure 2.13); HepG2 cells form spheroids whereas the released HC04 hepatocytes are in the form of long, multi-layered cell sheets and in some instances the imprint of the non-woven fibre can be seen on the cell sheets. The disparity in the scaffold-associated HC04 cell numbers derived from the AB vs. DNA results may be attributable to differences in scaffold penetration of the respective reagents used. This discrepancy was not observed for HepG2 cells, which do not populate the matrix as densely and may allow for more uniform reagent diffusion.

The albumin assay indicated that the cell-lines are metabolically superior, when grown in 3D as compared to a conventional 2D monolayer, particularly in the case of HC04 cells. The comparison of 3D vs. 2D was carried out using an approximately 70% confluent 2D monolayer as this cell confluency is typically the benchmark used in conventional experimentation to represent the most optimal log phase of 2D hepatocyte growth. More mature, confluent 2D-cultured cells experience increased cellular stress and eventual cell death (39). Some fluctuation in albumin secretion was observed for both cell-lines, which is not unusual (39) and Glicklis *et al.* (126) also reported a decline in albumin production on day 7 in their 3D alginate scaffolds. Prestwich (82) suggests a possible cyclic production of albumin, as well as urea and EROD activity of hepatocytes (primary and HepG2-C3A cells) cultured on hydrogel surfaces or in 3D by encapsulation in Extragel, a synthetic extracellular matrix; our data suggests this to be accurate. HepG2 3D cultures had lower levels of albumin production as compared to HC04 3D cultures. This may be as a result of restrictions on mass transfer of essential nutrients caused by the formation of spheroids. This was observed by Dvir-Ginzberg *et al.* (127) when the spheroids in their alginate scaffolds reached sizes of 100 µm or larger. The compaction of the spheroids over time and the deposition of ECM proteins (127, 128) could lead to the decreased

ability to remove cell secretions and reduce albumin levels in 3D HepG2 culture supernatants compared to the HC04 hepatocytes.

An additional indicator of superior hepatocyte growth on the scaffolds is increased CYP gene expression. Hepatocytes absorb drugs from the blood stream and metabolize them through phase-I and phase-II reactions (129). During phase-I metabolism, 90% of all drugs are oxidized by CYP isozymes with different substrate selectivity. Seven isoforms account for 95% of this activity namely 1A1, 1A2, 2C9, 2C19, 2D6, 2E1, and 3A4, with 3A4 responsible for over 65% of the metabolism of current therapeutic agents (82). Cytochrome isozymes are downregulated within 24 h after plating fresh hepatocytes onto conventional 2D tissue culture plastic (82), thus *in vitro* culture models that reflect the increased physiological CYP levels of primary hepatic tissues and cells are sought after in the pharmaceutical industry as surrogates for predicting *in vivo* phase I drug metabolism (130). In several instances the 3D non-woven scaffolds developed in this study promoted increases in CYP gene transcripts in both the HC04 and HepG2 cell-lines relative to their respective monolayers. Gene expression increased in a time-dependent manner for the HC04 cells grown on the 200 µm pore size scaffolds that had not been grafted with PNIPAAm. Expression of the *CYP2C9* and *CYP3A4* isoforms, however, remained below that of the 2D monolayer cells. Similarly, after 21 days of growth on the non-grafted scaffolds, HepG2 cells displayed increased expression of three out of six CYP isoforms compared to 2D monolayer cells, while the remaining isoforms had levels of gene expression equivalent or less than that observed for the 2D monolayer. This contrasts with the results observed for the scaffolds grafted with PNIPAAm. All the CYP genes tested demonstrated increased levels of expression as compared to the 2D control on scaffolds with pores sizes 100 µm and 150 µm. This is a good indication that the grafted layer serves not only as a mechanism for cell release from the scaffolds but positively influences hepatocyte growth and metabolism.

Two scaffolds with thermoresponsive properties were successfully developed, namely PP-*g*-PNIPAAm-A and PP-*g*-PNIPAAm-B. Large tracts of viable cells or spheroids were released from these scaffolds in a temperature-dependant manner and, by comparison with control scaffolds, this thermal release was shown to be exclusively caused by the grafted PNIPAAm layer. Fluorescent microscopy did, however, reveal that not all the cells were released from these thermoresponsive scaffolds. A comparison of thermal release versus trypsin treatment of the cells growing on scaffolds PP-*g*-PNIPAAm-B1 and PP-*g*-PNIPAAm-B2 revealed a similar efficiency in cell release from the scaffolds (Table 2.4). Scaffold PP-*g*-PNIPAAm-B3 however was more permissive to trypsin treatment possibly owing to the more open pore structure of the scaffold. The cells that remain in the scaffolds may either be trypsin resistant due to the 3D

nature of the cell clusters and deposition of protective ECM proteins or may not be able to navigate out of the non-woven fibre network to be counted. Uneven grafting and scaffold areas devoid of PNIPAAm may be responsible for cells remaining on the scaffold. In addition, hepatocytes were, in some instances, observed to grow around the full circumference of the fibre, this means that when the phase transition of the PNIPAAm polymer triggers cell release it will simply repel the cells from the scaffold but will not be sufficient for the cells to separate from one another. It is for this reason that we believe some hepatocytes remain on the scaffold after the 2 h thermal release. Grafting efficiency and time for cell release are potential areas for further improvement. Currently the commercially available thermoresponsive 2D plates (UPCellTM, Cell Seed Inc, Tokyo, Japan) require just over 30 min for release of a monolayer of cells.

In the preliminary design of the automated cell culturing system, the following criteria were identified: 1: the system should allow for the cultivation of large numbers of cells which would be achieved with a high surface area 3D scaffold; 2: it should allow for thermal, non-enzymatic cell release via the use of a thermoresponsive scaffold, thereby preserving the cell surface composition; 3: the proposed cell culturing system must be easy to operate with minimal human intervention required and 4: the automated culture system should be a small, cost-effective bench-top device that would be affordable to most cell culture laboratories.

Scaling up cell proliferation in the automated system revealed that it is possible to culture high numbers of cells on the non-woven scaffolds in the bioreactor. The cell numbers, however, are not sufficiently high to warrant using the automated system over conventional culturing if cell proliferation is the primary aim. Further optimisation to obtain cell numbers significantly higher than what can be obtained in culture flasks would be required. The proof-of-concept thermal release of cells from the grafted non-woven scaffolds was superior to that of the control non-woven scaffolds but this would need to be confirmed in a duplicate set of experiments.

This chapter demonstrated the proliferation and superior nature of hepatocytes growing on non-woven scaffolds in 3D. In the following chapter, selected scaffolds will be used to culture hepatocytes in 3D and once the hepatocytes have populated the scaffold, the hepatocytes will be infected with the liver stage (sporozoite) of the human malaria parasite *P. falciparum*. Invasion of sporozoites *in vitro* has historically been very challenging and we hypothesise that the more physiologically representative state the hepatocytes growing in 3D will enhance the permissiveness of the hepatocytes to the parasite. Although the data represented in Chapter 3 does not currently make use of the thermoresponsive properties of the scaffolds, this

functionality may find an application in the future if the hepatocyte permissiveness to the malaria pathogen is indeed enhanced and researchers want to circumvent enzymatically removing the cells from the scaffolds in order to study surface antigens/proteins.

CHAPTER 3

APPLICATION OF A 3D SCAFFOLD: A SPOROZOITE-HEPATOCYTE MODEL

3.1. INTRODUCTION

3.1.1. Malaria

The liver constitutes the largest organ in the human body and is responsible for performing critical tasks such as plasma protein synthesis, hormone and bile production, glycogen storage, metabolism of xenobiotics, decomposition of erythrocytes and lipid digestion. The liver supports almost every organ in the body and is vital for our survival; however, this organ is also involved in many diseases, of which malaria ranks amongst one of the most important and widespread. An accurate estimation of the extent of morbidity and mortality caused by malaria is difficult but ~216 million cases and 655 000 deaths were reported for 2010 (131).

Malaria is caused by the protozoan parasite belonging to the genus *Plasmodium*. Five species account for almost all human infections (*P. falciparum, P. vivax, P. malariae, P. ovale* and *P. knowlesi)*. *P falciparum* causes the majority of infections in Africa and is responsible for most of the instances of severe disease and mortality (132). The parasite's life cycle, as illustrated in Figure 3.1, begins when the parasite is transmitted as a liver-infective sporozoite to the mammalian host through the bite of an infected female *Anopheles* mosquito. An average of 15-123 sporozoites are injected under the skin of the host and enter the blood circulation system where they migrate to the liver. There they infect hepatocytes and begin to develop into merozoites (133, 134). Tens of thousands of merozoites develop per invading sporozoite over a period of days to ~2 weeks (depending on the species) and are released into the blood stream where they rapidly adhere to and invade erythrocytes. Further infectious merozoites are subsequently generated through asexual replication inside erythrocytes, and this intra-erythrocytic cycle is also where malaria-associated pathology becomes detectable (135).

The malaria parasite's life cycle also comprises a phase of sexual reproduction, which takes place in the mosquito vector. The switch to sexual development starts in the human host, with the formation of male and female gamete precursors (gametocytes), and is a prerequisite for transmission of disease to the mosquito vector (136). Once ingested by the female mosquito the

male and female gametes form zygotes, which develop into oocysts. From these oocysts sporozoites emerge and travel to the salivary gland of the mosquito ready to be injected into the next host. Sporozoites are generated in multinucleated oocysts located between the epithelium and the basal lamina of the mosquito midgut. When a mature oocyst bursts, sporozoites are released into the mosquito's haemolymph; when the sporozoites reach the mosquito salivary glands they attach to and invade gland cells. Sporozoites transit through the cytoplasm of the gland cells and exit into the secretary cavity where they await the next blood meal for transmission to the host (137).

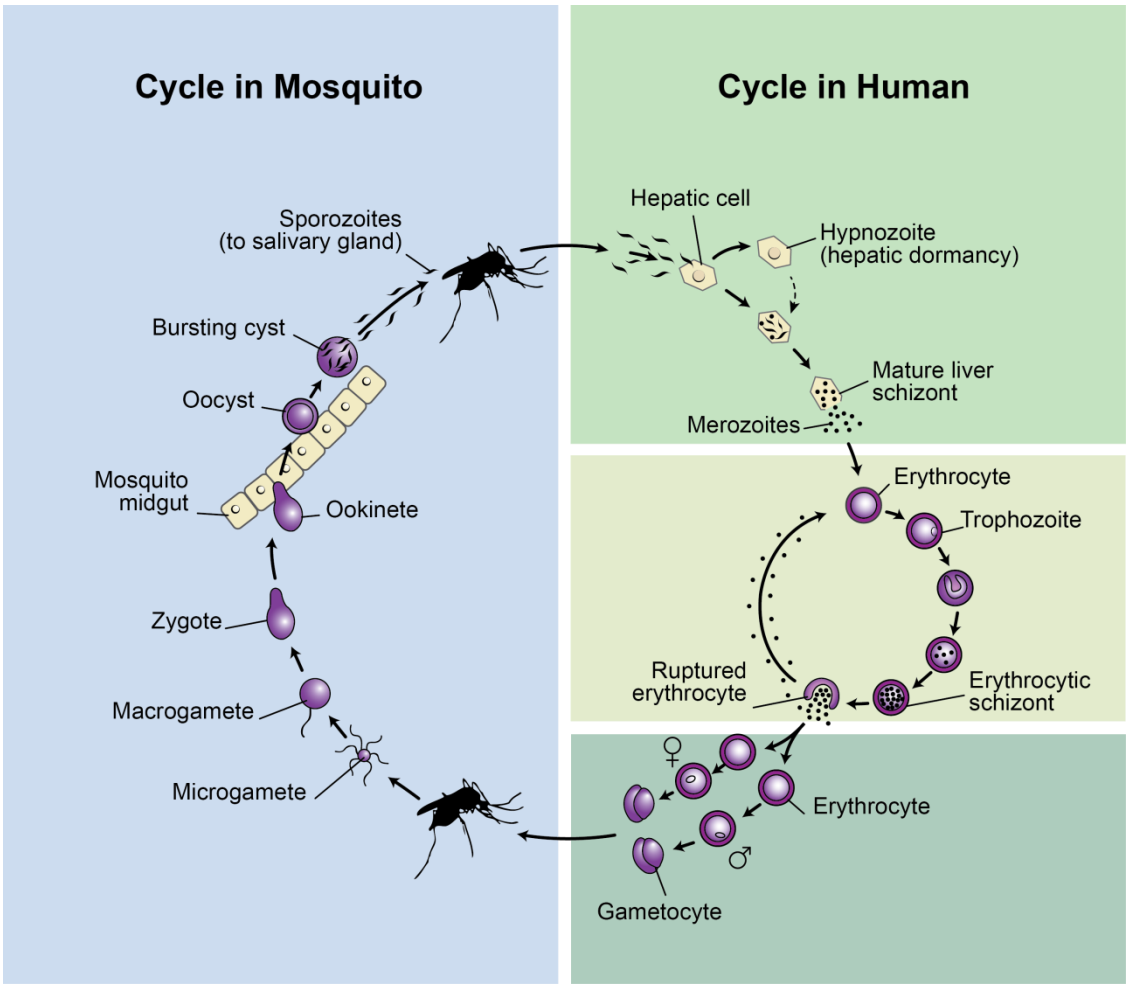

Figure 3.1. The life cycle of *P. falciparum* parasites in the human host and the *Anopheles* mosquito vector. Malaria develops in two phases: an exo-erythrocytic and an intra-erythrocytic phase. When an infected mosquito feeds on its host, sporozoites in the mosquito's saliva enter the bloodstream and migrate to the liver multiplying asexually and asymptomatically forming thousands of merozoites over a period of 5 - 16 days which, following rupture of their host cells, escape into the blood and infect erythrocytes. This is the beginning of the erythrocytic stage of the life cycle. Within the erythrocytes, the parasites multiply further. A merozoite infects an erythrocyte and matures into a schizont, which releases more merozoites into the circulatory system to invade fresh erythrocytes approximately every 48 h. Several such amplification cycles occur and it is at this stage that the clinical signs of malaria are observed. Some merozoites are triggered to form the sexual stage parasites (gametocytes), which are ingested by a female mosquito when taking a blood meal. The male and female gametes form zygotes, which develop into oocysts. After 8 - 15 days these oocysts sporozoites emerge and travel to the salivary gland of the mosquito ready to be injected into the next host. Adapted from (138).

3.1.2. Sporozoite hepatocyte invasion

The proposed journey of the sporozoite to the hepatocyte and subsequent liver stage development starts when the infectious sporozoite is deposited into the skin by the mosquito vector and subsequently enters the bloodstream through a capillary endothelial cell. Some sporozoites may also enter draining lymph nodes and can partially develop within the lymphoid endothelium. After being transported by the bloodstream through the body, the sporozoites eventually reach the liver. In the liver sinusoids, the blood flow is very slow and sporozoites are able to adhere to the liver endothelium via circumsporozoite protein recognition of heparan sulphate proteoglycans (HSPGs) protruding into the sinusoidal lumen through endothelial fenestrations (139). Following adhesion, the sporozoites glide along the endothelium looking for a point of entry to the space of Disse and the underlying hepatocytes (140). The sporozoite then traverses a number of hepatocytes before invading a hepatocyte with the formation of a parasitophorous vacuole membrane. Although contentious, transgenic mice (homozygous op/op known to have few Kupffer cells) (141) and intra-vital microscopy using infected live mice with red or green fluorescent *P. berghei* sporozoites (142) have pointed to Kupffer cells (resident macrophages in the liver) as the main gateway into the liver. In addition, it has been shown that sporozoites can transmigrate Kupffer cells and macrophages *in vitro* (142, 143).

At least two cell-invasive motilities have been documented for malaria parasites: cell-infection (137) and cell-traversal motility (144). Cell-infection motility is accompanied by vacuole formation and is followed by parasite development into exo-erythrocytic (EE) forms, whereas cell-traversal motility involves plasma-membrane disruption and is followed by migration through the cytoplasm and eventual escape from the cell. In their 2002 paper, Mota *et al.* revealed that cell traversal motility can be identified by a conventional cell-wound assay and they proposed that this motility is necessary for sporozoites to be activated for hepatocyte infection (145). Once inside the hepatocyte the sporozoites develop into EE forms, undergo schizogony and produce thousands of erythrocyte-infectious merozoites that enter the sinusoid packaged in extrusomes / merosomes (in order to avoid immune detection) and are subsequently released in the bloodstream (146, 147).

3.1.3. *In vitro* culturing of hepatocytes for malaria sporozoite invasion

In recent years, the malaria parasite has become ever-more resistant to the current line of available drugs and in certain regions is increasingly resistant to the last line of defence, artemisinin (148). Most available antimalarials are designed to target the pathogenic blood

stages in humans and to address the constant threat of drug resistance (149). Thus there is a renewed interest in new methods to tackle malaria, in particular the development of solutions that combat EE development including liver-stage infection as well as gametocyte formation. Despite being asymptomatic, the liver stage of *Plasmodium* infection is both immunologically active (150) and one where a rich array of host–parasite interactions takes place (146, 151, 152). In endemic areas relapse of vivax malaria is a major cause of malaria in young children, and an important source of malaria transmission. Relapse also occurs in *P. ovale* infections (153). This recurrence arises from persistent liver stages of the parasite (hypnozoites) (153). Molecules that efficiently target the parasite stages in the liver would offer protection from the development of the blood stages and resultant malaria symptoms. As only approximately 100 sporozoites may be introduced by a bite, there are also likely to be many orders of magnitude fewer parasites at this stage than in an active blood stage infection, reducing the possibility of resistance arising (154). New compounds targeting this stage of the disease are therefore highly desirable; at the same time the liver stage represents the most suitable opportunity for developing long-term vaccine solutions.

Much of what researchers know today about the *Plasmodium* EE stages is as a result of research done using *Plasmodium* spp. that infects rodents, specifically*, P. berghei* and *P. yoelii*. These two species present differences in infectivity, which depend not only on the species but also on the clone and the genetic background of the rodent host (133). *In vitro* systems have been developed to study the EE stages of these malaria parasites in various human and mouse cell-lines including HepG2, Huh-1/2, Huh-7, HSS-102, HC04, WI38 and HeLa cell-lines grown in 2D (155). The sporozoites of human and primate malaria parasites will readily infect primary cells but these cells cannot be grown continuously in culture and are thus not ideal for experimental purposes. However, Sattabongkot *et al*. (113) developed the hepatocyte cell-line, HC04, that could support the complete development of the EE stage parasites from *P. falciparum* and *P. vivax* but infectivity was low; ~0.066% and 0.041% for *P. falciparum* and *P. vivax* infections, respectively. As a direct result of the low levels of infectivity, down-stream applications to study the parasite including global strategies like genomic and proteomic investigations are less feasible. Similarly, effective testing of antimalarial drugs on *P. falciparum*-infected hepatocytes remains a major challenge, primarily due to inconsistent and unreliable *in vitro* culturing systems developed for sporozoite invasion into hepatocytes. Thus, a new, reliable *in vitro* model that more easily permits researchers to study the *P. falciparum*-liver interaction is needed to expedite a more relevant understanding of malaria liver infection.

Chapter 3: An application of a 3D scaffold: A sporozoite-hepatocyte model

With the knowledge that the infectious sporozoites traverse several hepatocytes prior to cell infection, it was hypothesised that the newly developed 3D system described in Chapter 2 may provide a suitable basis for developing an improved host-pathogen model of malaria infection. Thus, the major focus of this chapter was to establish if a greater level of *in vitro P. falciparum* sporozoite invasion could be achieved in hepatocytes that have been cultured on 3D non-woven scaffolds compared to conventional 2D systems. Although *P. berghei* sporozoites have previously been produced *in vitro* in low numbers (156), an effective *in vitro* system for the generation of sporozoites poses as a major hurdle to this field of malaria drug discovery (155), especially for *P. falciparum*. Thus, the maintenance of mosquito colonies infected with malaria parasites is a pre-requisite for liver stage research. To date, this has not been achieved for *P. falciparum* in South Africa, limiting our research to the asexual stages of these parasites. The first objective of this chapter was, therefore, to establish methods to infect an *Anopheles* mosquito colony with *P. falciparum* gametocytes, to allow sexual replication in the mosquitoes and obtain a reliable source of *P. falciparum* sporozoites for subsequent use in the 3D hepatocyte cell culture model.

3.2. MATERIALS AND METHODS

3.2.1. *In vitro* cultivation of asexual *P. falciparum* cultures

Continuous asexual cultures of *P. falciparum* parasite strains 3D7, 7G8 and NF54 (MRA-1000 ATCC, MR4, ATCC® Manassas, Virginia) were maintained *in vitro* according to a modified Trager and Jensen method which supports intracellular parasite development (157). The erythrocyte and serum preparation, culture thawing and general maintenance of asexual stage parasites are described below.

Type A+ or O+ blood was collected in EDTA vacuum tubes, transferred to centrifuge tubes using aseptic technique and centrifuged at 2500*g* for 5 min at room temperature. The plasma and buffy coat were aspirated and an equal volume of wash medium [RPMI with L-glutamine and HEPES (Lonza Walkersville) supplemented with 0.4% (w/v) D-glucose (Sigma-Aldrich Chemie), 88 mg/L hypoxanthine (Sigma-Aldrich Chemie) and 48 mg gentamycin (Sigma-Aldrich Chemie)], was added. The erythrocytes were re-suspended and centrifuged at 2500*g* for 5 min, after which the supernatant was aspirated. The procedure was repeated 3 to 4 times to reduce the presence of leukocytes. Washed erythrocytes were re-suspended in an equal volume of wash medium and stored at 4°C. The wash medium was aspirated and replaced twice a week to preserve the erythrocytes.

Human serum (male, type A+, negative for HIV, hepatitis and syphilis, aspirin, antibiotic and drug free) was purchased from the Interstate Blood Bank (Tennessee, USA). The units of serum were filter sterilised through both a 47 mm type A/D glass fibre filter (PAL Corporation, Ann Arbor, Michigan, USA) and a 47 mm 0.22 PES filter (PAL Corporation). The units of serum were pooled (a minimum of four donors per pool) and aliquots were frozen at -20°C. The human serum was not heat inactivated on the advice of Megan Dowler from the Walter Reed Army Institute of Research (personal communication). Ethical approval for the use of donor blood and serum was conferred by the University of Pretoria and CSIR research ethics committees.

Glycerol-frozen aliquots of asexual *P. falciparum* 3D7, 7G8 and NF54 parasites were removed from storage at -80°C and quickly thawed in a water bath at 37°C. The thawed aliquot was transferred to a centrifuge tube under sterile conditions in a laminar flow cabinet. The osmotic potential of the thawed stocks were gradually reduced by the drop-wise addition of 200 µL 12% (w/v) NaCl solution, followed by pipette-mixing for ~10 – 20 s and then the drop-wise addition of 1.8 mL 1.6% (w/v) NaCl, again followed by pipette-mixing for ~10 – 20 s. The parasites were

collected by centrifugation at 2500*g* for 5 min at room temperature. The supernatant was aspirated and 10 mL culture medium [wash medium with 0.5% (m/v) AlbuMAX® II purified lipid-rich bovine serum albumin (Gibco®) for the 3D7 and 7G8 parasites, and RPMI with L-Glutamine and HEPES (Lonza Walkersville) with 88 mg/L hypoxanthine (Sigma-Aldrich Chemie) and filter sterilised human serum (A+ male, Interstate Blood Bank) for the NF54 parasites], preheated to 37°C, was added. This was followed by 500 µL freshly collected, washed, type A+, packed erythrocytes to establish a ~5% haematocrit culture. The erythrocytes were suspended and transferred to 75 cm^2 culture flasks (T75, Nunc) and gassed for 30 s with a special gas mixture containing 90% nitrogen, 5% oxygen and 5% carbon dioxide (Air Products, Johannesburg, South Africa). The flasks were sealed air-tight and incubated at 37°C.

Parasite growth was monitored daily by visual microscopic inspection of thin smears which were fixed with methanol (MeOH) and stained with a 10% (v/v) Giemsa stock solution (Merck) in phosphate buffered saline (PBS, pH 7.4, Lonza Walkersville). Parasitaemia was calculated by counting the equivalent of 1000 erythrocytes using the Miller technique for reticulocyte counting (158) at 1000x magnification with an Olympus BX41 microscope. This counting technique requires an evenly distributed erythrocyte smear across the microscope field and makes use of an ocular micrometer disk. It consists of two squares whose area has a ratio of 1:9; the small square occupies one corner of the large square. The principle involved in the use of the Miller ocular is the counting of the scarce element (parasites) in the large square and the estimation of the incidence of the common element (erythrocytes) from counts made in the small square only. This is performed on 10 randomly adjacent fields until a total of 100 erythrocytes were counted in the small squares. By extrapolation, the equivalent of 1000 erythrocytes were inspected for parasites and the percentage parasitaemia was calculated as follows:

$$\% \text{ Parasitemia} = \frac{100 \text{ X parasites in large squares}}{\text{Erythrocytes in small squares X } 9}$$

Parasitaemia was generally maintained between 3-5%. Culture medium was replaced daily and the parasites were gassed with the special gas mixture for 40 s before incubation at 37°C. Once thawed, the cultures were not grown for longer than 3 months to prevent genetic alteration. Ring-stage parasite-infected pellets (5-10% parasitaemia) were cryopreserved with equal volume of freezing media (20% glycerol/wash medium) on a regular basis and stocks were preserved at -80°C.

3.2.2. *In vitro* cultivation of sexual stage *P. falciparum* parasites (gametocyte cultivation)

Formal training in gametocyte culturing, mosquito feeding, mid-gut and salivary gland dissections was received at the Armed Forces Research Institute for Medical Sciences (AFRIMS) in Bangkok under the supervision of Dr Jetsumon Sattabongkot.

A method for the development of *in vitro P. falciparum* parasites' sexual stages (gametocytes) using strains 3D7, 7G8 and NF54 was subsequently developed using a combination of protocols by Carter *et al.* (159), the candle jar method from the AFRIMS (Dr Sattabongkot; personal communication) as well as from Megan Dowler (Walter Reed Army Institute of Research, WRAIR; personal communication). The methodologies were compared in order to obtain cultures with consistently high numbers of gametocytes and are described below.

3.2.2.1. Candle jar method

The candle jar method is used routinely at AFRIMS and Walter Reed Army Institute of Research with good success. A 5 mL asexual parasite culture grown in a T25 flask with a parasitaemia of between 3-5% was transferred aseptically to a 50 mL tube to which 1.8 mL fresh A+ erythrocytes was added for a 6% starting haematocrit in 23.2 mL culture media (no antibiotics, 10% human serum added). This was mixed well and 5 mL was added to each well of a 6-well tissue culture plate. The plate was then placed into a candle jar and the candle lit. The lid of the candle jar was secured with a very small gap until the candle burned out, thereafter, the lid was closed; vacuum grease was used around the lip of the lid to ensure a tight seal. Media changes were performed daily and a slide warmer set to 37°C was set up in the hood to prevent excessive cooling of the gametocyte cultures whilst outside of the incubator.

The gametocyte cultures were sub-cultured routinely on a Monday/Thursday cycle using the youngest culture in the series. One well of the six was used to start a new culture as described above. Each culture set started out in 6-well plates, the contents of the wells (25 mL) were then pooled and transferred to a T75 flask around day 10/11 or when candle jar space was not available for the newest subculture. Proper use of the candle jar results in the gas phase being 2-3% CO_2 and 14-17% O_2 compared to the 5% CO_2, 5% O_2 mixture used for gassing flasks. Only 3D7 and 7G8 parasite strains were available at the time of this experiment.

3.2.2.2. Flask method

The method for sexual stage culturing in a culture flask was based on the protocol developed by Carter *et al.* (159). An unsynchronised, asexual *P. falciparum* parasite stock culture at a parasitaemia above 4% was diluted to a starting parasitaemia of 0.5-0.7% at a 6% haematocrit. The diluted culture was made up to 15 mL using complete media (no antibiotics, 10% (/v/) human serum) in a T75 tissue culture flask and gassed with the special gas mixture (5% O_2, 5% CO_2 in N_2) for 40 s. Media changes were performed daily with pre-warmed media and a slide warmer set to 37°C was again used to prevent excessive cooling of the cultures whilst outside the incubator. After 4-5 days, when the asexual stage parasitaemia reached 5-10%, thin smears were made, fixed with MeOH and stained with a 10% (v/v) Giemsa stock solution (Merck) in phosphate buffered saline (PBS, pH 7.4, Lonza Walkersville) in order to examine the cultures for changes in morphology associated with stress, such as slightly triangular ring forms. When these signs were observed, the haematocrit was reduced to approximately 3.5% by increasing the amount of fresh media added from 15 mL to 25 mL. The cultures were maintained with daily media changes of 25 mL until mature gametocytes (stage V) were observed.

The gametocyte cultures initiated in flasks were not sub-cultured. New gametocyte cultures were started from the stock flask of asexual parasites. This method was tested using both 3D7 and 7G8 parasite strains as well as NF54 (MRA-1000 ATCC, MR4) parasites.

3.2.2.3. Monitoring of exflagellation

Gametocyte cultures were inspected for gametogenesis (exflagellation) of the male gametocyte (microgamete) by monitoring exflagellation microscopically from day 13 onwards. Terminally differentiated malarial gametocytes remain in a developmentally arrested state until they are taken up by the mosquito (160). The gametocytes then undergo gametogenesis in the mosquito mid-gut within minutes after ingestion of the infected blood meal. *In vitro* gametocyte cultures are assessed prior to mosquito feeding for the presence of exflagellation, an indication of parasite maturity and potential infectivity.

Exflagellation slides were made during the daily media change after removing the media and making a thin smear. Before fresh media was added, the contents of the flask were gently mixed and a small drop of culture material placed on a clean slide and covered with a petroleum jelly-ringed cover slip. The cover slip was gently tapped into contact with the drop. Exflagellation was best observed when the density of the drop allowed the cells to be closely packed together

in a single layer rather than crowded in overlapping layers. Exflagellation was checked after 15 min at 21°C at 200x magnification. In order to observe the exflagellating parasite one must rest one's eyes on the visible field and look for vibrating/jiggling movement and small areas where cells have been cleared to determine whether an exflagellating gametocyte is responsible. A magnification higher than 200x is not recommended as Brownian motion is then strongly visible and may obscure the motions caused by exflagellation. Rating exflagellation is very subjective but was rated using the scale currently used at Walter Reed: 1+: poor exflagellation (1-2 every 5 fields); 2+: some exflagellation (4-10 every 5 fields); 3+: good exflagellation (3-5 per field); 4+: excellent exflagellation (10-15 per field).

3.2.3. Mosquito rearing

The mosquitoes used in this study were kindly reared by Professor Lizette Koekemoer and staff at the Vector Control Reference Unit/Malaria Entomology Research Unit at the National Institute for Communicable Disease (NICD, Sandringham, Johannesburg). The mosquitoes fed are listed in Table 3.1.

Table 3.1. Mosquitoes fed for malaria infection studies. The mosquitoes were reared at the Vector Control Reference Unit/Malaria Entomology Research Unit at the National Institute for Communicable Disease in Johannesburg, South Africa.

Species	Colony name	Country of origin
Anopheles gambiae	SUA	Liberia
An. gambiae	TONGS	Ivory Coast
An. funestus	FUMOZ	Mozambique

3.2.4. Mosquito feeding and dissections

3.2.4.1. Mosquito preparation

Approximately 150 female *An. gambiae* and *An. funestus* mosquitoes (4-7 and 14-21 days post emergence (dpe), respectively) were collected from the insectary for feeding. *An. funestus* mosquitoes were used at 14-21 dpe as this was the age that the staff at the NICD were previously able to successfully infect these mosquitoes with *P. berghei*, a rodent malaria. The mosquitoes were placed in the Richard Hunt Insectary (a secure laboratory, NICD, Johannesburg, South Africa) at 26°C and 80% humidity and kept in a 16/8 h light/dark cycle. The mosquitoes food source (sugar pads: cotton wool soaked in a 10% sugar solution) were

removed 24 h prior to feeding the mosquitoes in order to starve the mosquitoes so that they would subsequently feed well on the blood.

Mosquito membrane feeders (Hemotek system, Discovery Workshops, UK) were set at 38°C and baudruche transparent membrane (supplied with the membrane feeder) was stretched over the feeder and secured using an O-ring. The gametocyte cultures produced in section 3.2.2.2 were used. For the purposes of mosquito feeding, the asexual parasites were not selectively killed once gametocytes began to form, thus, a mixed gametocyte population existed (stages I-V) containing a small percentage of asexual parasites. The sexual cultures consisted of predominantly mature gametocytes (stages IV-V) from days 14 through 17. Gametocyte cultures (approximately 2% gametocytaemia) were spun down for 5 min at 2500*g* in a centrifuge pre-warmed to 37°C and the pellet (approximately 500 µL) gently re-suspended in an equal volume fresh O+ erythrocytes and 2.5-3 mL warm human serum (from section 3.2.1.). This feed mixture was placed into the feeders; as a general rule, gametocytes from 1 flask filled one feeder, that is a 500 µL culture pellet with fresh blood and serum. The feeders with the blood were place on the netting covering the cartons of mosquitoes and the feeders and cartons were covered with a damp cloth. Blowing in the cartons as soon as the mosquitoes started feeding was performed at regular intervals every 5-10 min to increase the numbers of mosquitoes finding the feeder. The feed was completed when the feed mix was drained or crusty/dried or when visual inspection showed the mosquitoes were replete; this could be as soon as 15-20 min. Unfed mosquitoes were separated from the fed ones and the fed mosquitoes' sugar pads were replaced.

3.2.4.2. Mosquito mid-gut dissections and sporozoite isolation from salivary glands

Oocysts are visible in an infected mosquitoes' mid-gut from 7 days post-infected blood meal, but are easiest to see 9-10 days after the feed (Dr J Sattabongkot, personal communication). The mid-guts of 10 mosquitoes per fed colony were checked each day for oocysts 7-10 days after feeding. The mosquitoes were taken out of the carton and immobilised by placing them in the freezer for 2 min. They were then placed in a Petri dish and kept on ice so that they did not revive. Each mosquito was placed in a drop of sterile PBS and using a stereo-microscope, the dissection needles were placed firmly, but gently enough so as not to squash the mosquito, onto the thorax and the other needle was placed on the bottom segments of the mosquito's abdomen. The needle on the abdomen was gently pulled downward until the mid-gut was visible (Figure 3.2). The mid-guts were stained with 0.1% mercurochrome for several minutes to

stain the oocysts before placing a cover slip over them. They were viewed at 100x magnification (using bright field microscopy).

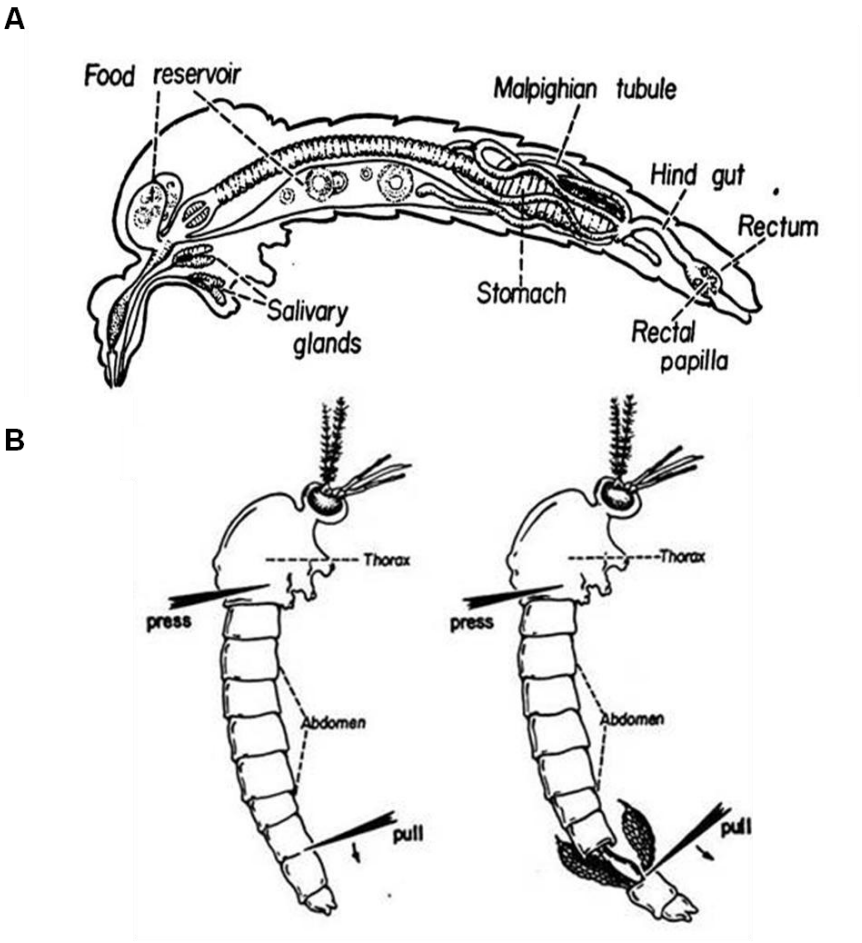

Figure 3.2. Mosquito mid-gut dissections. **A.** Diagrammatic side view of the female mosquito showing internal organs (ovaries omitted) (161). **B.** The position of the needles on the thorax and lower segment of the mosquito to dissect out the mid-gut (161).

Lying under the alimentary canal in the forward part of the thorax are the salivary glands. There are two sets of these, each having three lobes with a common duct which joins the duct from the other set a short distance before they enter the base of the hypopharynx (162). Each of these lobes is made up of a layer of secreting cells which produces the saliva that is injected into the wound as soon as the insect pierces the skin of the victim; it is in these glands that one finds the sporozoites. Sporozoites should be visible 16-22 days post feeding. Mosquitoes were dissected (20 individual mosquitoes per colony) every second day from days 16-22 to microscopically detect sporozoites. Mosquito salivary gland dissections were performed as described by Strome *et al.* (163) using a stereo microscope. Each knocked mosquito was placed in a drop of PBS and the dissection needles placed on the head and thorax as illustrated in Figure 3.3. The head of the mosquito was gently removed from the thorax to expose the

glands, which were then severed from the head. After recovering the gland a cover slip was placed on top of the gland to rupture it and the sporozoites viewed with phase contrast at 200x magnification.

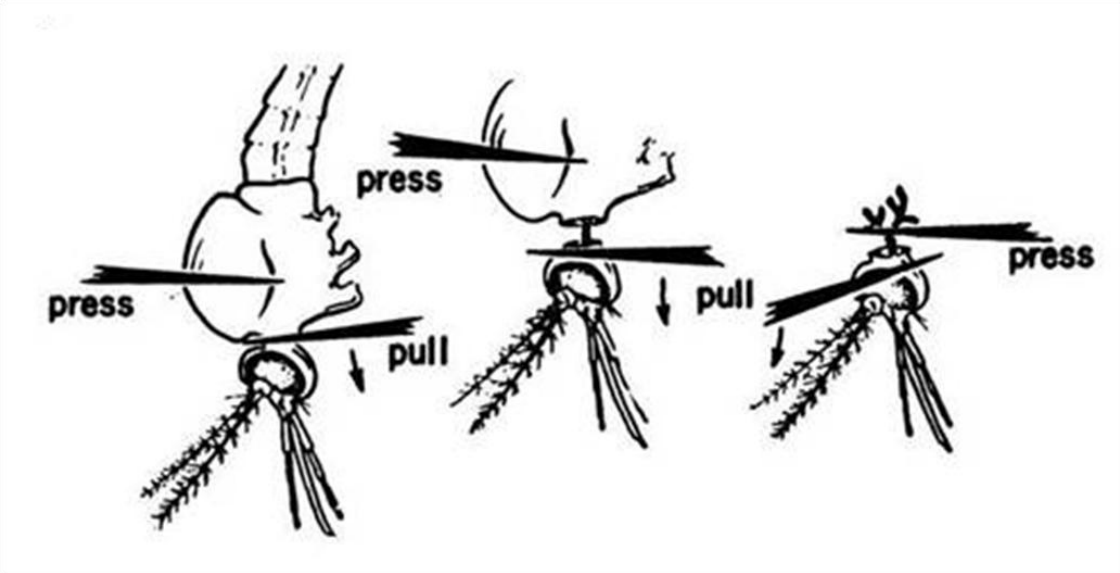

Figure 3.3. Mosquito salivary gland dissections. The position of the dissection needles on the thorax and head of the mosquito and removal of the salivary glands (161).

3.2.5. Populating 3D scaffolds and 2D wells with hepatocytes

The methodology applied was the same as in Chapter 2 section 2.2.3. Briefly, scaffolds (PP-*g*-PNIPAAM-B, Table 2.2) of size 5x5x3 mm were sterilised in 70% ethanol for 1 h, rinsed three times in 1x PBS and allowed to dry in a laminar hood. The scaffolds were soaked overnight at 37°C in the cell culture media specific for the cell-line used, to reduce any surface tension effects as well as to ascertain whether the scaffolds had been effectively sterilised prior to seeding the non-woven scaffolds with the hepatocytes (114). The HC04 hepatocytes were cultured in 1:1 DMEM:Hams F12 media (Lonza) with 2 mM L-glutamine and supplemented with 10% (v/v) FCS, 100 g/mL penicillin and 10 µg/mL streptomycin (Sigma-Aldrich Chemie). Hepatocytes growing in culture flasks were trypsinised and re-suspended to a final concentration of 2 x 10^6 cells/mL. A 200 µL aliquot of this cell suspension was gently dripped onto each of the non-woven scaffolds in a 96-well plate, resulting in a final concentration of 4 x 10^5 cells seeded into each scaffold.

The scaffolds were incubated at 37°C for 2 hpi to allow the cells to attach to the scaffolds. Thereafter, the scaffolds were removed from the 96-well tissue culture plate using sterile tweezers and placed into the well of a 6-well tissue culture plate with 3 mL media and cultured

under standard conditions. Scaffolds containing the HC04 hepatocytes were maintained in culture for a period of 14-16 dpi with media changes performed every 48 hpi.

Two days before infecting the hepatocytes with the sporozoites (see below), 2 x 10^4 HC04 hepatocytes were seeded into the wells of a 96-well plate and maintained under standard conditions. These served as the 2D control; three wells per time point were seeded as well as three wells to be used as the uninfected control. On the day of infection, the hepatocytes were approximately 60-70 % confluent (155).

3.2.6. Seeding sporozoites into 2D hepatocytes and 3D scaffolds

Prior to seeding the 2D hepatocytes and 3D scaffolds with the sporozoites, the scaffolds were aseptically removed from the media in the 6-well plate and each placed into individual wells of an empty 6-well plate; this was done so that when the sporozoites were seeded into the scaffold they were not able to float off into the surrounding media. The media was aspirated out of the wells of the 96-well plate where the 2D cells were growing.

Cryopreserved infectious *P. falciparum* NF54 sporozoites were obtained from Sanaria Inc (Rockville, MD, USA) as six vials of non-attenuated sporozoites in a liquid-nitrogen dry shipper with a temperature monitoring device so as to maintain the viability of the cryopreserved sporozoites. The vials contained 195 542 ± 8 151 sporozoites, each with sporozoite membrane integrity of 88.6% ± 1.35%, as determined by Sanaria Inc. A 6 day hepatocyte potency assay resulted in 22 parasites expressing PfMSP-1 per well, also as determined by Sanaria Inc. The sporozoites were shipped in a temperature monitored container ensuring the cold chain was not broken at any point.

Upon their arrival, the vials were transferred to a liquid nitrogen tank and stored in the liquid nitrogen vapour phase. The sporozoites (20 µL, ±195 000 sporozoites per vial) were thawed for 30 s in a circulating water bath set to 37°C. They were resuspended in 180 µL invasion media [1:1 DMEM:Hams F12 media (Lonza) with 2 mM L-glutamine and supplemented with 10% (v/v) human serum (Interstate Blood Bank), 200 g/mL penicillin and 20 µg/mL streptomycin (Sigma-Aldrich Chemie)] as stipulated in the protocol supplied with the parasites. The sporozoites were gently mixed and 40 µL (approximately 4 x 10^4 sporozoites) was added to each 3D scaffold (n=3) and 2D well (n=3; an approximate 1:2 ratio of sporozoite to hepatocytes). The sporozoites were allowed to invade for 6 h under standard incubation conditions following which media was gently added to the 3D scaffold and fresh media replaced the 40 µL in the 2D wells. 2D and 3D

scaffolds were harvested on days 3 and 7 post invasion; 2D samples were trypsinised and pelleted via centrifugation at 500*g* for 5 min, the supernatant was aspirated and the pellet was washed with an equal volume of PBS. All the samples were stored in liquid nitrogen to retain the stability of the samples.

3.2.7. gDNA isolation

Frozen 2D and 3D samples from section 3.2.6 were removed from liquid nitrogen storage and completely defrosted. gDNA was isolated with the DNeasy® Blood and Tissue Kit (Qiagen) according to the kit instructions. Proteinase K (20 µL) and 40 µL RNAse A (10 mg/mL, Fermentas Life Sciences, Ontario, Canada) were added to the samples and incubated at room temperature for 2 min. Following this, 200 µL Buffer AL was added to each sample. Buffer AL contains chaotropic salts and detergents, the chaotropic salts allows DNA to bind to the silica matrix (164) in the DNeasy spin column. The samples were vortexed and incubated at 56°C to lyse the cells. The samples were then placed into QIAShredder columns and centrifuged at 16 000*g* for 3 mins to ensure that the hepatocytes and sporozoites were fully lysed as well as to separate the cells from the 3D scaffolds. Ethanol (200 µL of 100%) was added to the samples and mixed well. Thereafter the samples were pipetted into a DNeasy spin column and centrifuged at 6 000*g* for 1 min. The DNA-bound membrane was then washed with 500 µL buffer AW1 followed by 500 µL buffer AW2. The samples were spun for 3 min at 16 000*g* to ensure that any residual ethanol was removed from the membrane. They were then placed in a clean 1.5 mL centrifuge tube and the gDNA eluted by gently pipetting 100 µL ddH_20 onto each of the membranes. The samples were incubated at room temperature for 1 min and thereafter spun at 16 000*g* for 1 min to elute the DNA.

The concentration of the gDNA was determined by measuring the absorbance at 260 nm by UV spectrophotometry with a NanoDrop-1000. For double stranded DNA one absorbency unit equals 50 ng/µL (165). Purity from protein contamination was estimated from the 260 nm/280 nm ratio which should be between 1.7 and 1.9 (165) as proteins have a maximum absorbance at 280 nm.

3.2.8. TaqMan® assay

The principle of the TaqMan® assay is based on a fluorogenic probe (TaqMan® probe), complementary to the target sequence being added to the PCR reaction mixture. This probe is an oligonucleotide with a reporter dye (fluorophore; FAM) attached to the 5' end and a quencher

dye (TAMRA) attached to the 3' end. While the probe is not hydrolysed, the quencher and fluorophore remain in close proximity to each other. During the PCR reaction the probe anneals in the selected specific region between the forward and reverse primers; the polymerase then carries out the extension of the primer and replicates the template to which the TaqMan® probe has bound. The 5' exonuclease activity of the polymerase cleaves the probe, releasing the fluorophore away from the close vicinity of the quencher. The fluorescence of the fluorophore increases and is detected by the light cycler.

Three controls were included in the TaqMan® assay. gDNA was extracted from asexual parasite cultures (trophozoites) with a parasitaemia of 5%, 2.5%, 1%, 0.1% and 0.01% using the same methodology described in sections 3.2.7. gDNA was also extracted from ± 3 $x10^4$ sporozoites to be used as a positive control as well as from uninfected hepatocytes growing in the 3D non-woven scaffolds and in 96-well tissue culture plates as described in section 3.2.6.

Primers to detect the 18s rRNA gene in *P. falciparum* were supplied by Dr Jetsumon Sattabongkot, (AFRIMS, Bangkok, Thailand); they were designed by Professor Osamu Kaneko (Institute of Tropical medicine (NEKKEN), Nagasaki University, Nagasaki, Japan). The primer and probe sequences are as follows: forward primer: 5'- GTG TGT CTA ACA CAA GGA AGT -3'; reverse primer: 5'- ACA ATT CAT CAT ATC TTT CAA TCG GTA-3' and probe: 5'- FAM TTG TAC ACA CCG CCC GTC GCT C TAMRA-3'.

Primers to detect the β-actin gene of HC04 hepatocytes, which serves as the control gene for data normalisation, were from the paper of Tanaka *et al.* (166). Their sequences are as follows: forward primer: 5'-CAG TGT GAC ATG GTG CAT CT-3'; reverse primer: 5'- GTG AGG ATC TTC ATG AGG TAG TCA-3' and TaqMan® probe: 5'-FAM-ACG TTG CTA TCC AGG CTG TGC T- TAMRA-3'. The β-actin hepatocyte gene was used to correct for the differing number of hepatocytes within the 2D and 3D culture systems to generate a relative ratio of EEF's per hepatocyte in the 3D vs the 2D system. The primers and probes were synthesised by Integrated DNA Technologies (Leuven, Belgium).

Each 20 µL reaction contained 1 x TaqMan® Universal Master Mix II (Applied Biosystems), 200 nM of both the forward and reverse primers, 50 nM probe, 10 µg gDNA template and the balance up to 20 µL, nuclease-free water. The thermal cycles were as follows: 95°C for 10 min followed by 55 cycles of denaturing at 95°C for 15 s and extension at 60°C for 1 min. Three biological replications were run and each with technical triplicates.

The presence of the *P. falciparum* 18s rRNA gene was determined as well as the hepatocyte β-actin gene in each of the samples in order to generate a ratio to correct for the differing number of hepatocytes in the 2D and 3D system. The ratio generated from the 3D system was then compared relative to the 2D ratio to gauge which system permitted greater sporozoite invasion per hepatocyte.

3.3. RESULTS

3.3.1. Gametocyte production and exflagellation

Previously described methods for the production of *P. falciparum* gametocytes were compared to determine optimal conditions for gametocyte production for subsequent use in mosquito feeding to obtain sporozoites for hepatocyte infection studies. Several conditions could induce *P. falciparum* parasites to differentiate from asexual forms to their sexual gametocytes, and both the candle jar and flask methods described here depend on high parasite numbers and reduced haematocrit resulting in parasite stress to induce gametocytogenesis (Dr Sattabongkot and colleagues at AFRIMS, Megan Dowler at the Walter Reed Army Institute of Research; personal communications, (159, 167)). Indicators of parasite stress include triangular ring stages as well as hazy or faint looking trophozoites and schizonts (159).

Comparison of the candle jar method to the flask method indicated that, for the majority of *P. falciparum* strains used, the flask method was superior in its ability to produce gametocytes (Figure 3.4). The candle jar method proved to be cumbersome and impractical given incubator space as a limiting factor. Additionally, this culturing method resulted in the formation of many spiculated cells (possible erythrocyte artefacts) as well as pyknotic, dead parasites showing signs of degradation including dark and lumpy parasite staining (168). Degenerate stage IV and V gametocytes appear as dark, lumpy, constricted or broken parasites with pigments often dispersed in irregular clumps (168) such as the gametocytes observed in Figure 3.4 (red box). Comparatively, gametocytes could be routinely produced in T75 culture flasks (flask method, (159)) for 7G8 and NF54 *P. falciparum* strains. For this method, the overall morphology of both sexual and asexual parasites in the culture was consistent with normal / healthy parasites and very few pyknotic, dead parasites were observed (Figure 3.4). Moreover, the erythrocytes themselves were much better adapted to this culturing method compared to the high number of spiculated erythrocytes observed with the candle jar method.

In addition to testing the various gametocyte production methods, several strains of *P. falciparum* parasites were evaluated for their ability to produce gametocytes. The 3D7 *P. falciparum* parasite strain continually failed to produce gametocytes even under different experimental methods used (Figure 3.4). However, qualitative morphological monitoring indicated that *P. falciparum* NF54 parasites proved superior to 7G8 parasites in their ability to generate gametocytes of various developmental stages (Figure 3.4).

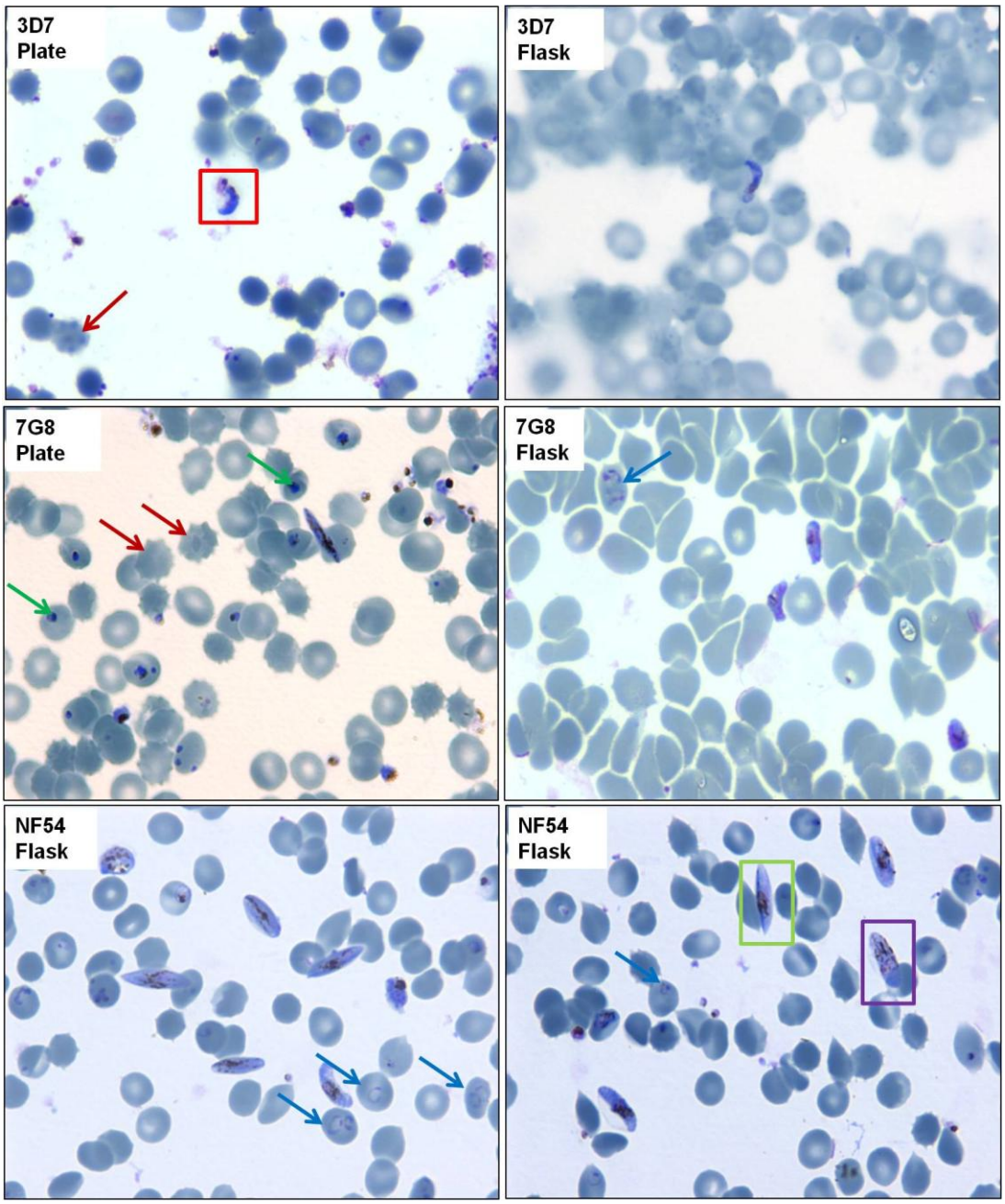

Figure 3.4. A qualitative comparison of the different gametocyte producing methods using 3 parasite strains after 10 days in culture. Culturing *P. falciparum* 3D7 and 7G8 parasites in 6-well plates in the candle jar did not result in good gametocyte production; many spiculated erythrocytes were observed as indicated by the red arrows and the green arrows indicate dead parasites. The 3D7 parasite as outlined in the red box appears dark and lumpy, an indication of degeneration (168). Using the flask method to initiate gametocytes in 3D7 and 7G8 parasites fewer dead parasites were observed but gametocyte production remained suboptimal as very few gametocytes were observed. Ten days after initiating gametocyte production using the flask method with *P. falciparum* NF54 parasites, good gametocyte production was observed as judged by the abundance of gametocytes observed across the microscope slide. The cultures consisted of predominantly stage IV and V parasites as indicated by the green and purple box respectively, though it was not uncommon to see earlier stages. Ten days after gametocyte initiation asexual parasites were still observed as indicated by the blue arrows. All parasites were stained with Giemsa stain and observed at 1000x magnification using an Olympus BX41 light microscope.

Quantitative analysis of various observed parameters of the gametocyte production methods was subsequently performed. The parameters measured include the number of spiculated cells, asexual parasites, dead/pyknotic parasites, parasites outside erythrocytes, degenerate gametocytes and healthy gametocytes (Figure 3.5). Three represented microscope fields were counted per parasite strain and culturing method and the variables are expressed as a percentage of the total erythrocytes per field. Based on these results, it is evident that the candle jar method results in extreme stress for both the parasites as well as erythrocytes in the culture. High levels (~2-fold and 3.5-fold increase for the 3D7 and 7G8 parasites, respectively) of spiculated cells were observed when culturing with the candle jar method vs. using the flask method. Additionally, dead asexual parasites and parasites outside erythrocytes were observed at higher numbers in the candle jar method compared to the flask method. From Figure 3.5, it is also clear that the flask method was the only method able to produce ~7 ± 3% gametocytaemia.

Comparison of strain-specific differences in gametocyte production again iterated that *P. falciparum* NF54 parasites are the most reliable gametocyte producing strain. Producing gametocytes from *P. falciparum* 7G8 parasites (flask method) still resulted in 8 ± 2% spiculated cells in addition to 3 ± 2% asexual parasitaemia still present in the culture 10 days after induction of gametocyte production. This indicates that these parasites are unable to maximally convert asexual parasites to gametocytes. In contrast, for the *P. falciparum* NF54 parasites, very few (4 ± 2%) spiculated cells, pyknotic or degenerate parasites were observed, indicating that overall this parasite strain was adequately adapted to the culture conditions for gametocyte production. Additionally, this was the only strain able to produce ~7 ± 3% gametocytaemia; 9.5-fold more than for the 7G8 parasites.

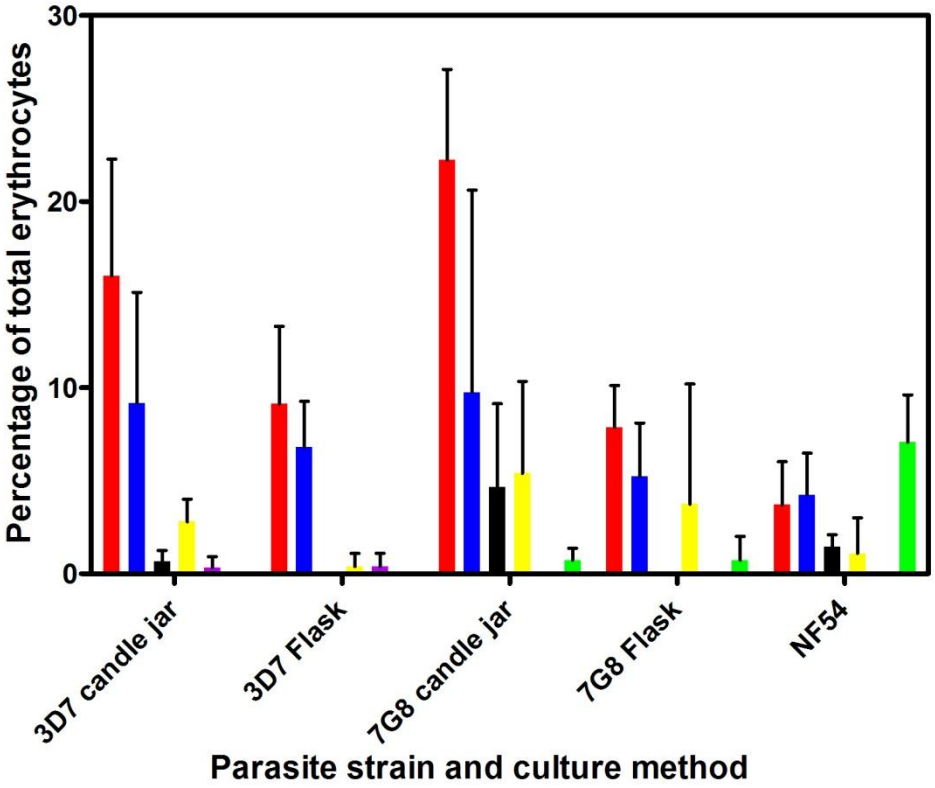

Figure 3.5. A comparison of culture health and gametocyte production between the candle jar and flask method and the three parasite strains. Various observed parameters in each of the culture methods (flask/plate) and for each of the different parasite strains (3D7, 7G8 and NF54) after 10 days in culture were measured. NF54 parasites were only cultured using the flask method. The number of spiculated erythrocytes (red bars), asexual parasites (blue bars), dead/pyknotic parasites (black bars), parasites outside the erythrocytes (yellow bars), degenerate gametocytes (purple bars) and healthy gametocytes (green bars) were counted. Data are from one representative experiment for each strain and culture method tested and are represented as the average of the percentage of the total number of erythrocytes from three adjacent microscopes field ± standard deviations.

After identifying the flask method and *P. falciparum* NF54 strains as the optimal combination for the production of gametocytes, the stage-specificity, production of male and female gametocytes and kinetics of gametocytogenesis could be evaluated. All five previously described stages of gametocyte maturity during gametocytogenesis of NF54 strain *P. falciparum* parasites could be detected (Figure 3.6 A). Stage descriptions are as described by Carter and Miller (168). Stage I gametocytes are the earliest stage at which gametocytes may be distinguished from a trophozoite; they are small rounded parasites one third to half the diameter of an erythrocyte, the cytoplasm is clear or light staining and is never vacuolated or amoeboid. Stage II gametocytes are identified by one side of the parasites becoming extended giving the parasite an overall half-moon shape; one side is smoothly rounded and the other side straight, and the two ends are sharply pointed. At this stage the parasite occupies up to half the erythrocyte; the erythrocyte is not distorted; pigment formation is almost complete and the granules tend to spread out along the axis of elongation (Figure 3.6). Stage III gametocytes are

identified when the pointed ends of stage II begin to become bluntly rounded and if still visible the erythrocyte becomes markedly distorted along the axis of the steadily elongating parasite (Figure 3.6). Stage IV gametocytes continue to grow along the direction of its axis and the two ends become pointed once again; pigment granules remain widely spread over the length of the parasite which is not bent or curved. Stage V gametocytes represent the point at which the gametocytes reach full morphological maturity and are crescent shaped (Figure 3.6).

In addition to the ability to successfully produce all stages of gametocytes, both male and female mature gametocytes were seen in the cultures from days 10 - 16 in fully mature stage V gametocyte cultures (Figure 3.6 B). At this stage, male and female gametocytes can be differentiated from one another. The mature macrogametocyte (female) is characterised by blue staining cytoplasm and is more elongated than the microgametocyte (male). The chromatin and pigment granules of the females are closely aggregated at the centre of the parasite; both chromatin and pigment granules are more spread out in the male (168) (Figure 3.6). Based on this morphological evaluation, it is therefore clear that an optimised protocol was established for gametocyte production with *P. falciparum* NF54 parasites, resulting in mature male and female gametocytes necessary for mosquito feeding studies.

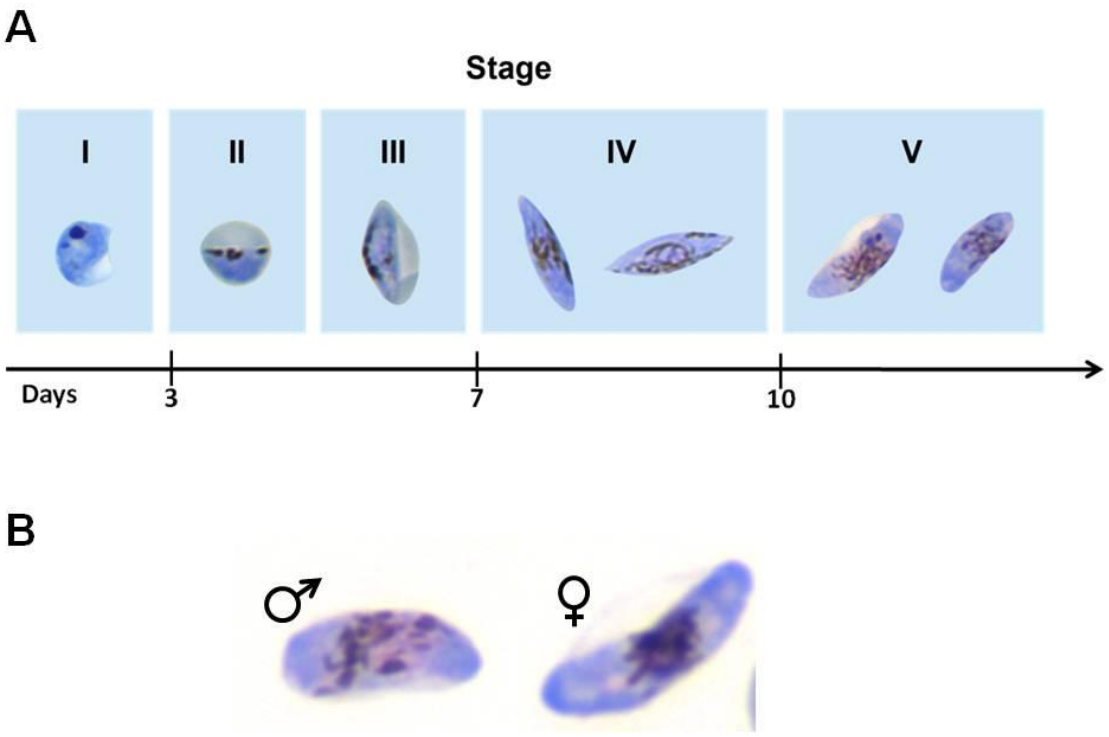

Figure 3.6. Gametocyte staging and sexing. **A.** Identification of Giemsa stained *P. falciparum* NF54 gametocyte stages I-V visualised at 1000x magnification using a light microscope (Olympus BX41). Stage II and III parasites were visualised after 3 days in culture stage IV were present after 7 days in culture and mature gametocytes were prevalent after 10 days in culture. **B.** The mature macrogametocyte (female) is characterised by blue staining cytoplasm and is more elongated than the microgametocyte (male). The chromatin and pigment granules of the females are closely aggregated at the centre of the parasite; both chromatin and pigment granules while tending to centralise are more spread out in the male (168).

In addition to the morphological evaluation of gametocyte production, the kinetics of gametocyte production could be monitored as a measure of successful gametocyte production, which should correlate to a reduction in the number of asexual forms of the parasite (169). Under optimal conditions, the flask method resulted in the production of *P. falciparum* NF54 sexual stage parasites which could be first detected on day 3 after gametocyte induction based on microscopic detection of stage I and II parasites (Figure 3.5). At this stage, the culture was still predominated with asexual forms of the parasite (parasitaemia ~8%) as assessed microscopically and these asexual forms decreased around day 8 when gametocyte production increased (Figure 3.7). The production of sexual stage parasites steadily increased until gametocytaemia reached a peak of 2-6% of predominantly stage IV-V on day 15 under optimal conditions (Figure 3.7). The highest gametocytaemia observed at 6% was correlated to a rapid increase in parasitaemia to 8% on day 3, peaking at ~12% on day 5 followed by a decrease to 2% by day 7 (Figure 3.7A). Comparatively, a parasitaemia of 8% reached by day 9 may not be sufficient to trigger gametocyte formation and resulted in only a 2% gametocytaemia (Figure 3.7B). Few or no asexuals were observed from day 13 onwards (Figure 3.7). This was,

however, not a general phenomenon for each gametocyte culture and in some instances asexual parasites were observed up to day 16 (data not shown).

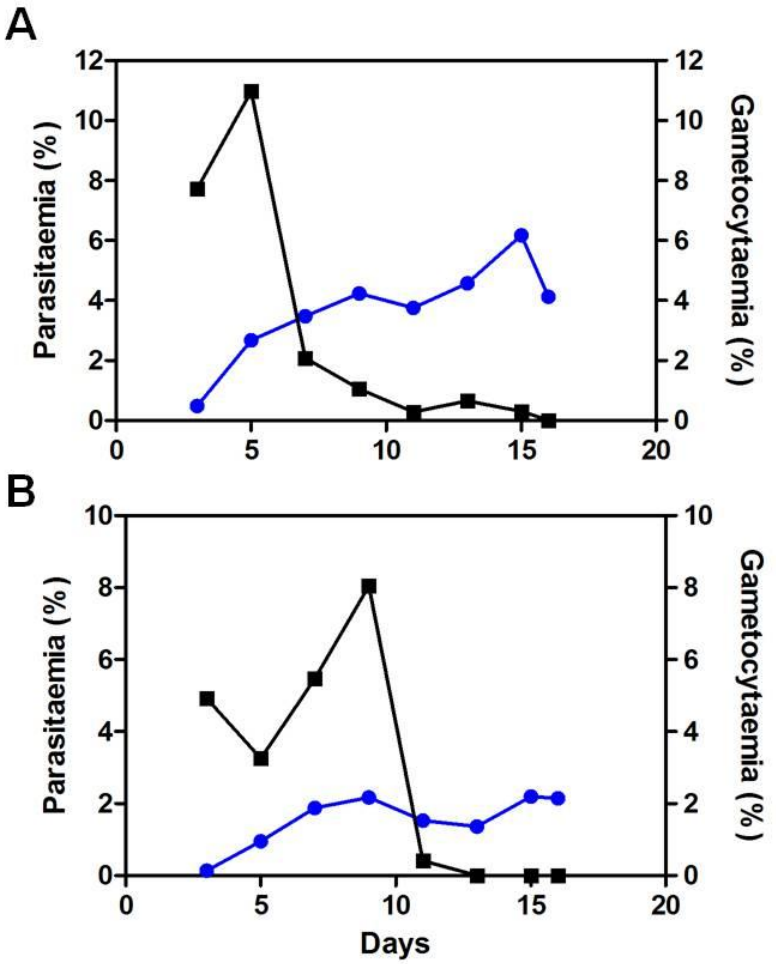

Figure 3.7. *P. falciparum* gametocytogenesis**.** Two independent gametocyte cultures were initiated using a mixed (asynchronous) population of parasites at 0.6% parasitaemia. The process of gametocytogenesis is depicted graphically in a high yielding culture (maximum gametocytaemia of 6%) (A) and a lower yielding culture (maximum gametocytaemia of 2%) (B). The number of asexual parasites (black line, solid squares) increased followed by a rapid decrease leading to a parasitaemia (asexual) of zero by day 16. Sexual forms were first detected on day 3 in both cultures (blue line, solid circle).

A certain proportion of the ring forms that appear in culture develop into gametocytes; this percentage represents the rate of conversion of asexual parasites to gametocytes (168) and is calculated using the following equation:

$$\text{Rate of conversion of asexual parasites to gametocytes} = \left[\frac{\text{No. of stage II gametocytes per 100 erythrocytes counted 48 h after ring forms}}{\text{No. of ring forms per 100 erythrocytes}} \right] \times 100$$

The two independent cultures described above (Figure 3.7) were examined on day 3, counting the number of ring-stage asexual parasites and again on day 5 for stage II gametocytes to

determine the conversion rate. The conversion rate of rings to gametocytes was 27% (2% final gametocytaemia, Figure 3.7B) and 32% (6% final parasitaemia, Figure 3.7A), respectively in the two independents cultures.

The conversion rates between the cultures do not appear to be significantly different, even though a 3-fold difference in end-point gametocytaemia is observed both cultures saw a conversion rate of ~30%. However, a correlation does appear to exist between high early parasitaemia and end-point gametocytaemia. The gametocyte cultures were initiated using an asynchronous asexual culture; the difference in end-point gametocytaemia may, therefore, be correlated to early prevalence of ring form asexual parasites. As such, the ratio of ring stage parasites to trophozoites was calculated for the first few days of the gametocyte culturing period (Table 3.2) and the two cultures were compared.

Table 3.2. The ring:trophozoite ratio. An initial high ring to trophozoite ratio was observed in culture A which rapidly declined; Culture B was observed to have an even ratio of rings to trophozoites which declined more slowly.

	Culture A	Culture B
	Ring:trophozoite ratio	
Day 3	2.3	1
Day 5	0.2	1.25
Day 7	0.083	0.59
Conversion rate	32%	27%
Final gametocytaemia	6%	2%

Culture A (Figure 3.7A) was observed to have an initial high number of rings as compared to trophozoites on day 3 of gametocyte culture (2.3 times more, Table 3.2). The number of rings re-emerging after 48 hours was substantially less as a ratio (rings:trophozoites) of 0.2 was calculated. This ratio further decreased by day 7. Culture B (Figure 3.7B) whose asexual parasitaemia increased more slowly than culture A had an even ratio of rings to trophozoites on day 3; the population of rings increase slightly 48 h later as evident by the higher observed ratio (1.25) and then as in culture A, the ring population was observed to decline.

One of the measures of functionality of *P. falciparum* gametocytes is to determine exflagellation of male gametocytes (microgametes) and this was used here to determine if the gametocytes

produced above are useful for mosquito infections. Exflagellating microgametes were observed on day 14-16 by monitoring exflagellation microscopically (Figure 3.8). Exflagellation can be identified by a small locus that rapidly vibrates/jiggles and is indicative of the presence of a viable male microgamete which, along with the female macrogamete, is necessary for oogenesis in the mosquito vector. Once good exflagellation is observed, a gametocyte culture is regarded as ready for mosquito feeding. Exflagellation rated 3+ or 4+ (as outlined in section 3.2.2.3) would be observed before a culture was deemed ready to be fed to the mosquitoes.

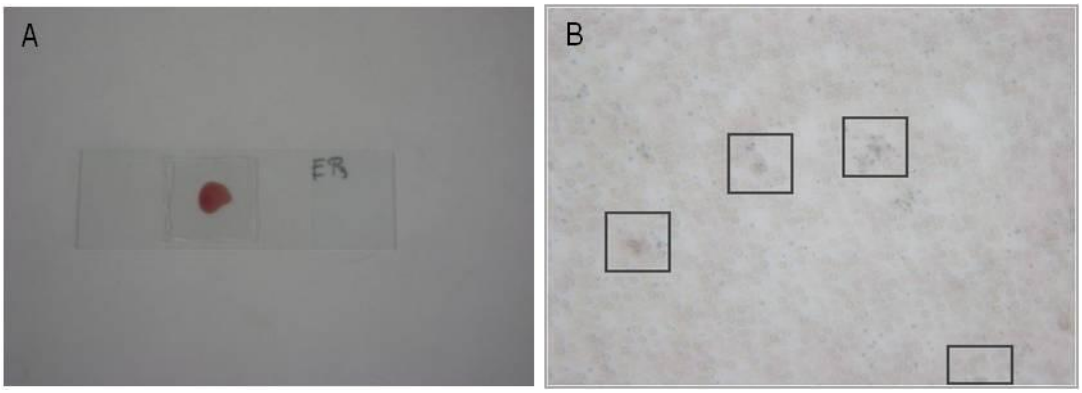

Figure 3.8. Mature microgamete exflagellation. **A.** An exflagellation slide; a drop of blood from a day 14-16 gametocyte culture is placed on a microscope slide and covered with a petroleum jelly rimmed cover slip and left to stand at room temperature for 20 min. **B.** A microscope image depicting four exflagellating microgametes in the microscope field (in grey boxes) in a blood droplet that had been at room temperature for 20 min. Visualised at 200x magnification.

3.3.2. Sporozoite invasion in 2D and 3D

3.3.2.1. Mosquito feeding and dissections

Mosquitoes were fed a parasite culture every two weeks over a period of 6 months. The mid-guts were dissected 7-10 days post feeding to determine if oocysts developed. Additionally, salivary glands were dissected 16-22 days post feeding to determine the presence of sporozoites. Although dissections were successful and were positive in detecting *P. berghei* in control systems (work conducted by Te-Chang M. Lo at the NICD), no oocysts or sporozoites could be detected after feeding *P. falciparum* NF54 gametocytes to the *An. funestus* mosquitoes as illustrated in Figure 3.9.

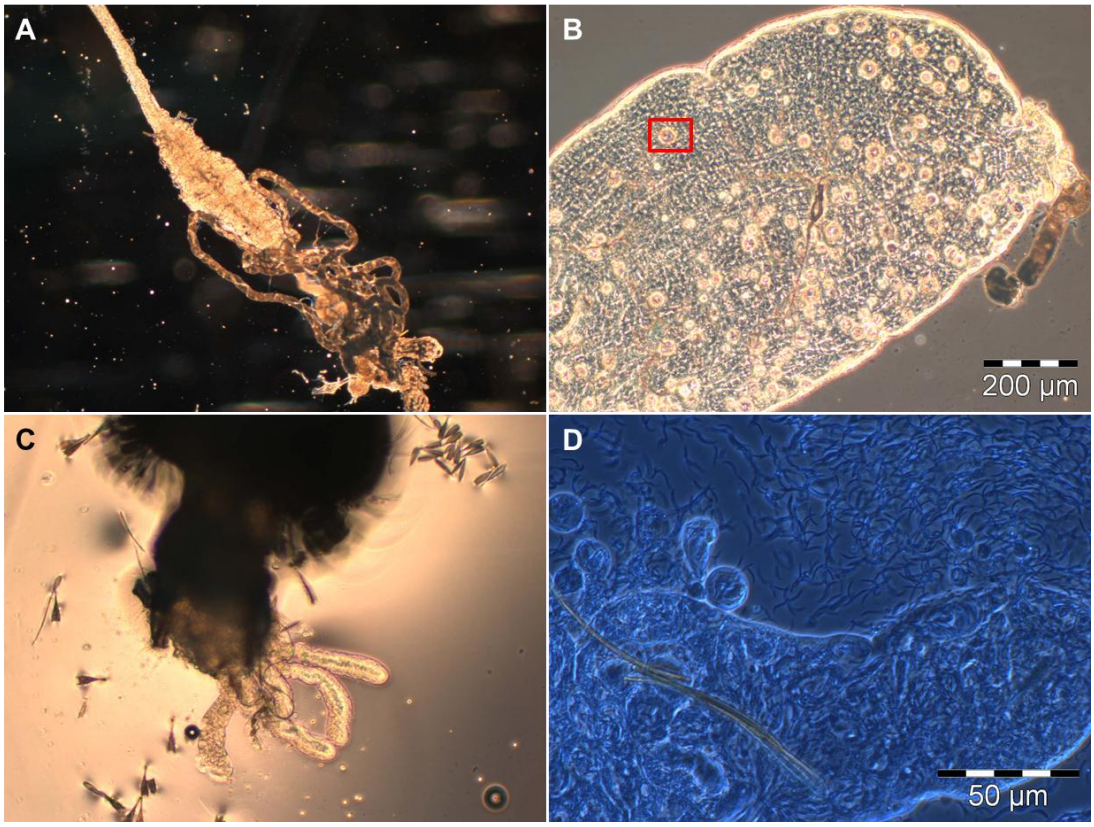

Figure 3.9. Mosquito mid-gut and salivary gland dissections. **A.** Photographed mosquito midgut and malpighian tubule at 50x magnification. **B.** FUMOZ midgut at 100x magnigfication; a *P. berghei* oocyst is outline in the red box; **C.** A bright field micrograph of uninfected mosquito salivary glands still attached the head at 50x magnification; **D**. *P. berghei* sporozoites surrounding a salivary gland. Photos B and D kindly supplied with permission by Te-Chang M. Lo, Malaria Entomology Research Unit, School of Pathology, Faculty of Health Sciences, University of the Witwatersrand, South Africa.

3.3.2.2. Sporozoite invasion of HC04 cells.

In order to enable testing of the scaffolds, *P. falciparum* NF54 sporozoites produced at Sanaria Inc. (USA) were obtained for the study. HC04 hepatocytes were maintained on PP-*g*-PNIPAAM-B scaffolds for 16 days prior to invasion with sporozoites as per section 3.2.6 (Figure 3.10 A). Another scaffold, Nylon-cont (Table 2.2. Chapter 2) was subsequently included as this scaffold has smaller pores (40 – 80 µm) and permits the hepatocytes to more densely populate the scaffold (Figure 3.6 B). This scaffold was used so that the sporozoites would be less able to navigate out of the scaffold via the pores.

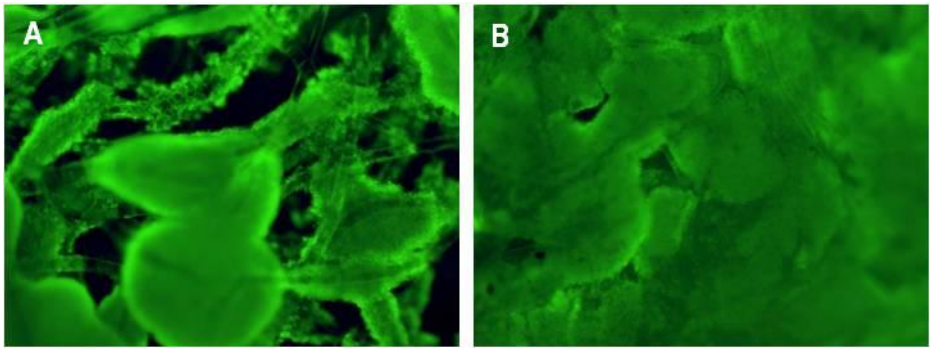

Figure 3.10. HC04 hepatocytes populating the non-woven scaffolds. **A**: PP-*g*-PNIPAAM-B and **B**: Nylon-Cont non-woven scaffolds after 16 days of growth. The cells were stained using fluorescein diacetate and visualised at 40x magnification using a standard fluorescence microscope (Olympus BX41) equipped with a 490 nm bandpass filter with a 510 nm cut-off filter for fluorescence emission.

3.3.2.3. Quantification of sporozoite invasion in HC04 cells

A qRT-PCR TaqMan® assay was performed to detect the parasites' 18S rRNA gene as an indication of sporozoite presence/invasion in HC04 cultures. The HC04 β-actin gene was used to normalise the data i.e. to correct for the differing number of hepatocytes in the 2D and 3D system. Presently the aim was not to accurately quantify parasite infection but to express invasion as a ratio of invasion in the 3D system relative to invasion in the 2D control system.

qRT-PCR was successful in detecting the *P. falciparum* parasites' 18S rRNA gene for quantification of parasites in control samples i.e. asexual parasites (5%, 2.5%, 1%, 0.1% and 0.01% parasitaemia) and purified sporozoites. Additionally, the HC04 β-actin gene was detected in uninfected hepatocytes growing in the 3D non-woven scaffolds as well as in 2D 96-well tissue culture plates. Low levels of *P. falciparum* parasites' 18S rRNA gene (very high C_T value) were detected in invaded 2D hepatocytes; average C_T values of 48.3 ± 1.3 at 3 dpi and 46.9 ± 2.7 at 7 dpi were observed (Appendix Table A1; Figure 3.11). The *P. falciparum* parasites'18S rRNA gene was however not detected in the invaded 3D hepatocytes.

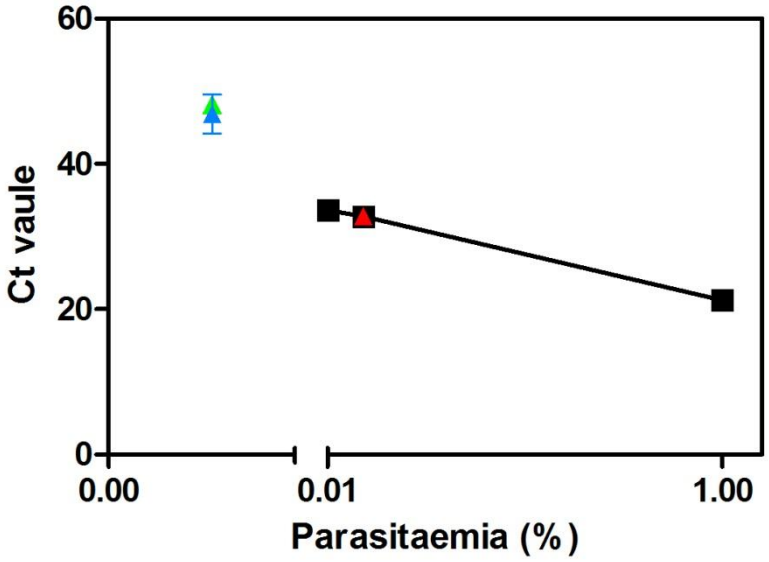

Figure 3.11. TaqMan® expression data. Asexual *P. falciparum* parasitaemia (0.01%, 0.1% and 1%) are plotted on the graph against the Ct value at which the *P. falciparum* 18s rRNA gene is first detected (black squares). The 18s rRNA gene in the positive sporozoite control (30 000 sporozoites) is plotted (red triangle); the Ct value corresponds to approximately 0.1% asexual parasitaemia. The 18s rRNA gene was detected in the 2D day 3 (blue triangle) and 7 (green triangle) samples and this parasitaemia as compared to the asexual controls falls somewhere between 0% and 0.01% parasitaemia (plotted midway for representative purposes only).

In order to determine whether the detection of the *P. falciparum* 18s rRNA gene in 2D and 3D invaded hepatocytes was being limited by the concentration of the probe or the amount of DNA being added to each reaction, the probe concentration was increased to 200 nM and the DNA concentration increased from 10 ng to 30 ng. The signal detected for each of the 2D and 3D invaded hepatocytes was not increased by the addition of increased probe concentration and additional DNA (Appendix, Table A2).

As no signal was detected in the hepatocytes growing on the 3D PP scaffolds, the experiment was repeated using the Nylon-Cont non-woven scaffold; due to the nylon having a smaller fibre diameter a non-woven mat with smaller pores is formed. It was hypothesised that if the pores were smaller, the hepatocytes would be able to more densely populate the non-woven scaffold thus allowing less of an opportunity for the sporozoites to migrate away from the hepatocytes via the porous network. The nylon non-woven scaffolds, when grafted with PNIPAAm, did not permit thermal release of hepatocytes and coupled with the denser pore network did not make this the best scaffold for work conducted in Chapter 2; it may however be better suited for sporozoite invasion compared to the PP non-woven scaffolds.

The manner in which the nylon non-woven scaffolds were seeded with sporozoites was also modified slightly. Instead of resuspending the sporozoites in 180 µL invasion media, the sporozoites (in a 20 µL pellet) were resuspended in 40 µL invasion media up to a final volume of 60 µL thus a smaller liquid volume containing the approximately 4 x 10^4 sporozoites was used to seed each of the six independent non-woven scaffolds. This was done in order that the small drop of media did not leak out of the scaffold. The protocol used to seed the 2D hepatocytes remained unchanged.

The 18s rRNA gene was detected in the 2D samples with an average C_T value of 48.98±0.7 and 48.31±1.1 at 3 and 7 dpi, respectively. The gene was again not detected in the invaded 3D hepatocytes (Appendix, Table A3) and, thus, the β-actin expression data was not used to normalise the data to correct for differing number of hepatocytes in the 2D and 3D systems.

3.4. DISCUSSION

The trigger that causes asexual parasites to form gametocytes remains unclear and there may be multiple factors that contribute to this (170). Several methods have been proposed to produce gametocytes *en masse* including the manipulation of the culture conditions and/or addition of pharmacological agents (170). Examples include the addition of lysed erythrocytes to an asexual culture (168, 171); using human serum in place of serum substitutes (172) or the addition of antimalarial drugs such as chloroquine (173). A sudden decrease of the haematocrit in fast growing ring-stage cultures causing parasite stress and subsequent conversion to large numbers of gametocytes has also been proposed (159, 174) and Ifediba and Vanderberg concluded that gametocyte production could be enhanced by reducing the haematocrit for part of the culture period (175). The sudden decrease in haematocrit and a high parasite load may reflect conditions of physiological stress in the human host that are known to correlate with increased numbers of transmission stages in blood circulation (167).

In this study two methods were tested for the generation of gametocytes. The candle jar method is used by Dr Sattabongkot and colleagues at AFRIMS and Megan Dowler at the WRAIR to generate sufficient amounts of gametocytes to feed to mosquitoes. In this study, the candle jar method was abandoned after 3D7 and 7G8 parasites failed to produce gametocytes and this method proved to have practical constraints. The second method was the flask method, which uses the reduction of the haematocrit when signs of culture stress become evident (via microscopic evaluation) to stimulate gametocytogenesis. The final culture conditions for the flask method involved starting the gametocyte culture on day 0 in a 15 mL culture volume with a 0.6% asexual parasitaemia (unsynchronised *P. falciparum* NF54 parasites) and 6% haematocrit. Using this method, a maximal gametocytaemia of approximately 2-6% was achieved using NF54 parasites. This high percentage gametocytaemia is in line with what the Parasitology Core Facility at the John Hopkins Malaria Research Institute claim to generate using the same protocol (176), however, this is higher than what has currently been described in literature.

Lelièvre *et al*. achieved a gametocytaemia (mature gametocytes stages IV-V) of approximately 1-2% using the 3D7HT-GFP parasite strain using AlbuMAXII in place of human serum, continuous addition of hypoxanthine and asexual parasite reduction using *N*-acetyl-D-glucosamine (177). Using AlbuMAXII Lelièvre *et al*. were not successful in generating gametocytes using NF54 parasites; it is, however, our experience that culturing NF54 parasites using AlbuMAXII in place of human serum is difficult which may account for their observed

results. In their 2012 paper, Roncales *et al*. compared several methods of gametocyte production with the most successful method resulting in a gametocytaemia of just under 1.5% (169). This was achieved using the *P. falciparum* NF54 parasite strain with a starting asexual parasitaemia of 0.75% and a haematocrit of 2%. During the culturing period, gametocytogenesis was stimulated by decreasing the asexual parasitaemia via sorbitol treatment and the addition of erythrocyte lysates [12]. Roncales *et al*. were not able to generate a significant number of gametocytes using the range of other methods tested, one of which was very similar to one used in this study. By starting with an asexual parasitaemia of 0.2%, reducing the haematocrit 3 days later and not chemically decreasing the asexual parasitaemia, they were only able to achieve a gametocytaemia using 3D7 parasites of 0.08 ± 0.03% and 0.19 ± 0.02% using Dd2 parasites. They did not test this method using NF54 parasites. Comparatively, in the work presented here we were able to achieve a >2% gametocytaemia when starting with a 0.6% asexual parasitaemia and a 6% haematocrit using NF54 parasites.

Culture synchronisation prior to gametocyte culture initiation should not influence the outcome of gametocytogenesis. In the protocol drafted by Carter *et al*. (178) the starting asexual parasitaemia should be 0.5% if the culture is mostly schizonts, 0.7% if the culture is mostly rings and 0.6% if the cultures comprised of a mixed population of asexual parasites. Since our cultures were not synchronised, a mixed population was observed, thus a starting parasitaemia of 0.6 % was always calculated to initiate a gametocyte culture. Mature male and female gametocytes (IV-V) were observed in culture from day 10; after days 14-16 in culture they were the predominant gametocyte stage present. Early stage gametocytes were also observed to be present in the cultures as well as a very small percentage of asexual parasites on occasion.

In contrast to the statement above, the initiating asexual culture's synchronisation status may indeed contribute to achieving higher end-point gametocytaemia. This hypothesis was further explored and upon further investigation, the gametocyte culture that reached 6% gametocytaemia (culture A) was observed to have a higher proportion of rings vs. trophozoites (approximately double) on day 3 after initiation when compared to the lower yielding gametocyte culture (culture B). From this it can be deduced that the asynchronous asexual culture used to initiate culture A was predominantly trophozoites on day 0 (assuming a 48 h life cycle). This would have resulted in the higher percentage asexual population observed earlier on in the gametocytogenesis process (Figure 3.7A). In contrast, culture B was comprised of an equal population of rings and trophozoites, thus, the asexual parasitaemia did not increase as rapidly as in culture A. After gametocyte induction, commitment occurs such that individual schizonts produce a progeny of merozoites that uniformly develop into either sexual or asexual parasites

(179). The re-emergence of rings was seen to decline more rapidly in culture A suggesting commitment to sexual stage development. This difference in end-point gametocytaemia also suggests that the trigger to form gametocytes occurs early on in the culturing protocol and for a finite period of time i.e. rings formed at later time points or after increasing the media volume due to a less rapid asexual increase are not induced to form gametocytes. As such, even though the conversion rates were ~30% for both the high and lower yielding gametocyte cultures, culture A simply had more rings at the point of gametocyte induction. Thus, a gametocyte culture initiated using a synchronised culture of asexual trophozoites may yield more gametocytes; this hypothesis remains to be validated.

Using the flask method several factors were identified to contribute towards the successful differentiation of asexual parasites into gametocytes. Firstly, *P. falciparum* asexual parasites do need to undergo a degree of stress to allow gametocyte production. The parasite cultures exceeded an asexual parasitaemia of approximately 5-10% before the amount of media added to the flasks during the daily media changes was increased. The efficacy of reducing the haematocrit to enhance gametocyte production was first documented by Ifediba and Vanderberg (175) in 1981. Sexual conversion induced *in vitro* by a sudden decrease in haematocrit concentration and a high parasite load was affirmed by Buchholz *et al.* (167). Minimising the time that the gametocyte cultures spend outside of the incubator is another factor, which aids in good gametocyte production. *In vivo*, mature gametocytes remain in a developmentally arrested state until they are taken up by the mosquito. It is within the mosquito mid-gut where the gametocytes then undergo gametogenesis within minutes after ingestion of the infected blood meal. Male gametogenesis (exflagellation) is triggered by a temperature decrease of at least 5°C and an increase in pH (160). Even though mature gametocytes are only observed from day 10 *in vitro*, to ensure that gametogenesis does not spontaneously occur during daily culture maintenance due to changes in temperature outside of the incubator, cultures were placed on a slide warmer set to 37°C; media was also thoroughly warmed prior to its addition to the culture flask (180) as a standard practice. This is a practice advocated by the researchers at AFRIMS (Bangkok), Megan Dowler (WRAIR, personal communication) and is stated in various protocols available for gametocyte culture (176, 178).

The successful generation of gametocytes in this study using NF54 *P. falciparum* parasites may be due to strain specific differences - NF54 *P. falciparum* parasites may simply be better at producing gametocytes than the other strains tested. This was certainly our experience as by using this method we were not successful in generating a significant number of gametocytes using 3D7 and 7G8 parasites. Even under the optimal conditions described above, 3D7 and

7G8 *P. falciparum* parasites failed to produce significant gametocytaemia using this method. The observation that 3D7 and 7G8 parasites do not produce gametocytes to the same extent as NF54 parasites is in agreement with Bennett *et al.* (181) who suggest that not all laboratory strains produce gametocytes to a similar extent even if they are stimulated by the same induction method. Gametocyte production can be lost in parasites that have been maintained *in vitro* for extended periods of time; *P. falciparum* parasite isolates have been shown to undergo deletions in a subtelomeric portion of chromosome 9 of about 300 kb (182). These parasites lack cyto-adherence to C32 melanoma cells and produce greatly reduced numbers of gametocytes (179). As standard practice in our laboratories, parasites are not maintained in culture for longer than 3 months, however, it is unknown to us whether our 3D7 and 7G8 parasites underwent prolonged asexual propagation, thus losing their ability to produce gametocytes, prior to us receiving them. The NF54 parasites used in this study were obtained from MR4 and were originally sourced from the lab of Megan Dowler (WRAIR) where they were used routinely to produce gametocytes for mosquito feeding.

In this study, *P. falciparum* gametocytes were generated for mosquito membrane feeding to ultimately obtain sporozoites for hepatocyte invasion studies. Culture adaptations therefore include the use of only human serum, antibiotics were omitted from the culture medium and the population of asexual parasites was not decreased via sorbitol or *N*-acetyl-D-glucosamine treatment. This was done to simplify the culturing process to allow for simple, high-throughput culturing and to generate a blood meal that would be palatable to the mosquitoes without, in any, way influencing the natural infection process we aimed to mimic. The NF54 *P. falciparum* gametocyte cultures were fed to *Anopheles spp*. mosquitoes at the NICD. However, none of the mosquitoes dissected 9-11 days post feeding had developed *P. falciparum* oocysts in their mid-guts nor were we able to obtain any sporozoites from the salivary glands of the mosquitoes at the later time points.

A number of factors may have contributed to this. Firstly, altitude may play a role as the Edenvale/ Sandringham area (where the NICD is situated) is approximately 2200 m above sea level. Altitude is an important factor in malaria transmission and it is generally stated that transmission does not normally occur above 1800 m (183). This effect is, however, usually related to lower temperatures associated with higher altitudes but temperature is a controlled parameter inside the insectary. Secondly, the mosquitoes may not be susceptible to the particular strain of malaria parasites used to infect them or the malaria parasites cultured *in vitro* may have become less infectious. Parasite genotype-vector genotype interactions are a major determinant of infection outcome (155, 184). In our study, only *An. gambiae* and *An. funestus*

were fed; other common mosquito species used for feeding that could possibly be used are *An. freeborn, An. stephensi* or and/*or An. arabiensis*. Of these *Anopheles* mosquitoes each presents with different permissiveness for malaria infection: *An. freeborni >> An. gambiae = An. arabiensis > An. stephensi* (155, 185). Finally, the presence of exflagellating microgametes was used to indicate that a gametocyte culture is functional and ready to be fed to the mosquitoes. This is, however, only an indication that viable male microgametes were present in the culture and not an indication of guaranteed infectivity. Female macrogametes, which along with the microgamete are required to form the oocysts, were observed in the *in vitro* cultures and therefore all the basic elements for successful infection were deemed to be in place. However, there is currently no measure of female macrogamete viability, which could influence oocyst formation. In the absence of detecting ookinetes or oocysts, it is currently difficult to determine if the gametocyte production protocol produced viable forms of both male and female gametes. Future feeds may make use of xanthurenic acid in the feed mix; xanthurenic acid has been identified as the putative inducer of gametogenesis in the mosquito (186). Bhattacharyya and Kumar demonstrated that by increasing the concentration of exogenous xanthurenic acid (optimum 100 mM), a gradual increase in the number of oocysts in the mid-gut of infected mosquitoes is observed (160). Alternatively, although a more challenging approach, ookinetes could be generated *in vitro* and fed to the mosquitoes (187).

P. berghei sporozoites have, however, been successfully produced at the NICD by infecting guinea pigs with the parasite and allowing the mosquito to feed on the sick animals. In this study we chose not to test our hypothesis that *Plasmodium* sporozoites may infect hepatocytes growing in 3D better than those growing in 2D by using *P. berghei* sporozoites. *P. berghei* is different to *P. falciparum* and we aimed to create a system based on the human parasite. It has previously been reported that depending on the host cell type *P. berghei* sporozoites can use several distinct pathways for invasion (188). Infection of human HepG2, HuH7 and even HeLa cell-lines by *P. berghei* does not depend on CD81 or host membrane cholesterol; invasion of hepatocytes by *P. falciparum* and *P. yoelii* depend upon these mechanisms for invasion. The existence of distinct invasion pathways may explain why *P. berghei* sporozoites are capable of infecting a wider range of host cell types *in vitro*. Therefore, optimising our 3D system using these sporozoites may not ultimately translate into a better system for *P. falciparum in vitro* studies. As a result of our inability to generate infected mosquitoes from gametocytes to produce sporozoites, cryopreserved *P. falciparum* sporozoites were purchased from Sanaria Inc. (USA) and these were used in the pilot 2D vs 3D hepatocyte invasion study.

In this study, qRT-PCR was used as the determinant of successful hepatocyte invasion of *P falciparum* sporozoites into either the 2D or 3D hepatocytes. An additional control that could be included would be to perform the TaqMan® assay on the DNA from Sanaria's 6 day hepatocyte potency assay which resulted in 22 parasites per well and correspond our C_T values to the ones obtained for these samples; this will give an insight as to whether this end-point analysis is sensitive enough for parasite quantification. The lack of plentiful sporozoites limits the testing of various new and exciting 3D culture methods and once infected mosquitoes are available to us in our own laboratories, several modifications to our 3D culturing system will be tested. An initial experiment would be to test parasite movement/penetration during the first hour in contact with the scaffold using immunofluorescence of the CSP. Once invasion has been established methods used to analyse the parasitaemia will then extend to flow cytometry to possibly assess the developmental stage the parasite is able to reach in 2D and 3D systems, qRT-PCR using RNA to assess gene copy number of the parasite *in vitro* can also be investigated. In our study, co-culture of the invaded 2D and 3D cultures with erythrocytes was also performed as outlined in (113) on 7, 14 and 21 dpi without successfully detecting any asexual parasites; this will also be conducted in future studies to assess whether the full sporozoite life cycle can be completed in the *in vitro* systems.

In vivo, hepatocytes are not directly accessible to sporozoites travelling in the bloodstream of a mammalian host; parasite passage across the sinusoidal cell layer is therefore mandatory for the onset of a malaria infection (141). The sinusoidal layer is composed of specialized fenestrated endothelia interspersed with Kupffer cells and several biochemical and physiological studies as well as various microscopic and genetic approaches have all suggested that sporozoites reach hepatocytes by passing through Kupffer cells (142, 143, 189-191). This is not the case *in vitro* where most *Plasmodium s*pecies are able to mature to liver stages in cultures of pure primary hepatocytes or hepatoma cells i.e. in the absence of Kupffer cells (141, 155). However, even in the absence of the sinusoidal barrier it remains difficult to obtain high levels of sporozoite-invaded hepatocytes *in vitro*. This non-invasiveness may be attributed to several factors. *In vivo* the switch from 'migration mode' to 'invasion mode' is hypothesised to be triggered by parasite circumsporozoite protein recognition of the presence of cells covered by HSPGs (140). Using a rodent model system Coppi *et al*. (192), demonstrated that *P. berghei* sporozoites use the sulphation level of host HSPGs to navigate in the mammalian host. Sporozoites were shown to migrate through cells expressing low-sulphated HSPGs, such as those in skin and endothelium, while highly sulphated HSPGs of hepatocytes activate sporozoites for invasion. *In vitro* this may not be a feature that is easily reproducible as the cell lines used for invasion may not display optimal levels of HSPG's on their surfaces for the

parasites to switch from migration mode to invasion mode, thus, the absence of the sinusoidal layer *in vitro* may ultimately be a disadvantage as the sporozoites are not sufficiently triggered to undergo invasion mode. This may lead researchers to re-consider the design of *in vitro* systems and co-culturing with macrophages or stromal cells may be a possible improvement. Another method to overcome this is the addition of calcium ionophores (145) or uracil derivatives or forskolin (193) to stimulate sporozoite apical regulated exocytosis which decreases migration and enhances infectivity (155). However, Prudêncio *et al*. draw attention to the fact that such measures should be carefully considered as these additives may confound ones data (155).

Additional reasons why sporozoites do not invade hepatocytes *in vitro* may be as a result of cell density or cell confluence. It has been demonstrated *in vitro* that EE forms of the parasite grow to a lesser extent when the cell density is high, preferring to invade hepatocytes at approximately 60-70% confluence (155). The hepatocytes growing in our 3D system may, therefore, simply be too dense for invasion. Until a more plentiful source of sporozoites is available to us one possible change we could make to test our hypothesis that 3D cells will permit more sporozoites to invade is to change the type of 3D cell support used. By making use of a “basement membrane” in place of the non-woven fibres, such as Matrigel (BD Biosciences) or Geltrex™ Matrix (Invitrogen) we may have greater success in achieving a higher level of invasion. A basement membrane is thin extracellular matrices underlying cells *in vivo*. BD Matrigel Basement Membrane Matrix is a solubilized basement membrane preparation extracted from the Engelbreth-Holm-Swarm (EHS) mouse sarcoma, a tumour rich in extracellular matrix proteins. Its major components are laminin, collagen IV, heparan sulfate proteoglycans and entactin/nidogen. BD Matrigel Basement Membrane Matrix is effective for the attachment and differentiation of both normal and transformed anchorage dependent cell types including hepatocytes (194). The Matrigel basement membrane was used by Al-Olayan *et al.* (156) to culture *P. berghei* sporozoites *in vitro*. They hypothesised that the Matrigel mimics the basal lamina of the mosquito midgut and when co-cultured with *Drosophila melanogaster* S2 cells they were successful in generating this stage of the parasites life cycle.

In his 2004 paper entitled “Beyond the Petri dish” Zang (2) proposes that in a true 3D system the pores need to be smaller than an individual cell and that 3D matrices produced from animals (such as Matrigel) offer a good alternative to the synthetically produced scaffolds. Whilst this is not problematic for normal hepatocyte 3D cultures, in the context of sporozoite invasion of hepatocytes, the reticulated surface of the Matrigel would permit denser more uniform hepatocyte coverage of the hydrogel, thus affording the sporozoites less of an opportunity to

"escape" the matrix. It may also reduce the time such an assay takes to perform. Typically it takes 14-21 days to populate the PP or nylon scaffolds with hepatocytes to the point where almost all the fibres are covered with cells, the architecture of the Matrigel is such that the cells would form a 3D layer over the top of the matrix in a relatively short period of time. The "flatter" surface would also allow us to monitor the level of confluence more closely, but, due the 3D nature of the hepatocytes growing on this matrix the sporozoites would be still be able to migrate into the 3D cell network thus able to traverse multiple hepatocytes prior to settling in their final host cells.

In addition to the modification strategy for growing the hepatocytes in 3D, readdressing the cell-line used for these experiments may yield a solution. Whereas HC04 hepatocytes are known to support the *in vitro* growth of *P. falciparum* (113), they typically have lost some of the features of the cells they were derived from through immortalisation and several cell culture passages. By using primary cells, though more expensive and less convenient for routine work we may be able to get better "proof of principle" of our hypothesis.

Robust protocols for the generation of high yielding *in vitro* gametocyte cultures were successfully developed in this study. Further modifications to the mosquito membrane feeding protocols will be explored until sporozoite infected mosquitoes are observed. This will then allow us to fully explore the possibility of enhanced sporozoite invasion in 3D hepatocyte systems.

CHAPTER 4

CONCLUDING DISCUSSION

New insight into cell phenotype and function *in vitro* and the desire to have cells functioning as closely to their *in vivo* counterparts has intensified the demand for materials that support 3D cell growth to enhance cell function in ways that resemble tissues *in vivo*. Cells growing *in vitro* are traditionally grown on 2D surfaces of tissue culture plastic and bear little resemblance to the complexities of the 3D tissues from which they were derived (5). Two-dimensional monolayer cultures are convenient for routine work but impose unnatural geometric and mechanical constraints upon the cells. The inherent problem with cells growing on 2D surfaces is the lack of dorsal anchorage points, which affects the balance between cells spreading or retracting. In tissues, cells connect to each other as well as to the ECM and it has been shown in various culture applications that the growth and function of cells as multi-cellular, 3D structures is significantly different to the 2D monolayer cultures (3, 5, 10-12). A change of environment for the cells, therefore, translates into a change in function and capacity for growth and differentiation. It is thus evident that the context in which cells are grown plays a significant role in their proper functioning and it has been proposed that the predictive accuracy of the drug discovery process and the analysis of host-pathogen interactions can be enhanced by engineering the cell culture microenvironment to create growth conditions that more accurately mimic the *in vivo* behaviour of cells (195). Thus, much effort has been dedicated to the fabrication and testing of materials that can support 3D cell growth. This study aimed to contribute two aspects to this field, specifically a non-woven 3D scaffold capable of supporting high numbers of cells, specifically hepatocytes, metabolically superior to their 2D counterparts. Secondly the non-woven scaffold should permit on-demand non-invasive release of the cells growing on and in the scaffold.

Despite the obvious advantages of 3D cell culture, the application of this technology as a tool for routine tissue culture applications has been slow. This is largely due to a number of identified limitations including: poor reproducibility between batches of biomimetic scaffolds, limited ability to scale up or down, difficulty in post-culturing processing and/or cell extraction from the matrix, lack of proven automated solutions, little flexibility in accommodating the many different cell-lines and types, characterising cells cultured in 3D geometries is difficult, poor visualisation and cost (98). By combining 3D cell culture with thermoresponsive technology, this study set out to investigate the potential of 3 non-woven fabrics (PP, PET and nylon) grafted with PNIPAAm to promote 3D hepatocyte proliferation in the scaffolds and subsequent non-

invasive cell harvesting of viable cells to overcome the problem of cell extraction from the 3D matrix for downstream applications. Ultimately, this 3D culturing technology was aimed to contribute towards studies such as host-parasite interactions, using the malaria parasite hepatocyte invasion system as model.

This study was successful regarding establishment of thermoresponsive 3D cell culturing technologies. This was measured by several factors as outlined below, providing novel data on and extending the current *status quo* regarding 3D cell culturing. High-density cell culture was achieved in this work and the number of cells cultured on selected non-woven scaffolds was comparable to the commercially available hydrogel 3D cell culture system, Algimatrix™. Hydrogel scaffolds are of the most commonly used and well characterised 3D scaffolds on the market; our scaffolds can, therefore, be considered in line with what would be acceptable to the consumer market in terms of cell numbers supported on the scaffold. A PP scaffold grafted with PNIPAAm was identified as being capable of promoting both good cell proliferation and displayed thermoresponsiveness and thus, was capable of non-invasive thermal release of the hepatocyte within the scaffold. This demonstrated the first “on-demand” method of cell harvesting using the thermoresponsive properties of PNIPAAm from 3D scaffolds thus circumventing the need to use salts or enzymes for scaffold degradation; a previously difficult result to achieve for downstream cell processing. The time it takes to release the cells from the 3D matrix is an area upon which future research may wish to improve. Currently thermal release of cells from 2D thermoresponsive plates takes approximately 30-40 min; halving the time it takes to release the cells from the 3D scaffolds would place our technology in line with what is commercially available. This may be achieved by further optimising the grafting method to adjust the graft thickness on the surface of the non-woven scaffolds. By using the scaffold identified to be thermoresponsive in a semi-automated cell culture device we were able to culture a large number of hepatocytes, however, cell release from this device would require further optimisation. This device would potentially allow researchers to grow large numbers of cells in 3D and harvest them non-invasively. Future work may aim to miniaturise the bioreactor such that several experiments could be run in parallel.

The second objective of this study was to test the hypothesis that hepatocytes growing in 3D would be more permissive to *P. falciparum* sporozoite invasion as a model system compared to hepatocytes growing on conventional tissue culture plastic in 2D. However, this was dependent on the successful production of *P. falciparum* gametocytes *in vitro* and the subsequent infection of *Anopheles* mosquitoes. We were successful in generating high yielding gametocyte cultures using NF54 *P. falciparum* parasites; gametocytogenesis reached 6% on occasion, a percentage

higher that currently reported in literature. We were, however, unsuccessful in infecting the mosquitoes with the parasite and were thus unable to generate an in-house source of sporozoites.

Due to the biological complexity of the malaria-*Anopheles* system, we may have been better positioned to study a less complex host-pathogen interaction, to show proof of concept of our 2D vs 3D system. The major vector of *P. falciparum* in Africa is *An. gambiae* which is widely distributed throughout the Afro-tropical belt (196) *An. gambiae sp.* is divided into two morphologically indistinguishable molecular forms, known as M and S. The susceptibility of the S and M molecular forms to *P. falciparum* relay contrasting findings; S and M forms exhibited similar susceptibility in Cameroon whereas in Senegal the S form were more susceptible than M form mosquitoes.(196-198), thus, it can be inferred that the susceptibility of *Anopheles* mosquitoes to *Plasmodium* infection is under genetic control. Multiple lines of evidence also suggest that mosquito bacterial communities influence vector competence (196). The protective role of *Anopheles* midgut bacteria against malaria infections was demonstrated by using antibiotic treatment to clear the gut microbiota, which resulted in enhanced *Plasmodium* infections (199, 200) and it has been observed that co-infections of bacteria with *Plasmodium* reduced the number of developing oocysts in the mosquito midgut, in the laboratory as well as field conditions (196). However, in a study by Boissiere (196) it was found that an abundance of *Enterobacteriaceae* is higher in *P. falciparum*-infected mosquitoes, suggesting that some microbe-parasite interactions may, in fact, contribute to the successful development of the malaria parasite. The inability to infect the mosquitoes in our insectary may hinge on one of the afore-mentioned factors which would need to be more extensively studied in the future.

When the *in vitro* invasiveness of commercially sourced *P. falciparum* sporozoites was tested in hepatocytes growing in 3D it was ultimately unsuccessful; this complex parasite may ultimately require a more advanced *in vitro* system to enhance *in vitro* sporozoite invasiveness. The results of this study can, however, be used as the basis to hypothesise a different strategy, perhaps one involving a different type of 3D scaffold or basement membrane, or possibly investigating macrophage-hepatocyte co-cultures. The possibility remains that this may be a host-pathogen interaction that will always be difficult to work with *in vitro.* However, due to the fact that the pursuit for novel drugs and vaccine strategies is expensive and at present animal testing currently offers the best means to study the malaria liver stage, this is an important area of research where all options for an *in vitro* model system need to be exhausted. *In vitro* assays are invariably cheaper, would allow high throughput screening of novel compounds and are ethically more acceptable.

In conclusion, this work demonstrated the potential of 3D cell culture and on-demand cell release in the grafted non-woven scaffolds and the possible application of an automated 3D cell culture and non-invasive release was demonstrated. In the human body virtually all organs are functionally integrated and looking to the future of 3D cell culture for the study of toxicology and host-pathogen interactions, investigators are already developing integrated 'human-on-a-chip' models that consist of interconnected compartments, each containing a cell type representing a different organ, linked through a microfluidic circulatory system (201); this concept is illustrated in Figure 4.1. This *in vivo* mimicry would vastly improve upon the speed with which new drugs reach the bedsides of patients and enhance our understanding of complex-host pathogen models for improved rational design of drugs and prophylaxis.

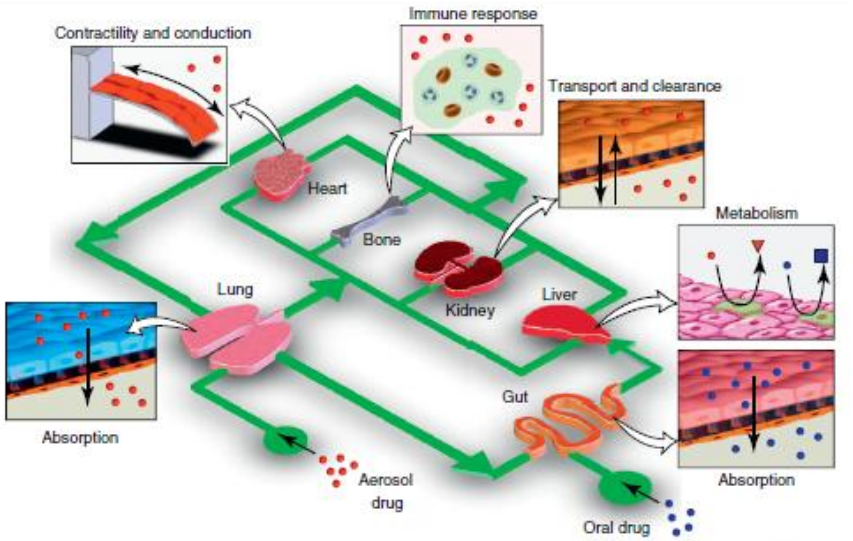

Figure 4.1. An illustration of the **"**human-on-a-chip" concept. Biomimetic microsystems representing different organs can be integrated into a single micro-device and linked by a microfluidics circulatory system in a physiologically relevant manner to model a complex, dynamic process of drug absorption, distribution, metabolism and excretion, and to more reliably evaluate drug efficacy and toxicity (202).

The investigation of useful biomaterials for *in vitro* mimicry is becoming more diverse bringing knowledge from a variety of disciplines (203) and bridging the divide between materials scientists and biologists alike. The changing future of cell culture will facilitate the translation of basic science to the clinical setting and the development and use of a series of increasingly complex 3D model systems. In order to achieve this, transdisciplinary research is fast becoming a more common practice and ultimately will be a priority for fast tracking novel materials from their conception to intended application. Our work was a collaboration between chemists, engineers, material scientists and biologists, all of whom played a critical role in the development of the novel thermoresponsive 3D scaffold. By engaging in transdisciplinary research we were able to address issues that could not otherwise be solved by one scientific discipline alone. The success of our collaborations can be summed up by four key factors as

outlined by Kessel and Rosenveld (204), these are: the willingness of the participating scientists to commit sufficient time to collaborative endeavours; openness to learning each other's disciplinary languages and jargon; the capacity to build mutual confidence and trust between researchers and overcoming the challenge of working as equals, with no knowledge or discipline or practice assuming priority. Additional factors contributing the success of this type of research between different scientific expertise and institutes is learning how to respect the value(s) of others and to be less concerned about submerging ones professional identity in the team process. To provide a broad foundation for such a process, the institutional infrastructure of scientific research, that is universities, journals, and funders, also all need to be aligned in support of transdisciplinary team science. Moreover, issues such as barriers between departments and faculties, authorship, peer review and funding applications can either support team science or constitute limiting factors (204). This study is a testament to the possibility of collaborative work. Much effort and time was dedicated to meetings and planning and the team co-operation lead to the successful development of the novel 3D scaffold.

This body of work represents the successful efforts to graft PNIPAAm onto 3D non-woven scaffolds for thermal release of cultured cell growing in 3D. We successfully demonstrated high density 3D cell proliferation using hepatocytes on the 3D scaffold comparable to that observed using the commercially available Algimatrix^{TM} system; thermal release of the hepatocytes from selected grafted non-woven's was also successfully demonstrated. Hepatocytes growing on the 3D scaffolds were observed to be metabolically superior to their 2D counterparts further validating the use of this scaffold for cell culture experiments. Applications of this scaffold may, therefore, be for drug and toxicity screening or high density proliferation and release of cells for the study of surface antigens and/or proteins that would have otherwise have been destroyed by enzymatic removal of the cells from the scaffold. A pilot scale-up experiment of the thermoresponsive scaffolds in a semi-automated system indicated that with further optimisation these scaffolds may be useful for very high density cell proliferation and recovery. When using the 3D scaffolds for a proof-of-concept experiment using the hepatocyte-sporozoite interaction we were not successful as hoped. However, these data obtained from this experiment will guide future experiments in the pursuit of an *in vitro* system that permits optimal sporozoite invasion – this would be an important development in the fight against this devastating pathogen.

REFERENCES

[1] Lee J, Cuddihy MJ, Kotov NA. Three-dimensional cell culture matrices: state of the art. Tissue Engineering. 2008;14:61-86.
[2] Zhang S. Beyond the Petri Dish. Nat Biotechnol. 2004;22:151-2.
[3] Cukierman E, Pankov R, Stevens DR, Yamada KM. Taking cell-matrix adhesions to the third dimension. Science. 2001;294:1708-12.
[4] Editorial. Goodbye, flat biology? Nature. 2003;424:861-.
[5] Bokhari M, Carnachan RJ, Cameron NR, Przyborski SA. Novel cell culture device enabling three-dimensional cell growth and improved cell function. Biochem Biophys Res Commun. 2007;354:1095-100.
[6] Bokhari M, Carnachan RJ, Cameron NR, Przyborski SA. Culture of HepG2 liver cells on three dimensional polystyrene scaffolds enhances cell structure and function during toxicological challenge. J Anat. 2007;211:567-76.
[7] InfiniteBio. 2009 [cited 18 July 2012]; Available from: http://www.infinitebio.com
[8] Page H, Flood P, Reynaud E. Three-dimensional tissue cultures: current trends and beyond. Cell Tissue Res. 2012:1-9.
[9] Wolfgang M-K. Three-dimensional cell cultures: from molecular mechanisms to clinical applications. Am J Physiol Cell Physiol. 1997;273:C1109-23.
[10] Schmeichel KL, Bissell MJ. Modeling tissue-specific signaling and organ function in three dimensions. J Cell Sci. 2003;116:2377-88.
[11] Beningo KA, Dembo M, Wang Y-l. Responses of fibroblasts to anchorage of dorsal extracellular matrix receptors. Proc Natl Acad Sci U S A. 2004;101:18024-9.
[12] Witte RP, Kao WJ. Keratinocyte-fibroblast paracrine interaction: the effects of substrate and culture condition. Biomaterials. 2005;26:3673-82.
[13] Scaglione S, Braccini A, Wendt D, Jaquiery C, Beltrame F, Quarto R, et al. Engineering of osteoinductive grafts by isolation and expansion of ovine bone marrow stromal cells directly on 3D ceramic scaffolds. Biotechnology and Bioengineering. 2006;93:181-7.
[14] Peretz H, Talpalar AE, Vago R, Baranes D. Superior survival and durability of neurons and astrocytes on 3-dimensional aragonite biomatrices. Tissue Eng. 2007;13:461-72.
[15] Tian Z, Si JC, Q., Zhou L, Chen S, Xiao P, Wu E. Antitumor activity and mechanisms of action of total glycosides from aerial part of *Cimicifuga dahurica* targeted against hepatoma. BMC Cancer. 2007;7:237-47.
[16] Liver Disease. US Department of Health and Human Services, National Institutes of Health 2012 [cited 31 August 2012]; Available from: http://www.nlm.nih.gov/medlineplus/liverdiseases.html
[17] Haycock JW. 3D cell culture: a review of current approaches and techniques. Methods in Molecular Biology 2011;695:1-15.
[18] Ratner BD, Hoffman AS, Schoen FJ, Lemons JE. Biomaterials science: An introduction to materials in medicine. San Diego: Elsevier Academic Press; 2004.
[19] Pavesio A. Development of a biodegradable scaffold for dermo-epidermal skin grafts. Building a bionic body? - Biomaterials research for healthcare 2000 [cited 1 August 2012]; Available from: http://ec.europa.eu/research/press/2000/pr2703en-an.html
[20] Carletti E, Motta A, Migliaresi C. Scaffolds for tissue engineering and 3D cell culture. 3D Cell Culture : Methods and Protocols: Springer Protocols; 2010. p. 17-39.
[21] Li S. Hydrolytic degradation characteristics of aliphatic polyesters derived from lactic and glycolic acids. J Biomed Mater Res. 1999;48:342-53.
[22] Yannas IV, Burke JF, Huang C, Gordon PL. Correlation of *in vivo* collagen degradation rate with *in vitro* measurements. J of Biomed Mater Res. 1975;9:623-8.
[23] Rezwan K, Chen QZ, Blaker JJ, Boccaccini AR. Biodegradable and bioactive porous polymer/inorganic composite scaffolds for bone tissue engineering. Biomaterials. 2006;27:3413-31.
[24] Armentano I, Dottori M, Fortunati E, Mattioli S, Kenny JM. Biodegradable polymer matrix nanocomposites for tissue engineering: A review. Polymer Degradation and Stability. 2010;95:2126-46.

[25] Nguyen KT, West JL. Photopolymerizable hydrogels for tissue engineering applications. Biomaterials. 2002;23:4307-19.
[26] Lutolf MP, Hubbell JA. Synthetic biomaterials as instructive extracellular microenvironments for morphogenesis in tissue engineering. Nat Biotech. 2005;23:47-55.
[27] Tibbitt MW, Anseth KS. Hydrogels as extracellular matrix mimics for 3D cell culture. Biotechnology and Bioengineering. 2009;103:655-63.
[28] Szot CS, Buchanan CF, Freeman JW, Rylander MN. 3D *in vitro* bioengineered tumors based on collagen I hydrogels. Biomaterials. 2011;32:7905-12.
[29] Eyrich D, Brandl F, Appel B, Wiese H, Maier G, Wenzel M, et al. Long-term stable fibrin gels for cartilage engineering. Biomaterials. 2007;28:55-65.
[30] Masters KS, Shah DN, Walker G, Leinwand LA, Anseth KS. Designing scaffolds for valvular interstitial cells: Cell adhesion and function on naturally derived materials. Journal of Biomedical Materials Research Part A. 2004;71A:172-80.
[31] Kleinman HK, Martin GR. Matrigel: basement membrane matrix with biological activity. Semin Cancer Biol. 2005;15:378-86.
[32] Azab AK, Orkin B, Doviner V, Nissan A, Klein M, Srebnik M, et al. Crosslinked chitosan implants as potential degradable devices for brachytherapy: In vitro and in vivo analysis. Journal of Controlled Release. 2006;111:281-9.
[33] Elkayam T, Amitay-Shaprut S, Dvir-Ginsberg M, Harel T, Cohen S. Enhancing the drug metabolism activities of C3A - A human hepatocyte cell line - by tissue engineering within alginate scaffolds. Tissue Engineering. 2006;12:1357-68.
[34] Dawson E, Mapili G, Erickson K, Taqvi S, Roy K. Biomaterials for stem cell differentiation. Advanced Drug Delivery Reviews. 2008;60:215-28.
[35] Hayman MW, Smith KH, Cameron NR, Przyborski SA. Growth of human stem cell-derived neurons on solid three-dimensional polymers. Journal of Biochemical and Biophysical Methods. 2005;62:231-40.
[36] Hayman MW, Smith KH, Cameron NR, Przyborski SA. Enhanced neurite outgrowth by human neurons grown on solid three-dimensional scaffolds. Biochemical and Biophysical Research Communications. 2004;314:483-8.
[37] Li Y, Ma T, Yang S-T, Kniss DA. Thermal compression and characterization of three-dimensional nonwoven PET matrices as tissue engineering scaffolds. Biomaterials. 2001;22:609-18.
[38] Flendrig LM, la Soe JW, Jorrning GGA, Steenbeek A, Karlsen OT, BovÃ©e WMMJ, et al. *In vitro* evaluation of a novel bioreactor based on an integral oxygenator and a spirally wound nonwoven polyester matrix for hepatocyte culture as small aggregates. Journal of Hepatology. 1997;26:1379-92.
[39] Gómez-Lechón MJ, Castell J, Danato T, Pahernik S, Thasler W, Koebe HG, et al. New non-woven polyurethane-based biomaterials for the cultivation of hepatocytes: expression of differentiated functions. J Mater Sci Mater Med. 2000;11:37-41.
[40] Wong C, Nuhiji E, Sutti A, Keating G, Liu X, Kirkland M, et al. Enhanced cell growth using non-woven scaffolds of multilobal fibres. Textile Research Journal. 2012;In Press.
[41] Williamson MR, Coombes AGA. Gravity spinning of polycaprolactone fibres for applications in tissue engineering. Biomaterials. 2004;25:459-65.
[42] Patel M, Bhrambhatt D. Nonwoven Technology. [cited 2012 18 July]; Available from: http://textlnfo.files.wordpress.com/2011/10/nonwoven-fabrics1.pdf
[43] Edwards SL, Mitchell W, Matthews JB, Ingham E, Russell SJ. Design of nonwoven scaffold strutures for tissue engineering of the anteriour cruciate ligament. AUTEX Research Journal. 2004 4:86-94.
[44] Owen SC, Shoichet MS. Design of three-dimensional biomimetic scaffolds. J of Biomed Mater Res. 2010;94A:1321-31.
[45] Shin H, Jo S, Mikos AG. Biomimetic materials for tissue engineering. Biomaterials. 2003;24:4353–64.
[46] Owen SC, Shoichet MS. Design of three-dimensional biomimetic scaffolds. Journal of Biomedical Materials Research A. 2010;94A:1321-31.

[47] Allen LT, Tosetto M, Miller IS, O'Connor D, Penney SC, Lynch I, et al. Surface-induced changes in protein adsorption and implications for cellular phenotypic responses to surface interaction. Biomaterials. 2006;27:3096-108.
[48] Shin H, Jo S, Mikos AG. Modulation of marrow stromal osteoblast adhesion on biomimetic oligo[poly(ethylene glycol) fumarate] hydrogels modified with Arg-Gly-Asp peptides and a poly(ethyleneglycol) spacer. J Biomed Mater Res. 2002;61:169-79.
[49] West JL, Hubbell JA. Polymeric biomaterials with degradation sites for proteases involved in cell migration. Macromolecules. 1999;32:241-4.
[50] Ranieri JP, Bellamkonda R, Bekos EJ, Vargo TG, Gardella JA, Jr., Aebischer P. Neuronal cell attachment to fluorinated ethylene propylene films with covalently immobilized laminin oligopeptides YIGSR and IKVAV. II. J Biomed Mater Res. 1995;29:779-85.
[51] Schense JC, Bloch J, Aebischer P, Hubbell JA. Enzymatic incorporation of bioactive peptides into fibrin matrices enhances neurite extension. Nature Biotechnology 2000;18:415 - 9
[52] Panitch A, Yamaoka T, Fournier MJ, Mason TL, Tirrell DA. Design and biosynthesis of elastin-like artificial extracellular matrix proteins containing periodically spaced fibronectin CS5 domains. Macromolecules. 1999;32:1701-3.
[53] Rezania A, Healy KE. Biomimetic peptide surfaces that regulate adhesion, spreading, cytoskeletal organization, and mineralization of the matrix deposited by osteoblast-like cells. Biotechnol Prog. 1999;15:19-32.
[54] Stile RA, Healy KE. Thermo-responsive peptide-modified hydrogels for tissue regeneration. Biomacromolecules. 2001;2:185-94.
[55] Elbert DL, Hubbell JA. Conjugate addition reactions combined with free-radical cross-linking for the design of materials for tissue engineering. Biomacromolecules. 2001;2:430-41.
[56] Borkenhagen M, Clémence JF, Sigrist H, Aebischer P. Three-dimensional extracellular matrix engineering in the nervous system. Journal of Biomedical Materials Research. 1998;40:392-400.
[57] Hern DL, Hubbell JA. Incorporation of adhesion peptides into nonadhesive hydrogels useful for tissue resurfacing. Journal of Biomedical Materials Research. 1998;39:266-76.
[58] Rowley JA, Madlambayan G, Mooney DJ. Alginate hydrogels as synthetic extracellular matrix materials. Biomaterials. 1999;20:45-53.
[59] Eid K, Chen E, Griffith L, Glowacki J. Effect of RGD coating on osteocompatibility of PLGA-polymer disks in a rat tibial wound. J Biomed Mater Res. 2001;57:224-31.
[60] Maheshwari G, Brown G, Lauffenburger DA, Wells A, Griffith LG. Cell adhesion and motility depend on nanoscale RGD clustering. J Cell Sci. 2000;113:1677-86.
[61] Irvine DJ, Ruzette AV, Mayes AM, Griffith LG. Nanoscale clustering of RGD peptides at surfaces using comb polymers. 2. Surface segregation of comb polymers in polylactide. Biomacromolecules. 2001;2:545-56.
[62] Loebsack A, Greene K, Wyatt S, Culberson C, Austin C, Beiler R, et al. *In vivo* characterization of a porous hydrogel material for use as a tissue bulking agent. Journal of Biomedical Materials Research. 2001;57:575-81.
[63] Sceats E. *In vitro* tissue models: Working in the third dimension. Innovations in Pharmaceutical Technology 2012 [cited 28 August 2012; Available from: http://www.zyoxel.com/docs/IPT_Article_ZyoxelLtd_Dec2010.pdf?cat=3&article=699
[64] Provenzano PP, Inman DR, Eliceiri KW, Trier SM, Keely PJ. Contact guidance mediated three-dimensional cell migration is regulated by Rho/ROCK-dependent matrix reorganization. Biophys J. 2008;95(11):5374-84.
[65] Harma V, Virtanen J, Makela R, Happonen A, Mpindi J-P, Knuuttila M, et al. A comprehensive panel of three-dimensional models for studies of prostate cancer growth, invasion and drug responses. PLoS ONE. 2010;5:e10431.
[66] Barrila J, Radtke AL, Crabbe A, Sarker SF, Herbst-Kralovetz MM, Ott CM, et al. Organotypic 3D cell culture models: using the rotating wall vessel to study host-pathogen interactions. Nat Rev Micro. 2010;8:791-801.
[67] Kim JB. Three-dimensional tissue culture models in cancer biology. Semin Cancer Biol. 2005;15:365-77.

[68] Yamada KM, Cukierman E. Modeling Tissue Morphogenesis and Cancer in 3D. Cell. 2007;130:601-10.
[69] Kunz-Schughart LA, Freyer JP, Hofstaedter F, Ebner R. The use of 3-D cultures for high-throughput screening: the multicellular spheroid model. J Biomol Screen. 2004;9:273-85.
[70] Kievit FM, Florczyk SJ, Leung MC, Veiseh O, Park JO, Disis ML, et al. Chitosan-alginate 3D scaffolds as a mimic of the glioma tumor microenvironment. Biomaterials. 2010;31:5903-10.
[71] Fischbach C, Chen R, Matsumoto T, Schmelzle T, Brugge JS, Polverini PJ, et al. Engineering tumors with 3D scaffolds. Nat Meth. 2007;4:855-60.
[72] Poincloux R, Collina O, Lizárraga F, Romaoa M, Debraye M, Piela M, et al. Contractility of the cell rear drives invasion of breast tumor cells in 3D Matrigel. PNAS. 2011;108:1943-8.
[73] Gurski LA, Jha AK, Zhang C, Jia X, Farach-Carson MC. Hyaluronic acid-based hydrogels as 3D matrices for in vitro evaluation of chemotherapeutic drugs using poorly adherent prostate cancer cells. Biomaterials. 2009;30:6076-85.
[74] Fischbach C, Kong HJ, Hsiong SX, Evangelista MB, Yuen W, Mooney DJ. Cancer cell angiogenic capability is regulated by 3D culture and integrin engagement. PNAS. 2009;106:399-404.
[75] Egeblad M, Rasch MG, Weaver VM. Dynamic interplay between the collagen scaffold and tumor evolution. Current Opinion in Cell Biology. 2010;22:697-706.
[76] Krause S, Maffini MV, Soto AM, Sonnenschein C. The microenvironment determines the breast cancer cells' phenotype: organization of MCF7 cells in 3D cultures. BMC Cancer. 2010;7:263.
[77] Millerot-Serrurot E, Guilbert M, Fourre N, Witkowski W, Said G, Van Gulick L, et al. 3D collagen type I matrix inhibits the antimigratory effect of doxorubicin. Cancer Cell Int 2010;13:26.
[78] DiMasi JA, Hansen RW, Grabowski HG. The price of innovation: new estimates of drug development costs. Journal of Health Economics. 2003;22:151-85.
[79] Friedman D. The silicone guinea pig. Technol Rev. 2004:62-8.
[80] Dambach DM, Andrews BA, Moulin F. New technologies and screening strategies for hepatotoxicity: Use of *in vitro* models. Toxicologic Pathology. 2005;33:17-26.
[81] Rangarajan A, Hong SJ, Gifford A, Weinberg RA. Species- and cell type-specific requirements for cellular transformation. Cancer Cell. 2004;6:171-83.
[82] Prestwich GD. Evaluating drug efficacy and toxicology in three dimensions: Using synthetic extracellular matrices in drug discovery. Acc Chem Res. 2007;41:139-48.
[83] Li C-L, Tao T, Nan K-J, Na Z, Guo Y-A, Jie C, et al. Survival advantages of multicellular spheroids vs. monolayers of HepG2 cells *in vitro*. Oncology Reports. 2008;20:1465-71.
[84] Miranda JP, Rodrigues A, Tostoes RM, Leite S, Zimmerman H, Carrondo MJT, et al. Extending hepatocyte functionality for drug-testing applications using high-viscosity alginate–encapsulated three-dimensional cultures in bioreactors. Tissue Eng: Part C. 2010;15:1223-32.
[85] The world is not flat: exploring cells and tissues in three dimensions. Science Daily 2010 [cited 19 July 2012]; Available from: http://www.sciencedaily.com/releases/2010/10/101019111716.
[86] Honer zu Bentrup K, Ramamurthy R, Ott CM, Emami K, Nelman-Gonzalez M, Wilson JW, et al. Three-dimensional organotypic models of human colonic epithelium to study the early stages of enteric salmonellosis. Microbes and Infection. 2006;8:1813-25.
[87] Carvalho HM, Teel LD, Goping G, O'Brien AD. A three-dimensional tissue culture model for the study of attach and efface lesion formation by enteropathogenic and enterohaemorrhagic *Escherichia coli*. Cell Microbiol. 2005;7:1771-81.
[88] Nickerson CA, Goodwin TJ, Terlonge J, M. O, Buchanan KL, Uicker WC, et al. Three-dimensional tissue assemblies: Novel models for the study of *Salmonella enterica* Serovar *Typhimurium* pathogenesis. Infect Immun. 2001;69:7106-20.
[89] Straub TM, Honer zu Bentrup K, Orosz-Coghlan P, Dohnalkova A, Mayer BK, Bartholomew RA, et al. *In vitro* cell culture infectivity assay for human noroviruses. Emerg Infect Dis. 2007;13:396-403.

[90] Carterson AJ, Honer zu Bentrup K, Ott CM, Clarke MS, Pierson DL, Vanderburg CR, et al. A549 lung epithelial cells grown as three-dimensional aggregates: alternative tissue culture model for *Pseudomonas aeruginosa* pathogenesis. Infect Immun. 2005;73:1129-40.
[91] Smith YC, Grande KK, Rasmussen SB, O'Brien AD. Novel three-dimensional organoid model for evaluation of the interaction of uropathogenic *Escherichia coli* with terminally differentiated human urothelial cells. Infect Immun. 2006;74:750-7.
[92] Margolis LB, Fitzgerald W, Glushakova S, Hatfill S, Amichay N, Baibakov B, et al. Lymphocyte trafficking and HIV infection of human lymphoid tissue in a rotating wall vessel bioreactor. AIDS Res Hum Retroviruses 1997;13:1411-20.
[93] Duray PH, Yin SR, Ito Y, Bezrukov L, Cox C, Cho MS, et al. Invasion of human tissue ex vivo by Borrelia burgdorferi. J Infect Dis 2005;191:1747-54.
[94] Jessup JM, Frantz M, Sonmez-Alpan E, Locker J, Skena K, Waller H, et al. Microgravity culture reduces apoptosis and increases the differentiation of a human colorectal carcinoma cell line. *In Vitro* Cell Dev Biol Anim 2000;36:367-73.
[95] Chisari FV. Unscrambling hepatitis C virus-host interactions. Nature. 2005;436:930-2.
[96] Chen SL, Morgan TR. The Natural History of Hepatitis C Virus (HCV) Infection. Int J Med Sci 2006;3:47-52.
[97] Sainz B, TenCate V, Uprichard S. Three-dimensional Huh7 cell culture system for the study of Hepatitis C virus infection. Virol J. 2009;6:103.
[98] Comley J. 3D cell culture, easier said then done. Drug Discovery World. 2010 24 April 2012;Summer 2010:25-41.
[99] Episkin™, EpiDerm™, and Rat Skin Transcutaneous Electrical Resistance (TER): *In vitro* test methods for assessing the dermal corrosivity potential of chemicals. The Inreagnecy Coordinating Comittee on the Validation of Alternative Methods 2012 [cited 4 September 2012]; Available from: http://iccvam.niehs.nih.gov/docs/dermal_docs/epis_brd0801.pdf
[100] Maltman DJ, Przyborski SA. Developments in three-dimensional cell culture technology aimed at improving the accuracy of *in vitro* analyses. Biochem Soc Trans 2010;38:1072-5.
[101] Levenberg S, Huang NF, Lavik E, Rogers AB, Itskoviz-Eldor J, Langer R. Differentiation of human embryonic stem cells on three-dimensional polymer scaffolds. PNAS. 2003;100:12741-6.
[102] Non-enzymatic methods for cell harvesting. Tech Notes Vol 1 Issue 3 1993 [cited 11 August 2012]; Available from: http://www.nuncbrand.com/files/en-1176.pdf
[103] Okano T, Yamada N, Okuhara M, Sakai H, Sakurai Y. Mechanism of cell detachment from temperature-modulated, hydrophilic-hydrophobic polymer surfaces. Biomaterials. 1995;16:297-303.
[104] Caykara T, Kiper S, Demirel GK. Thermosensitive poly(*N*-isopropylacrylamide-co-acrylamide) hydrogels: Synthesis, swelling and interaction with ionic surfactants European Polymer Journal. 2006;42:348-55.
[105] Curti PS, de Moura MR, Veiga W, Radovanovic E, Rubira AF, Muniz EC. Characterization of PNIPAAm photografted on PET and PS surfaces. Appl Surf Sci. 2005;245:223-33.
[106] Yamato M, Utsumi M, Kushida A, Konno C, Kikuchi A, Okano T. Thermo-responsive culture dishes allow the intact harvest of multilayered keratinocyte sheets without dispase by reducing temperature. Tissue Eng. 2001;7:473-82.
[107] Kushida A, Yamato M, Konno C, Kikuchi A, Sakarai Y, Okano T. Decrease in culture temperature releases monolayer endothelial cell sheets together with deposited fibronectin matrix from temperature-responsive culture surfaces. J of Biomed Mater Res. 1999;45:355-62.
[108] Kumashiro Y, Yamato M, Okano T. Cell attachment–detachment control on temperature-responsive thin surfaces for novel tissue engineering. Annals of Biomedical Engineering. 2010;38:1977-88.
[109] Roy I, Gupta MN. Smart polymeric materials: Emerging biochemical applications. Chemistry & Biology. 2003;10:1161-71.
[110] Nobuhikou K, Yasu T, Hiroto U, Masataka S, Shigemasa H, Masatoshi K, et al. Mechanical stress promotes the expression of smooth muscle-like properties in marrow stromal cells. Experimental Hematology. 2004;32:1238-45.

[111] Cavelier C, Justice B, Felder RA. Automated 3D cell culture. 2010 [cited 6 October 2012]; Available from: http://www.hamiltoncompany.com/downloads/L90013%20-%20Automated%203D%20Cell%20Culture%20Application%20Note.pdf
[112] Dvir-Ginzberg M, Gamlieli-Bonshtein I, Agbaria R, Cohen S. Liver tissue engineering within alginate scaffolds: Effects of cell-seeding density on hepatocyte viability, morphology, and function. Tissue Eng. 2003;9:757-66.
[113] Sattabongkot J, Yimamnuaychoke N, Leelaudomlipi S, Rasameesoraj M, Jenwithisuk R, Coleman RE, et al. Establishment of a human hepatocyte line that supports *in vitro* development of the exo-erythrocytic stages of the malaria parasites *Plasmodium falciparum* and *P. vivax*. Am Journal Trop Med Hyg. 2006;74:708-15.
[114] Wagner WR, Muzzio DJ, Rilo HR, Deglau T, Ataai MM, Michalopoulos GK, et al. Effect of growth factors and defined medium on primary hepatocyte culture on polyester carriers with varying surface treatments. Tissue Eng. 1997;3:289-301.
[115] Shor L, Güçeri S, Wen X, Gandhi M, Sun W. Fabrication of three-dimensional polycaprolactone/hydroxyapatite tissue scaffolds and osteoblast-scaffolds interactions *in vitro*. Biomaterials. 2007;28:5291-7.
[116] Mandal BB, Kundu SC. Cell proliferation and migration on silk fibroin 3D scaffolds. Biomaterials. 2009;30:2956-65.
[117] Al-Nasiry S, Geusens N, Hanssens M, Luyten C, Pijnenborg R. The use of Alamar Blue assay for quantitative analysis of viability, migration and invasion of choriocarcinoma cells. Human Reproduction. 2007;5:1304-9.
[118] Rago R, Mitched J, Wilding G. DNA fluorometric assay in 96-well tissue culture plates using Hoechst 33258 after cell lysis by freezing in distilled water. Anal Biochem. 1990;191:31-4.
[119] Kessler MA, Meinitzer A, Wolfbeis OS. Albumin blue 580 fluorescence assay for albumine. Analytical Chemistry. 1997;248:180-2.
[120] Bradford MM. A rapid and sensitive method for the quantitation of microgram quantities of protein utilizing the principle of protein-dye binding. Anal Biochem. 1976;72:248-54.
[121] Clark K, Dhoogra M, Louw AI, Birkholtz L-M. Transcriptional responses of *Plasmodium falciparum* to a-difluoromethylornithine-induced polyamine depletion. Biol Chem. 2008;389:111-25.
[122] Livak KJ, Schmittgen TD. Analysis of relative gene expression data using Real-Time Quantitative PCR and the $2^{-\Delta\Delta CT}$ method. Methods. 2001;25:402-8.
[123] Canavan HE, Cheng X, Graham DJ, Ratner BD, Castner DG. Cell sheet detachment affects the extracellular matrix: A surface science study comparing thermal liftoff, enzymatic, and mechanical methods. Journal of Biomedical Materials. 2005;75A(1):1-13.
[124] Rozen S, Skaletsky H. Primer3 on the WWW for general users and for biologist programmers. Methods Mol Biol. 2000;132:365-586.
[125] Kee NW, Leong DTW, Hutmacher DW. The challenge to measure cell proliferation in two and three dimensions. Tissue Eng. 2005;11 182-91.
[126] Glicklis R, Merchuk JC, Cohen S. Modeling mass transfer in hepatocyte spheroids via cell viability, spheroid size, and hepatocellular functions. Biotecnol Bioeng. 2004;86:672-80.
[127] Dvir-Ginzberg M, Elkayam T, Aflalo ED, Agbaria R, Cohen S. Ultrastructural and functional investigations of adult hepatocyte spheroids during *in vitro* cultivation. Tissue Eng. 2004;10:1806-17.
[128] Glicklis R, Shapiro L, Agbaria R, Merchuk JC, Cohen S. Hepatocyte behavior within three-dimensional porous alginate scaffolds. Biotechnol Bioeng. 2000;67:344-53.
[129] Hamilton GA, Jolley SL, Gilbert D, Coon JD, Barros S, LeCluyse EL. Regulation of cell morphology and cytochrome P450 expression in human hepatocytes by extracellular matrix and cell-cell interactions. Cell Tissue Res. 2001;306:85-99.
[130] Lübberstedt M, Müller-Vieira U, Mayer M, Biemel KM, Knöspel F, Knobeloch D, et al. HepaRG human hepatic cell line utility as a surrogate for primary human hepatocytes in drug metabolism assessment *in vitro*. J Pharmacol Toxicol Methods. 2011;63:59-68.
[131] World Health Organization. World malaria report 2011 [cited 10 August 2012]; Available from: http://www.who.int/malaria/world_malaria_report_2011/en/index.html.
[132] Greenwood B, Bojang K, Whitty C, Targett G. Malaria. Lancet. 2005;365:1487-98.

[133] Prudencio M, Rodriguez A, Mota MM. The silent path to thousands of merozoites: the *Plasmodium* liver stage. Nature Reviews Microbiology. 2006 Nov;4(11):849-56.
[134] Rosenberg R, Wirtz RA, Schneider I, Burge R. An estimation of the number of malaria sporozoites ejected by a feeding mosquito. Trans R Soc Trop Med Hyg. 1990;84:201-12.
[135] Cowman AF, Crabb BS. Invasion of red blood cells by malaria parasites. Cell. 2006;124:755–66.
[136] Baker DA. Malaria Gametocytogenesis. Molecular and Biochemical Parasitology. 2010;172:57-65.
[137] Kappe SH, Kaiser K, Matuschewski K. The *Plasmodium* sporozoite journey: a rite of passage. Trends Parasitol 2003;19:135-43.
[138] Life cycle of the malaria parasite Epidemiology of Infectious Diseases 2011 [cited 18 June 2012]; Available from: http://ocw.jhsph.edu
[139] Coppi A, Tewari R, Bishop JR, Bennett BL, Lawrence R, Esko JD, et al. Heparan sulfate proteoglycans provide a signal to Plasmodium sporozoites to stop migrating and productively invade host cells. Cell Host & Microbe. 2007;2:316-27.
[140] Montagna GN, Matuschewski K, Buscagli CA. *Plasmodium* sporozoite motility: an update. Frontiers in Bioscience. 2012;17:726-44.
[141] Baer K, Roosevelt M, Clarkson AB, Jr., van Rooijen N, Schnieder T, Frevert U. Kupffer cells are obligatory for *Plasmodium yoelii* sporozoite infection of the liver. Cell Microbiol. 2007;9:397-412.
[142] Frevert U, Engelmann S, Zougbede S, Stange J, Ng B, Matuschewski K, et al. Intravital observation of *Plasmodium berghei* sporozoite infection of the liver. PLoS Biol. 2005;3:e192.
[143] Pradel G, Frevert U. Malaria sporozoites actively enter and pass through rat kupffer cells prior to hepatocyte invasion. Hepatology. 2001;33:1154-65.
[144] Mota MM, Pradel G, Vanderberg JP, Hafalla JCR, Frevert U, Nussenzweig RS, et al. Migration of Plasmodium sporozoites through cells before infection. Science. 2001;291:141-4.
[145] Mota MM, Hafalla JCR, Rodriguez A. Migration through host cells activates *Plasmodium* sporozoites for infection. Nature Medicine. 2002;8:1318-22.
[146] Silvie O, Mota MM, Matuschewski K, Prudencio M. Interactions of the malaria parasite and its mammalian host. Curr Opin Microbiol. 2008;11:352-9.
[147] Vaughan AM, Aly SIA, Kappe SHI. Malaria Parasite Pre-Erythrocytic Stage Infection: Gliding and Hiding. Cell Host & Microbe. 2008;4:209-18.
[148] Wongsrichanalai C, Meshnick SR. Declining artesunate-mefloquine efficacy against falciparum malaria on the Cambodia-Thailand border. Emerging Infectious Diseases. 2008;14:716-9.
[149] Fidock DA. Drug discovery: Priming the antimalarial pipeline. Nature. 2010;465:297-8.
[150] Epiphanio S, Mikolajczak SA, Goncalves LA, Pamplona A, Portugal S, Albuquerque S, et al. Heme oxygenase-1 is an anti-inflammatory host factor that promotes murine plasmodium liver infection. Cell Host Microbe. 2008;15:331-8.
[151] Tarun AS, Peng X, Dumpit RF, Ogata Y, Silva-Rivera H, Camargo N, et al. A combined transcriptome and proteome survey of malaria parasite liver stages. Proceedings of the National Academy of Sciences. 2008 January 2, 2008:305-10.
[152] Albuquerque SS, Carret C, Grosso AR, Tarun AS, Peng X, Kappe SH, et al. Host cell transcriptional profiling during malaria liver stage infection reveals a coordinated and sequential set of biological events. BMC Genomics. 2009;17:270.
[153] White NJ. Determinants of relapse periodicity in *Plasmodium vivax* malaria. Malar J. 2011;10:297.
[154] Delves M, Plouffe D, Scheurer C, Meister S, Wittlin S, Winzeler EA, et al. The activities of current antimalarial drugs on the life cycle stages of *Plasmodium*: A comparative study with human and rodent parasites. PLoS Med. 2012;9:e1001169.
[155] Prudencio M, Mota MM, Mendes AM. A toolbox to study liver stage malaria. Trends in Parasitology. 2011;27:565-74.

[156] Al-Olayan EM, Beetsma AL, Butcher GA, Sinden RE, Hurd H. Complete development of mosquito phases of the malaria parasite *in vitro*. Science. 2002 January 25, 2002;295:677-9.
[157] Trager W, Jensen JB. Cultivation of erythrocytic and erythrocytic stages of plasmodia. New York and London: Academic Press; 1980.
[158] Brecker G, Schneiderman M. A time saving device for counting of reticulocytes. American Journal of Clinical Pathology. 1950;20:1079-83.
[159] Carter R, Ranford-Cartwright LC, Alano P. The culture and preparation of gametocytes of *Plasmodium falciparum* for immunochemical, molecular, and mosquito infectivity studies. Totowa, New Jersey: Humana Press Inc; 1993.
[160] Bhattacharyya MK, Kumar N. Effect of xanthurenic acid on infectivity of *Plasmodium falciparum* to *Anopheles stephensi*. International Journal for Parasitology. 2001;31:1129-33.
[161] Hunter GW, Weller TH, Jahnes WG. An Outline for teaching mosquito stomach and salivary gland dissection. American Journal of Tropical Medicine and Hygeine. 1946;26:221-8.
[162] Doane RW. Insects and Disease: A popular account of the way in which insects may spread or cause some of our common diseases. Rahway, N.J.: The Quinn and Boden Co. Press; 1910.
[163] Strome CPA, DeSantis PL, Leef JL. A convenient technique for the dissection of mosquito salivary glands. Journal of Tissue Culture Methods. 1980;6:9-11.
[164] Marco M, Chipperfield R, Bimboim H. A procedure for the large-scale isolation of highly purified plasmid DNA using alkaline extraction and binding to glass powder Anal Biochem. 1982;121:382-7.
[165] Sambrook J, Russel D. Molecular cloning, a laboratory manual. New York: Cold Spring Harbor Laboratory Press; 2001.
[166] Tanaka T, Inoue K, Hayashi Y, Abe A, Kyoko Tsukiyama-Kohara K, Nuriya H, et al. Virological significance of low-level hepatitis B virus infection in patients with hepatitis C virus associated liver disease. Journal of Medical Virology. 2004;72:223-9.
[167] Buchholz K, Burke TA, Williamson KC, Wiegand RC, Wirth DF, Marti M. A high-thoroughput screen targeting malaria transmission stages opens new avenues for drug development. Journal of Infectious Diseases. 2011;203:1445-53.
[168] Carter R, Miller LH. Evidence for environmental modulation of gametocytogenesis in *Plasmodium falciparum* in continuous culture. Bull World Health Organ. 1979;57 Suppl 1:37-52.
[169] Roncales M, Vadal-Mas J, Leroy D, Herros E. Comparison and optimisation of different methods of *In vitro* production of *Plasmosium falciparum* gametocytes. Journal of Parasitology Research. 2012;In Press.
[170] Baker DA. Malaria gametocytogenesis. Mol Biochem Parasitol. 2012;172:57-65.
[171] Schneweis S, Maier WA, Seitz HM. Haemolysis of infected erythrocytes - a trigger for formation of *Plasmodium falciparum* gametocytes? Parasitology Research. 1991;77:458-60.
[172] Smalley ME, Brown J. *Plasmodium falciparum* gametocytogenesis stimulated by lymphocytes and serum from infected Gambian children. Transactions of the Royal Society of Tropical Medicine and Hygiene. 1981;75:316-7.
[173] Buckling A, Ranford-Cartwright LC, Miles A, Read AF. Chloroquine increases *Plasmodium falciparum* gametocytogenesis *in vitro*. Parasitology. 1999;118:339-46.
[174] Young JA, Fivelman QL, Blair PL, De La Vega P, Le Roch KG, Zhou Y, et al. The *Plasmodium falciparum* sexual development transcriptome: A microarray analysis using ontology-based pattern identification. Molecular and Biochemical Parasitology. 2005;143:67-79.
[175] Ifediba T, Vanderberg JP. Complete *in vitro* maturation of *Plasmodium falciparum* gametocytes. Nature. 1981;294:364-6.
[176] Parasitology Core Facility 2010 [cited 15 August 2012]; Available from: http://www.parasitecore.org/PFGAMETO.html

[177] Lelievre J, Almela MJ, Lozano S, Miguel C, Franco V, Leroy D, et al. Activity of clinically relevant antimalarial drugs on *Plasmodium falciparum* mature gametocytes in an ATP bioluminescence "transmission blocking" assay. PLoS One. 2012;7:e35019.
[178] Moll K, Ljungström I, Perlmann H, Scherf A, Wahlgren M. BioMalPar. Methods in Malaria Research 2008 [cited 15 August 2012]; Available from: http://www.biomalpar.org/updatedMethods_In_Malaria_Research_5thedition.pdf
[179] Alano P, Roca L, Smith D, Read D, Carter R, Day K. *Plasmodium falciparum*: Parasites defective in early stages of gametocytogenesis. Exp Parasitol. 1995;81:227-35.
[180] Fivelman QL, McRobert L, Sharp S, Taylor CJ, Saeed M, Swales CA, et al. Improved synchronous production of *Plasmodium falciparum* gametocytes *in vitro*. Molecular and Biochemical Parasitology. 2007;154(1):119-23.
[181] Bennett TN, Kosar AD, Roepe PD. *Plasmodium falciparum* strain GC-03 exhibits hyper-gametocytogenesis in partially hemoglobin depleted red blood cells. Molecular and Biochemical Parasitology. 2005;139:261-5.
[182] Shirley MV, Biggs BA, Forsyth KP, Brown HJ, Thompson JK, Brown GV, et al. Chromosome 9 from independent clones and isolates of *Plasmodium falciparum* undergoes subtelomeric deletions with similar breakpoints *in vitro*. Mol Biochem Parasitol. 1990;40:137-46.
[183] Sanofi. Impact-Malaria. 2002-2012 [cited 2012 14 May 2012]; Available from:
[184] Lambrechts L, Halbert J, Durand P, Gouagna LC, Koella JC. Host genotype by parasite genotype interactions underlying the resistance of anopheline mosquitoes to Plasmodium falciparum. Malar J 2005;4.
[185] Vaughan JA, Noden BH, Beier JC. Sporogonic development of cultured Plasmodium falciparum in six species of laboratory-reared Anopheles mosquitoes. Am J Trop Med Hyg 1994;51:233-43.
[186] Billker O, Lindo V, Panico M, Etienne AE, Paxton T, Dell A, et al. Identification of xanthurenic acid as the putative inducer of malaria development in the mosquito. Nature. 1998;392:289-92.
[187] Ghosh AK, Dinglasan RR, Ikadai H, Jacobs-Lorena M. An improved method for the *in vitro* differentiation of *Plasmodium falciparum* gametocytes into ookinetes. Malar J. 2010;9:194.
[188] Silvie O, Franetich J-F, Boucheix C, Rubinstein E, Mazier D. Alternative invasion pathways for plasmodium berghei sporozoites. International Journal for Parasitology. 2007;37:173-82.
[189] Ishino T, Yano K, Chinzei Y, Yuda M. Cell-passage activity is required for the malarial parasite to cross the liver sinusoidal cell layer. PLOS Biology. 2004;2:77-84.
[190] Ishino T, Chinzei Y, Yuda M. A *Plasmodium* sporozoite protein with a membrane attack complex domain is required for breaching the liver sinusoidal cell layer prior to hepatocyte infection. Cellular Microbiology. 2005;7:199-208.
[191] Pradel G, Garapaty G, Frevert G. Proteoglycans mediate malaria sporozoite targeting to the liver. Molecular Microbiology. 2002;45:637-51.
[192] Coppi A, Tewari R, Bishop JR, Bennett BL, Lawrence R, Esko JD, et al. Heparan sulfate proteoglycans provide a signal to *Plasmodium* sporozoites to stop migrating and productively invade host cells. Cell Host Microbe. 2007;15:316-27.
[193] Ono T, Cabrita-Santos L, Leitao R, Bettiol E, Purcell LA, Diaz-Pulido O, et al. Adenylyl cyclase alpha and cAMP signaling mediate *Plasmodium* sporozoite apical regulated exocytosis and hepatocyte infection. PLoS Pathog. 2008;4:e1000008.
[194] Bi YA, Kazolias D, Duignan DB. Use of cryopreserved human hepatocytes in sandwich culture to measure hepatobiliary transport. Drug Metab Dispos 2006;34:1658-65.
[195] Bhadriraju K, Chen CS. Engineering cellular microenvironments to improve cell-based drug testing. Drug Discovery Today. 2002;7:612-20.
[196] Boissiere A, Tchioffo MT, Bachar D, Abate L, Marie A, Nsango SE, et al. Midgut microbiota of the malaria mosquito vector Anopheles gambiae and interactions with Plasmodium falciparum infection. PLoS Pathog. 2012;8:e1002742.
[197] Ndiath MO, Cohuet A, Gaye A, Konate L, C. M, Faye O, et al. Comparative susceptibility to *Plasmodium falciparum* of the molecular forms M and S of *Anopheles gambiae* and *Anopheles arabiensis*. Malar J. 2011;10:269.

[198] Wondji C, Frederic S, Petrarca V, Etang J, Santolamazza F, Della Torre A, et al. Species and populations of the *Anopheles gambiae* complex in Cameroon with special emphasis on chromosomal and molecular forms of *Anopheles gambiae* s.s. J Med Entomol. 2005;42:998-1005.
[199] Dong Y, Manfredini F, Dimopoulos G. Implication of the mosquito midgut microbiota in the defense against malaria parasites. PLoS Pathog. 2009;3:e1000423.
[200] Beier MS, Pumpuni CB, Beier JC, Davis JR. Effects of para-aminobenzoic acid, insulin, and gentamicin on *Plasmodium falciparum* development in anopheline mosquitoes (Diptera: Culicidae). J Med Entomol. 1994;31:561-5.
[201] Esch MB, King TL, Shuler ML. The role of body-on-a-chip devices in drug and toxicity studies. Annu Rev Biomed Eng. 2011;13:55-72.
[202] Huh D, Hamilton GA, Ingber DE. From 3D cell culture to organs-on-chips. Trends in Cell Biology. 2011;21:745-54.
[203] Roach P, Eglin D, Rohde K, Perry C. Modern biomaterials: a review—bulk properties and implications of surface modifications. J Mater Sci Mater Med. 2007;18:1263-77.
[204] Kessel F, Rosenfield PL. Toward transdisciplinary research historical and contemporary perspectives. Am J Prev Med. 2008;35:S225-S34.

APPENDIX A

Table A1. TaqMan® expression data. The grey shaded area represents the control samples. Expression data from invaded 2D and 3D hepatocytes are presented alongside their respective endogenous control. Data for three biological replications (n=3) of each sample are presented; the standard deviation (C_T SD) is calculated from the three technical replicates.

Sample Name	Target Name	CT Mean	CT SD	Target Name	CT Mean	CT SD
Non-invaded hepatocyte controls						
2D control	β-Actin	28.97	0.00			
3D control	β-Actin	30.24	0.09			
Parasite controls						
Sporozoite only	18S rRNA	32.38	*			
5 % Parasitemia	18S rRNA	20.10	0.13			
2.5 % Parasitemia	18S rRNA	20.37	0.09			
1 % Parasitemia	18S rRNA	20.97	0.02			
0.1% Parasitemia	18S rRNA	28.82	0.62			
0.01 % Parasitemia	18S rRNA	40.52	0.82			
Invaded 2D hepatocytes				**Hepatocyte control**		
2D Day 3	18S rRNA	48.28	**	β-Actin	29.78	0.08
2D Day 3	18S rRNA	49.53	**	β-Actin	29.66	0.03
2D Day 3	18S rRNA	46.94	**	β-Actin	30.78	0.05
2D Day 7	18S rRNA	44.98	**	β-Actin	30.72	0.03
2D Day 7	18S rRNA	48.74	0.21	β-Actin	29.58	0.11
2D Day 7	18S rRNA	**ND**		β-Actin	30.54	0.11
Invaded 3D hepatocytes				**Hepatocyte control**		
3D Day 3	18S rRNA	**ND**		β-Actin	29.75	0.09
3D Day 3	18S rRNA	**ND**		β-Actin	29.60	0.04
3D Day 3	18S rRNA	**ND**		β-Actin	29.68	0.11
3D Day 7	18S rRNA	**ND**		β-Actin	30.32	0.07
3D Day 7	18S rRNA	**ND**		β-Actin	29.96	0.15
3D Day 7	18S rRNA	**ND**		β-Actin	30.22	0.09

* Due to limited sample volume this control was initially not run in triplicate thus, the C_T SD was not calculated.
** Due to the assumed low abundance of the 18S rRNA target in the samples, this gene was not detected in each and every technical replicate thus the C_T SD was not calculated.
ND: Not determined.

Appendix A

Table A2. TaqMan® expression data for increased primer and probe concentrations. The grey shaded area represents the control samples. Data for three biological replications (n=3) of each sample are presented; the standard deviation (C_T SD) is calculated from the three technical replicates.

Sample Name	Target Name	CT Mean	CT SD
Parasite control			
Sporozoite only	18S rRNA	36.90	0.09
Invaded 2D hepatocytes			
2D Day 3 50 nM probe	18S rRNA	49.44	0.26
2D Day 7 50 nM probe	18S rRNA	52.05	0.80
2D day 3 200 nM probe	18S rRNA	53.05	2.00
2D day 7 200 nM probe	18S rRNA	49.92	0.97
Invaded 3D hepatocytes			
3D Day 3 50 nM probe	18S rRNA	ND	
3D Day 7 50 nM probe	18S rRNA	ND	
3D day 3 200 nM probe	18S rRNA	ND	
3D day 7 200 nM probe	18S rRNA	ND	

Appendix A

Table A3. TaqMan® expression data from invaded cells growing in 2D and nylon scaffolds. The grey shaded area represents the control samples. Expression data from invaded 2D and 3D hepatocytes are presented alongside their respective endogenous control. Data for three biological replications of each sample are presented the standard deviation (C_T SD) is calculated from the three technical replicates

Sample Name	Target Name	CT Mean	CT SD	Target Name	CT Mean	CT SD
Non-invaded hepatocyte controls						
2D control	β-Actin	29.47	0.02			
3D control	β-Actin	31.12	0.20			
Parasite controls						
Sporozoite only	18s rRNA	32.80	*			
5% Parasitemia	18s rRNA	19.98	0.17			
2.5% Parasitemia	18s rRNA	21.03	0.05			
1% Parasitemia	18s rRNA	21.23	0.06			
0.1% Parasitemia	18s rRNA	32.78	1.11			
0.01% Parasitemia	18s rRNA	33.63	1.29			
Invaded 2D hepatocytes				**Hepatocyte control**		
2D Day 3	18s rRNA	48.53	3.05	β-Actin	31.10	0.32
2D day 3	18s rRNA	48.64	3.13	β-Actin	29.93	0.04
2D day 3	18s rRNA	49.78	2.03	β-Actin	30.91	0.31
2D day 7	18s rRNA	49.07	**	β-Actin	30.35	0.17
2D day 7	18s rRNA	47.04	0.28	β-Actin	28.35	0.03
2D day 7	18s rRNA	48.82	1.93	β-Actin	28.97	0.16
Invaded 3D hepatocytes				**Hepatocyte control**		
3D day 3	18s rRNA	**ND**		β-Actin	28.83	0.02
3D day 3	18s rRNA	**ND**		β-Actin	28.85	0.04
3D day 3	18s rRNA	**ND**		β-Actin	27.74	0.04
3D day 7	18s rRNA	**ND**		β-Actin	29.39	0.08
3D day 7	18s rRNA	**ND**		β-Actin	29.37	0.13
3D day 7	18s rRNA	**ND**		β-Actin	28.89	0.10

* Due to limited sample this control was not run in triplicate thus the C_T SD was not calculated.
** Due to the assumed low abundance of the 18S rRNA target in the samples, this gene was not detected in each and every technical replicate thus the C_T SD was not calculated.
ND: Not determined.